الجامعة الإسلامية العالمية ماليزيا
INTERNATIONAL ISLAMIC UNIVERSITY MALAYSIA
يونيرسيتي إسلام انتارابغسا ملايسيا

MAGNETIC RESONANCE IMAGE RECONSTRUCTION USING 2D AUTOREGRESSIVE MOVING AVERAGE MODEL

BY

ATHAUR RAHMAN BIN NAJEEB

INTERNATIONAL ISLAMIC UNIVERSITY MALAYSIA

2008

MAGNETIC RESONANCE IMAGE RECONSTRUCTION USING 2D AUTOREGRESSIVE MOVING AVERAGE MODEL

BY

ATHAUR RAHMAN BIN NAJEEB

A dissertation submitted in partial fulfilment of the requirements of the degree of Master of Science in Computer and Information Engineering

Kulliyyah of Engineering
International Islamic University
Malaysia

FEBRUARY 2008

He is the Knower of the Unseen, Whom not an atom's weight eludes, either in the heavens or in the earth; nor is there anything smaller or larger than that which is not in a Clear Book. (Qur'an, 34:3)

ABSTRACT

Discrete Fourier Transform (DFT) is a method of choice for reconstructing Magnetic Resonance Images. It is used as basis for reconstructing images in all types of Data Acquisition techniques ranging from conventional techniques such as Projection Method to the latest Parallel Imaging Techniques. Despite the great success of DFT as reconstruction algorithm, it has some inherit limitation. When used with truncated data, it clearly exhibits artifacts. The data set for DFT is expected to be huge, while practically data acquired are small. DFT works best on smooth image function, while practically MRI data set consists of discrete data set. Application of FT on this data leads to artifacts such as truncation artifacts, spikes at discontinuity point of spectrum (Gibbs Ringging). Although spikes could be flatten by applying windows or filters, but this leads to additional problems such as tiny important pathological images could be suppressed as well. To overcome some of these limitations, few alternatives were proposed such as Modified Backprojection Method (MBM), Parametric Methods (PM), Neural Network Methods (NN), Wavelets Methods (WM), etc. Though, clear reconstructed images can be obtained with NN and WM, however, their data representation is doubtful. Studies show during processing several images with motion and a small tumor, NN and WM successfully reconstructed clear images without any indication of motions has taken place. Yet, the pathological tumor has been averaged away as well. Such clinically these methods are invalid and it is a clear indicative of failure. Parametric methods such as Autoregressive (AR) and Autoregressive Moving Average (ARMA) model give positive result. Research and studies conducted during 1980s and 1990s, clearly showing that ARMA can be a good replacement, but due to the computational complexity, it has not been practically implemented and need further clinical testing. Although there are many algorithms available to solve for ARMA, particularly, Transient Error Reconstruction Approach (TERA) were proven be successful. Taking advantage of current microprocessor speeds and successful implementation of previous variety forms of ARMA algorithms, this research tends to implement 2D ARMA on MRI Data set to reconstruct the images. Modified Transient Error Reconstruction Approach (m-TERA) method is proposed to solve for 2D ARMA model. Model orders are proposed to be computed dynamically rather than a fixed value as in TERA method. Different approach of AR parameter determination and final image calculation is also been proposed in comparison with TERA method.

Raw data for simulation of 2D m-TERA are obtained from Hospital HTAA, Kuantan with courtesy of Philip® Medical System. Images were reconstructed with proposed algorithm using Matlab®. Finally, reconstructed images from 2D m-TERA are compared with standard method 2D IFFT and performance analysis in term of resolution and reconstruction time is presented.

ملخص البحث

إن طريقة (دي أف تي) تعتبر احسن طريقة لإعادة تنظيم تصوير الرنين المغناطيسي. وتستعمل هذه الطريقة كأساس لاعادة تنظيم الصور في كل تقنيات الحصول على المعلومات إعتباراً من الطرق التقليدية كطريقة عرض الصور على الشاشة الى آخر التقنيات في طرق لصق الصور المتوازية. بالرغم من النجاح الساحق لمنظمات (دي أف تي) فأن لها محددات متوارثة، عند إستعمالها مع المعلومات المبتورة (غير المتكاملة). بالاضافة الى إن المعلومات اللازمة لهذه الطريقة تكون كميتها هائلة، بينما المعلومات المكتسبة تكون عمليا ضئيلة. هذه الطريقة تشتغل بصورة جيدة عندما تكون الصورواضحة، بينما هذا غير موجود في الواقع حيث إن معلومات تصوير الرنين المغناطيسي (أم آر آي) تتألف من مجموعة من المعلومات والتطبيقات لمنظومة (دي أف تي) لهذه المعلومات تؤدي الى وجود بعض الصور غير المرغوب فيها والتي تتداخل مع الصورة وتؤدي الى عدم استمرار صورة الطيف. بالرغم من إن التداخل سكن جعله مسطحا باستخدام الشبابيك أو المرشحات، إلا إن هذا يؤدي الى مشاكل إضافية وكمثال على ذلك فان الصور المرضية الصغيرة جدا قد لاتظهر وتطمس بسبب ذلك. للتغلب على هذا القصور، فقد تم إقتراح عدة بدائل مثل الطريقة المعدلة لعرض الصور (أم بي أم)، وطريقة الباراميترك (بي أم)، والطريقة الشبكية (أن أن)، بالاضافة الى الطريقة التذبذبية (دبليو أم)، الخ. على الرغم من إن الصور التي يتم الحصول عليها بطرق (أن أن) و (دبليو أم) تكون واضحة، ولكن النتائج يكون مشكوك فيها. بعض الدراسات أوضحت خلال عرض عدة صور مع تحريكها فأن هاتين الطريقتين (أن أن) و (دبليو أم) تعطي صور واضحة بدون الاشارة الى وجود حركة. علاوة على ذلك، فأن صور الاورام الخبيثة تم إيجاد معدلاتها للاعتماد عليها. وسريريا لايمكن إعتماد هذه الطرق وهذا دليل على فشلها. الطرق الباراميتركية وكمثال عليها (أي آر) و (أي آر أم أي) تعطي نتائج إيجابية. البحوث والدراسات خلال الثمانينات والتسعينات، أوضحت إن طريقة (أي آر أم أي) تعتبر بديل جيد، ولكن بسبب التعقيدات الحسابية، لم يتم تطبيقها عمليا وتحتاج الى تطبيقات سريرية مفصلة. بالرغم من وجود عدة طرق لوغاريتمية لحل مشاكل (أي آر أم أي)، بصورة خاصة ، فأن طريقة (تي إي آر أي) قد أثبتت نجاحها. للاستفادة من المعاملات

الميكروية وسرعتها و لنجاح تطبيقاتها في مجموعة اشكال لوغاريتمات (أي آر أم أي)، فان هذا البحث يقودنا الى تطبيق (أي آر أم أي) باتجاهين على معلومات صور الرنين المغناطيسي لبناء الصور.تم إقتراح طريقة (أم - تي إي آر أي) لحل الموديل (أي آر أم أي) ذو الاتجاهين. كما تم إقتراح اوامر الموديل ليتم حسابها ديناميكيا بدل من تحديد القيم كما هو في طريقة (تي إي آر أي). كما تم إقتراح تعيين متغيرات (أي آر) وحسابات الصور النهائية بالمقارنة مع طريقة (تي إي آر أي). تم حساب المعلومات الاولية بالنسبة الى (أم – تي إي آر أي) من مستشفى في كوانتان وبواسطة النظام الطبي المسمى (فيليب، ذو الماركة المسجلة). تم بناء الصور من المعلومات اللوغاريتمية بواسطة استخدام السوفت وير (مات لاب، المسجل ايضا). واخيرا، تم مقارنة الصور التي تم الحصول عليها من (أم - تي إي آر أي) ذو الاتجاهين مع الطريقة القياسية (آي أف أف تـي، ذو الاتجاهين) وتحليل تأدية هذه الطريقة بالنسبة الى ثبات واعادة البناء.

APPROVAL PAGE

I certify that I have supervised and read this study and that in my opinion; it conforms to acceptable standards of scholarly presentation and is fully adequate, in scope and quality, as a dissertation for the degree of Master of Science in Computer and Information Engineering.

.....
Momoh Jimoh E. Salami
Supervisor

I certify that I have read this study and that in my opinion it conforms to acceptable standards of scholarly presentation and is fully adequate, in scope and quality, as a thesis for the degree Master of Science in Computer and Information Engineering

.....
Amir Akramin Shafie
Internal Examiner

This dissertation was submitted to the Department of Electrical and Computer Engineering is accepted as a partial fulfillment of the requirements for the degree of Master of Science, Computer and Information Engineering

.....
Othman Khalifa
Head, Department of Electrical
and Computer Engineering

This dissertation was submitted to the Kulliyyah of Engineering and is accepted as a partial fulfillment of the requirements for the degree of Master of Science, Computer and Information Engineering

.....
Ahmad Faris Ismail
Dean, Kulliyyah of Engineering

DECLARATION

I hereby declare that this dissertation is the result of my own investigations, except where otherwise stated. I also declare that it has not been previously or concurrently submitted as a whole for any other degrees at IIUM or other institutions.

Athaur Rahman Bin Najeeb

Signature ..... Date …….

INTERNATIONAL ISLAMIC UNIVERSITY MALAYSIA

DECLARATION OF COPYRIGHT AND AFFIRMATION OF FAIR USE OF UNPUBLISHED RESEARCH

MR IMAGE RECONSTRUCTION USING AUTOREGRESSIVE MOVING AVERAGE MODEL

Affirmed by Athaur Rahman bin Najeeb

…….. ……..
Signature Date

I dedicate this humble work of mine to my parents Mr. and Mrs. Najeeb, my wife, Mrs. Akhari Begam, my children and all my teachers who have guided me throughout my life. Thank you for your love, patience and guidance, Jazakallahu Khairan.

ACKNOWLEDGEMENTS

Alhamdullilah, praises and prayers to the Almighty Allah SWT, the Creator, Sustainer, Master of All Knowledge for granting me patience, perseverance to accomplish this thesis successfully and for His Blessings and Guidance throughout this research work and my life. I would like to thank my supervisors, Prof. Dr. Momoh Jimoh E. Salami, Assoc. Prof. Dr. Othman Khalifa, and Assoc. Prof. Dr. Kamarul Arriffin (Kulliyyah of Medicine), for the support and advice they have provided throughout the duration of my research work. I am also indebted to Dr. Pawel F. Tokarczuk PhD (MRI Physicist and Scientist, Cardiff University), Dr. Matthew Clemence PhD (Clinical Science Support MR, Philips Medical Systems United Kingdom), Dr. Mirko Hrovat PhD, (MRI Research Scientist) and Prof. Dr. Mike Smith (University of Calgary, Canada) for teaching me the art of reconstruction work and providing the impetus for much of my work. I would also like to thank all the people with whom I have worked over the past three years without whom none of this work could have been done, and particularly Datuk Dr. Zainon (Head of Diagnostic Imaging, Hospital HTAA, Kuantan), Mr. Khalil Khamis and Mr. Eric Seng Chian Chang, from Philips® Medical (M) Sdn Bhd whom made possible to download raw data for simulation purpose. Finally I would like to thank the Research Center of my university, International Islamic University of Malaysia for funding this research and Philips® Medical Sdn Bhd for utilizing their Interra 1.5T MRI Scanner.

TABLE OF CONTENTS

LIST OF TABLES

LIST OF FIGURES

LIST OF ABBREVIATIONS

A.I.C.	Akaike Information Criterion
A.R.	Autoregressive
A.R.M.A.	Autoregressive Moving Average
C.A.T.	Criterion Autoregressive Transfer
C.N.R.	Contrast to Noise Ratio
C.P	Converter Programme
C.R.A.	Clinical Research Agreement
D.B.R.	Direct Backprojection Reconstruction
D.C.F.	Density Compensation Function
D.F.T.	Discrete Fourier Transform
E.P.I.	Echo Planar Imaging
F.B.R.	Filter Backprojection Reconstruction
F.F.T.	Fast Fourier Transform
F.I.D.	Free Induction Decay
F.O.I.	Field of Interest
F.P.E.	Final Prediction Error
F.P.E .	Final Prediction Method
F.R.F.	Fourier Reconstruction Formula
F.R.T.	Fourier Reconstruction Technique
F.T.	Fourier Techniques
G.R.	Gridding Reconstruction
G.R.A.P.P.A.	Generalized Auto calibrating partially parallel acquisitions
I.B.P.	Iterative Backprojection
L.R.T.	Likelihood Ratio Test
M.D.L.	Minimum Description Length
M.D.L.	Minimum Description Length
M.R.	Magnetic Resonance
M.R.I.	Magnetic Resonance Imaging
M.R.T.	Magnetic Resonance Tomography
M-T.E.R.A.	Modified Transient Error Reconstruction Technique
N.M.R.	Nuclear Magnetic Resonance
N.S.A.	Number of Signal Averages
N.V.	Noise Variance
P.I.T.	Parallel Imaging Techniques
P.S.D.	Pulse Sequence Diagram
P.S.F.	Point Spread Function
P.S.W.F.	Prolate Spherical Wave Function
R.F.	Radio Frequency
R.O.I	Region of Interest
R.T.R.	Radon Transform Reconstruction
S.E.N.S.E.	Sensitivity Encoding for fast MRI
S.M.A.S.H.	Simultaneous Acquisition of Spatial Harmonics
S.N.R.	Signal to Noise Ratio
S.V.D.	Singular Value Approaches

T.E.R.A.	Transient Error Reconstruction Technique
T.P.E.	Total Prediction Error

CHAPTER ONE

INTRODUCTION

1.1 OVERVIEW

Magnetic resonance imaging (MRI) formerly referred as magnetic resonance tomography (MRT) or in chemistry Nuclear Magnetic Resonance (NMR), is a non-invasive method used to produce images inside of an object. It is an alternate technology of scanning human body without using CT-Scan technologies. MRI is painless and safe diagnostic procedure that uses a powerful magnet and radio waves to produce detailed images of the body's organs and structures, without the use of X-rays, which is know to be harmful to human body after certain threshold frequency. By using radio-frequency technology, MRI scanners are able to penetrate soft tissues such as layers of muscles or blood vessels in contrast to earlier technology which were able to only detect dense tissues like bone structures.

Signals captured from patients go through several stages before been presented as a clear digital image, which has a higher contrast, resolution, more information and better quality compared to X-ray or CT-scans. By varying several scanning parameters, MRI scanners are able to provide 3D scanning to generate cross-sectional images in any plane (including oblique planes), while CT and X-Rays are limited to acquire images in the axial (or near axial) plane only.

Each MR image sequence composed of slices of the body area. Numerous images are created from this single anatomical part and presented as separate single image starting from upper layer to lowest layer. These numerous images clearly show all features of that particular region of interest (ROI). For example, one cerebral image

sequence may consists of 16 or 32 different images; each image displays one layer starting from upper layer of cerebral, going deep into lowest layer.

From signal processing view, imaging process involves a pair of transformations. The first transformation is imaging equation generation, which governs and specify how the signal data is collected and the second transformation is image equation reconstruction. The later determines how the measured data is processed to form image by applying algorithm which suits the property of decoded signal during first transformation. Figure 3.1 illustrates this concept (Liang and Lauterbur, 1999).

.

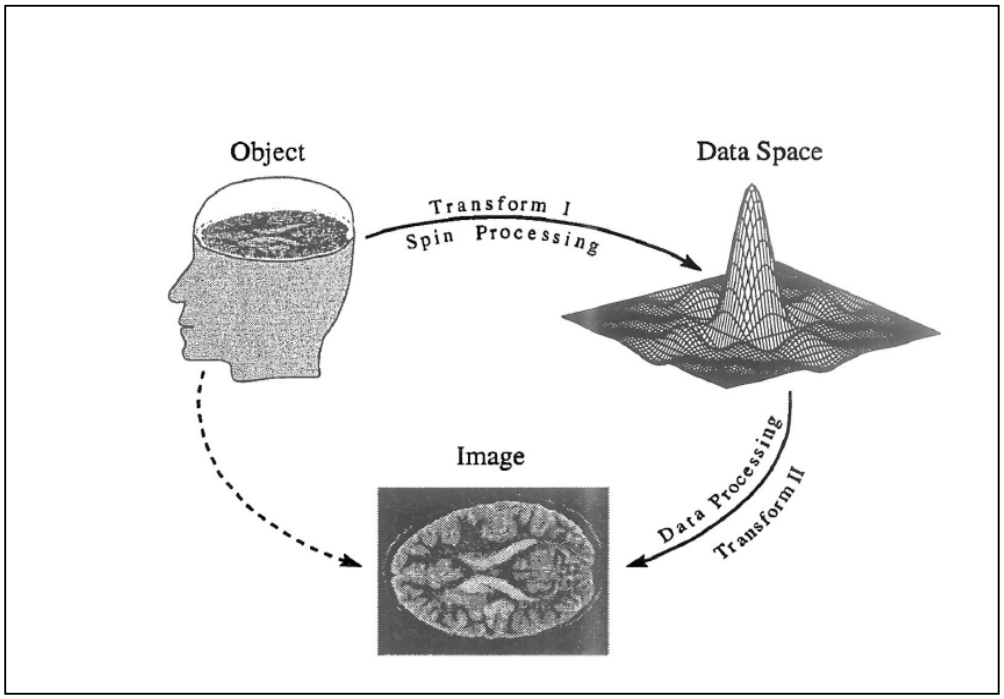

Figure 1.1: Signal Processing View of Image Reconstruction

Generally, imaging equation generation is also known as data acquisition techniques. This technique describes not only how signal data is acquired into a desirable format, but also about the design of signal acquiring hardware and how the

hardware interact among each other. In MRI, the data acquisition techniques can be described with a Pulse Sequence Diagram (PSD). PSD shows how hardware interacts in sequence to obtain radio-frequency signals emitted from object. Spatial information signals are captured in time domain and plotted on a 2D k-space following a pattern which could be either rectilinearly or spirally. This is discussed more in detail in Chapter Two.

Image reconstruction is applying an algorithm to decode the acquired k-space signal into a frequency signal which can be plotted directly to form image. Image reconstruction methods are central to many new applications of medical imaging. There is no surprise to see these techniques are dynamic fields which evolves each time when there are improvements on hardware. Moreover, image reconstruction itself is a field of study, where reconstruction algorithms are studied in great detail. Improvements and new approaches are introduced from time to time with one sole objective to improve the image quality with minimum reconstruction time.

One should differentiate between image reconstruction and image enhancement. Image enhancement is processing an image data, for example enhancing blurred images, improving contrast, etc. .Enhancement algorithms are applied on readily available images, but image reconstruction builds the image from raw data. Image reconstruction is to acquire image data from measured signal data. It starts with reading the k-space data, applies reconstruction formula and scale to a desired display.

In this introductory chapter, the background of this thesis is presented. The problem statement is discussed in Section 1.2 briefing the standard imaging equation and its inherit limitation. Research objectives are clearly mentioned. The adopted research methodology is listed and finally the layout of this thesis is discussed.

1.2 PROBLEM STATEMENT AND ITS SIGNIFICANCE

1.2.1 Imaging Equation

MRI is usually a Fourier transform based technique in the sense that, in data acquisition, spatial image information is encoded to generate data in the Fourier space (or k-space) (Liang and Lauterbur (1999)) which is then inverse Fourier transformed to get the desired image. Mathematically, the relation between acquired data and image data can be expressed as:

$$s(k) = \int_{-\infty}^{\infty} I(x) e^{-i2\pi kx} \tag{1.1}$$

where

k is the spatial frequency
x is the spatial position
$s(k)$ is the measured signal
$I(x)$ is the image function

In higher dimensional case such as 2D or 3D, equation 1.1 can be rewritten in vector notation as:

$$s(\vec{k}) = \int_{-\infty}^{\infty} I(\vec{r}) e^{-i2\pi \vec{k}\vec{r}} d\vec{r} \tag{1.2}$$

where $\vec{k}$ represents $(k_x k_y)$ or $(k_x k_y k_z)$ and $\vec{r}$ represents *(x,y)* or *(x,y,z)* for two or three dimensional cases respectively. This multidimensional equation can be solved as a sequence of 1D equation for any dimensions:

$$s(k_x, k_y) = \int_{-\infty}^{\infty} \left[\int_{-\infty}^{\infty} I(x, y) e^{-i2\pi(k_x x + k_y y)} dx \right] dy \tag{1.3}$$

The image data, *I(x)* is a MR image intensity representation, and is a multi-parameter coded function of spin density, relaxation time diffusion coefficients and so on. The exact function depends on data acquisition protocol. Whatever the function is, the goal is to ascertain $I(\vec{r})$ from acquired sample set of data, $s(\vec{k})$.This is known as

image reconstruction. Plotting $I(\vec{r})$ in frequency domain will display the image. This image should be exact representation of acquired raw data, $s(\vec{k})$. Any violation of data would produce inaccurate images or will introduce additional information in the final image. This would lead to misguided diagnosis of pathological conditions of patient.

The problem of reconstructing a function from its Fourier transform samples is to determine $I(x, y)$ from equation 1.3; for a given data values of $\vec{k}_n \in D$. D contains the set of k-space points where the measured data are collected. Standard method of obtaining $I(x, y)$ is applying Fourier transform on $s(\vec{k})$. Consequently, by considering only 1D, the true image function $I(x, y)$ can be shown as:

$$I(x) = \Delta k \sum_{n=-\infty}^{\infty} s_n e^{i2\pi n \Delta k x} \quad , |x| < \frac{1}{2\Delta x} \tag{1.4}$$

Where,

$I(x)$ is the true image data

Δk is the sampling interval

s_n is the acquired MRI data

n is the data interval , ranging from - $-\infty \le n \le \infty$

Equation 1.4 ([Haacke and Liang, 2000 ; Liang and Lauterbur, 1999 and Yan 2002] is often referred to as the reconstruction formula for infinite sampling. Practically, only a finite number of k-space points are collected. Assuming that $s(\vec{k})$ is known for $\vec{k}_n \in D$, where

$$D = \{n\Delta k, -N/2 \le n \le N/2 - 1\} \tag{1.5}$$

Therefore, for practical consideration of finite sampling, $\hat{I}(x)$ is given by (Yan, 2002):

$$\hat{I}(x) = \Delta k \sum_{n=-N/2}^{N/2-1} s_n e^{i2\pi n\Delta k x} + \Delta k \sum_{n<N/2, n\geq N/2} c_n e^{i2\pi n\Delta k} \tag{1.6}$$

$\hat{I}(x)$ is a feasible reconstruction of $I(x)$ with respect to the measured data, s_n for an arbitrary constant (finite) c_n; which is application dependent. c_n =0 is often selected as a minimum-norm constraint. As a result, the unmeasured Fourier series coefficient for c_n are all forced to be zero. Such that the minimum-norm feasible reconstruction can be expressed as

$$\hat{I}(x) = \Delta k \sum_{n=-N/2}^{N/2-1} s(n\Delta k) e^{i2\pi\Delta k x} \quad , |x| < \frac{1}{2\Delta x} \tag{1.7}$$

where

$\hat{I}(x)$ is the Fourier Reconstruction Image
N is the total number of sampled data points
Δk is the sampling interval

Equation 1.7 is known as Fourier Reconstruction Formula (FRF) which can be evaluated using a Fast Fourier Transform (FFT). FFT has been adopted as a standard image reconstruction technique as for its reliability and fast reconstruction time.

1.2.2 Challenges in Imaging Equation

Obviously, $\hat{I}(x)$ from equation 1.7 is not the true image function $I(x)$, as it is derived from finite sampling. $\hat{I}(x)$ is related to $I(x)$ by the convolution equation with a Point Spread Function (PSF), *h(x)*.

$$\begin{aligned} &\hat{I}(x) = I(x) * h(x); \\ &\textit{where } h(x): \\ &h(x) = \Delta k \frac{\sin(\pi N \Delta k)}{\sin(\pi \Delta k x)} e^{-i\pi\Delta k x} \end{aligned} \tag{1.8}$$

Note that h(x) is a periodic function, and within each period it displays characteristics similar to those of a sinc function. The width of its main lobe, as measured by the interval between the first two zero crossings is $\frac{2}{N\Delta k}$. Its effective width, W_h, is often taken to be the width of an approximating rectangular pulse with height *h(0)* of the same area. (Yan ,2002) which is:

$$W_h = \frac{1}{h(0)} \int_{-(1/2\Delta k)}^{1/2\Delta k} h(x)dx = \frac{1}{N\Delta k} \tag{1.9}$$

As the width of W_h is half of the main lobe, it can reduce the resolution of $\hat{I}(x)$. An implication from equation 1.9 is both of W_h and N cannot be reduced simultaneously. Reducing the W_h will improve the resolution of image produced, which in turn need a high number of data, N. Practically N is not a huge data set. For an image of size 256 by 256, total data captured is 65,536 is considered short data. Therefore the usage of direct FFT in reconstructing MR Image will lead to poor resolution. This problem is inherited with FFT reconstruction.

Since the data is collected at discrete points of s_n, certainly $I(x)$ is not a smooth function. At the discontinuity points, the convergence behavior of Fourier transform produces overshoots. As N approaches ∞ in $I(x)$, the value of maximum overshoot tends to a finite value(Liang and Lauterbur ,1999); Yan, 2002]. This maximum overshoot is formally called Gibbs phenomena. It manifests itself as spurious ringing around sharp edges in final images and produces Gibbs ringing artifact. It is a common image distortion that exists in Fourier images. Figure 1.2 illustrates the overshoot that occurs at discontinuity points. The maximum overshoot

or undershoot of the Gibbs ringing is about 9% of the intensity discontinuity and is independent of the number of data points used in reconstruction.

In addition to losses of resolution and Gibbs ringing, the finite sampling interval (Δk) also leads to another disadvantage of Fourier transform. It creates a limitation of imaging for finite regions of support. Any attempt to slower rate to reduce the Gibbs ringing, would lead to image aliasing.

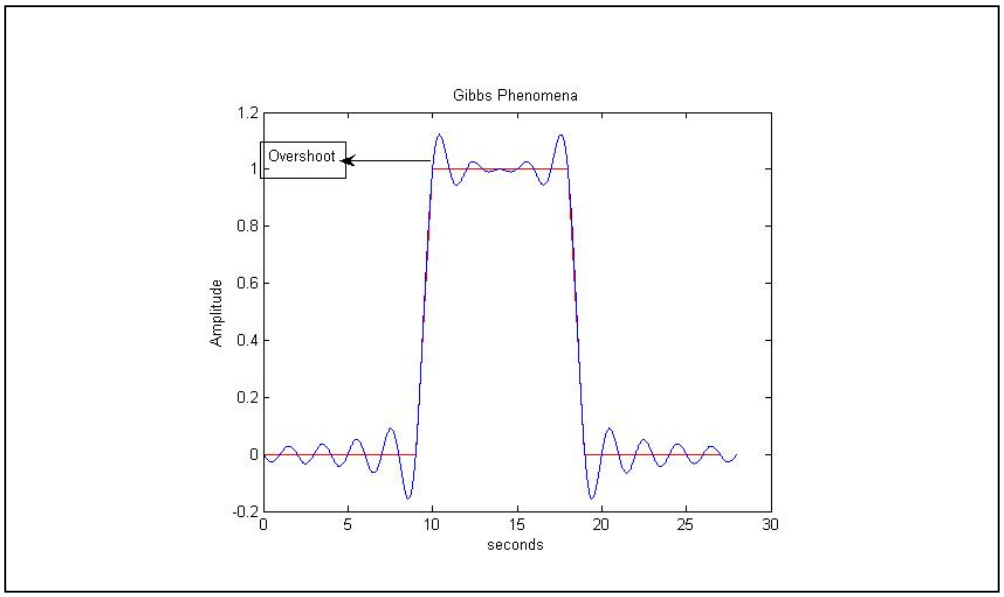

Figure 1.2: Illustration of Gibbs phenomena

Although Gibbs ringing can be reduced by applying some windowing technique, the trade off is lost in resolution. Such, seems an efficient algorithm, which combines reduction of Gibbs ringing and improving resolution within the minimum value of Δk would seem to overcome this issue. But energy level from various parts of human body produces different noise level. A filter designed to be used in abdomen imaging may not be good enough to be applied on cerebral imaging. Further

discussion on Gibbs ringing is presented in Chapter 2, while discussing issues in MR reconstruction.

Generally, Fourier Reconstruction Technique (FRT) leads to image with low resolution, spikes due to Gibbs phenomena, aliasing and provides significant low resolution images. There are many existing reconstruction techniques either to improve the limitation caused by Fourier Transform or to replace Fourier transform. Techniques such as Neural Network, Wavelet Reconstruction, Parametric Modeling, etc. were proposed to replace Fourier Reconstruction. But not all techniques are found suitable, as some of the techniques failed during clinical test. Further analysis of these reconstruction techniques is discussed in Chapter 3.

1.3 RESEARCH OBJECTIVES

This research is intended to propose study and analyze an alternative basic reconstruction algorithm which can be applied on MRI raw data to reconstruct the images in comparison to current techniques.

Parametric modeling which was explored by Smith (Smith, 1986) was one technique proven to be an efficient alternate option when compared to Fourier reconstruction technique. But this proposal has not been tested clinically due to its computational complexity. Taking advantage of current computing speed and considering the fact that speed of Fourier based reconstruction has reached the bottleneck of about 1200 images per second; this research thesis tends to revisit the application of Autoregressive Moving Average to reconstruct MR Images. ARMA is a parametric modeling technique widely used in spectroscopy analysis. Successful implementation of ARMA in other fields was the driving factor.

Modification is proposed to be applied on the Transient Error Reconstruction Technique (TERA), originally proposed by Smith (Smith et al)) to solve ARMA. Smith has successfully implemented 1D TERA method that is modeling the truncated axis with TERA and other axis with standard Fourier reconstruction.

The work of Smith is further extended in this thesis to 2 dimensional ARMA model which will be solved using Modified TERA (MTERA). Compared to Smith's work where he has used a fixed the model order, MTERA computes the model order dynamically for each rows and columns. This calculation requires high computation speed as model order computation involves nested algorithms. The proposed MTERA also adopts different Autoregressive (AR) coefficient determination and different approach of generating the final image data. This proposed modified algorithm is discussed in more detail in Chapter 4 and implemented in Chapter 5. Successful implementation of this work will contribute to a new perspective in Medical Imaging. The scope and objective of research work is listed as:

1. To develop MTERA as ARMA solution method for reconstructing MR Images.
2. To reconstruct MR images from k-space data using MTERA.
3. To reconstruct the same data with FRT for comparison.
4. To evaluate the performance of the MTERA based 2D ARMA reconstruction technique with respect to improving resolution and reducing Gibbs ringing artifact.

1.4 RESEARCH METHODOLOGY

The following are milestones in the realization of this thesis work:

1. Problem Statement and Research Objective

2. Literature Review
    a. Understanding MRI and MRI Physics
    b. Understanding ARMA and TERA methods
    c. Review and Analysis of MRI reconstruction techniques
2. Development of MTERA Algorithm
3. Raw data acquisition from MRI Scanner
4. Implementation of 2D FFT Reconstruction Technique
5. Implementation of 2D ARMA using MTERA
6. Testing and Data Analysis

1.4.1 Thesis Layout

This thesis is organized into six (6) chapters. Chapter 1 is an introductory chapter which begins with a brief introduction to image reconstruction followed by problem statement which discusses the limitation of current image reconstruction techniques. Research objectives and research methodology are presented as well.

Literature review is presented from 2 perspectives; how image is formed in a MRI scanner and analysis MRI Reconstruction techniques. Chapter 2 discusses fundamentals of MRI physics starting with a brief summary on history of MRI. This is followed by discussion on imaging principals and data acquisition techniques.

Finally, Chapter Two is ended with highlights of critical key issues that need attention for image reconstruction.

A through analysis of MRI Reconstruction techniques are presented in Chapter 3. This chapter begins with overview of different Reconstruction techniques and a comparative analysis of these techniques is presented.

The proposed algorithm is discussed in detail by introducing the concept of ARMA in Chapter 4. General steps in TERA method are listed and followed by detailed discussion of the proposed algorithm, MTERA.

The raw data organization and analysis are presented in Chapter 5. This chapter begins with an introduction to k-space plot, how raw data is downloaded from MRI scanner and how the data is organized in k-space plot. Discussion continues with details of converter program which was written to read the binary data and rearrange in image matrix format. Later, the implementation of MTERA is discussed and results are presented graphically by plotting the intensity graphs or pixel value graphs. Final images were compared between raw image, FFT images and 2D ARMA images.

Finally, conclusion and recommendation for future work is discussed in Chapter 6.

CHAPTER TWO

MAGNETIC RESONANCE IMAGING

2.1 INTRODUCTION

While this thesis is primarily concerned with reconstruction of MR images, the basic understanding on how MRI works is essential; since reconstructions of images are strongly related to data acquisition methods. In this chapter, fundamentals or physics of MR imaging are presented; starting with brief history of MRI developments until the procedures of MR image production. Some key issues in MR image reconstruction are also discussed. Finally, image acquisition techniques which provide basic equations for image reconstruction are presented as well.

2.2 HISTORICAL PERSPECTIVE

MRI is based on the technique of nuclear magnetic resonance. In 1946, Felix Bloch from Stanford University and Edward Purcell from Harvard University independently found that *when certain nuclei were placed in a magnetic field they absorbed energy in the radiofrequency range of the electromagnetic spectrum, and re-emitted this energy when the nuclei returned to their original state* (Semmlow, 2004] This phenomenon was termed Nuclear Magnetic Resonance (NMR) as:

- "Nuclear" as only the nuclei of certain atoms reacted in that way.
- "Magnetic" as a magnetic field was required;
- "Resonance" because of the direct frequency dependence of the magnetic and radiofrequency fields.

With this discovery, NMR spectroscopy was born and soon became an important analytical method in the study of the composition of chemical compounds. The inventors were awarded Nobel Prize for Physics in 1952. In the years after that till early 70s, NMR was developed and used for chemical and physical molecular analysis only. It was not until 1971 when Raymond Damadian showed that the nuclear magnetic relaxation times of tissues and tumors differ and this motivates for research of using NMR for detecting diseases. A breakthrough was on 1973, when MRI was first demonstrated on small test tube samples by Paul Lauterbur from State University of New York (Rodriguez ,2004). The research become more active and many others contributed following Lauterbur.

Perhaps the most important discovery which later became the backbone for current MRI is invented by Anil Kumar and Richard Ernst, whereby they proposed magnetic resonance imaging data acquisition using phase and frequency encoding which leads to use of Inverse Fourier Transform for image reconstruction (Kumar et al, 1975). The term MR Imaging emerges after this proposal and continues to be developed until full body imaging was demonstrated by Raymond Damadian in 1977 (Liang and Lauterbur ,1999). Since then, MRI keeps on advancing either in hardware design, data acquisition techniques or from signal processing aspects such as reconstruction algorithms or post processing. Reconstruction techniques changes whenever new hardware is added or new data acquisition technique were employed.

2.3 MRI PHYSICS

The purpose of this section is to present a general description of signal production which is the basis of MRI. The hardware components of MR imaging are introduced

followed by a summary of how signal is generated from human body for imaging purpose.

2.3.1 Hardware

There are five main hardware components in a MRI scanner which are the main magnet, the gradient system, the radio frequency (RF) system, the reconstructor (computer), and the control panel. The *main magnet* has a bore (hole) to place the subject. Its primary function is to generate magnetic field ($\vec{B}_0$). The main magnet is classified as either resistive, permanent or a superconducting magnet based on its magnetic strength. Each magnet is used for different kinds of scanning i.e angiograph, thorax, etc. Higher fields offer better signal to noise ratio and spectral resolution. (Liang and Lauterbur, 1999).

The *magnetic field gradient component* consists of three orthogonal gradients coils, the x-gradient coils, the y –gradient coils and the z-gradient coils (G_x, G_y, and G_z) . These coils are designed to produce time-varying magnetic fields and used for signal localization. They are measured in, millitesla per meter, mT/m. Higher value of mT/m the better signal it can produce.

The *RF component* consists of transmitter coil and a receiver coil. Also known as RF coils because they resonate at radio frequency and used to generate magnetic fields at RF frequency, which is used to elicit signals from human tissues.

The other 2 components are supporting hardware; *the constructor* receives the signal (after AD conversion) and reconstructs the data to a viewable image. While *the control panel* is to control the overall function of MRI and push the images for storage at different location. Figure 2.1 illustrates a typical MRI Scanner.

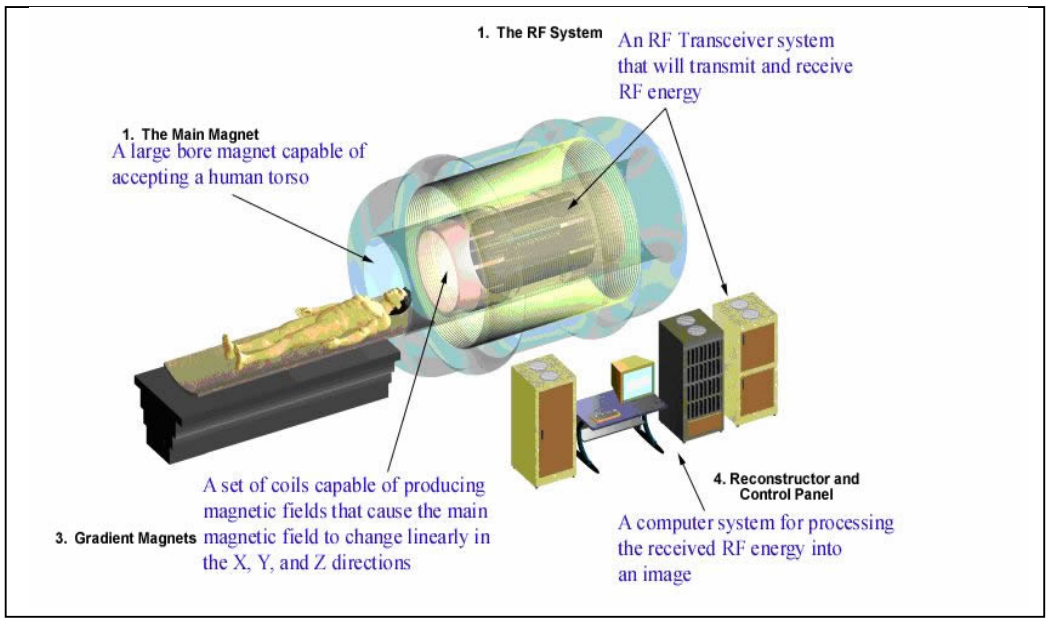

Figure 2.1: MRI Hardware
(Note: Courtesy of Philips®)

2.3.2 Image Formation.

Figure 2.2 illustrates nucleus behaviors during data acquisition process. The imaging process begins with the spinning of nucleus (consists of proton and neutron) atom about an axis; since atomic nuclei have charges, an angular momentum of nucleus spin ($\vec{J}$) would produce magnetic moment ($\vec{u}$) along the axes of spin. In most nuclei, the particles are paired so that the net magnetic properties cancelled by each of rotating protons and neutrons. However, if the number of protons or neutrons is odd, complete cancellation is not possible. Nuclei with an unpaired proton or neutron such as hydrogen 1, carbon 13, and sodium 23, among others, exhibit a net magnetic effect (Liang and Lauterbur, 1999]. Hydrogen which is available in high number in human body also exhibits large magnetic moment compared to other odd atomic number particle. This property is the basis for nuclear magnetism.

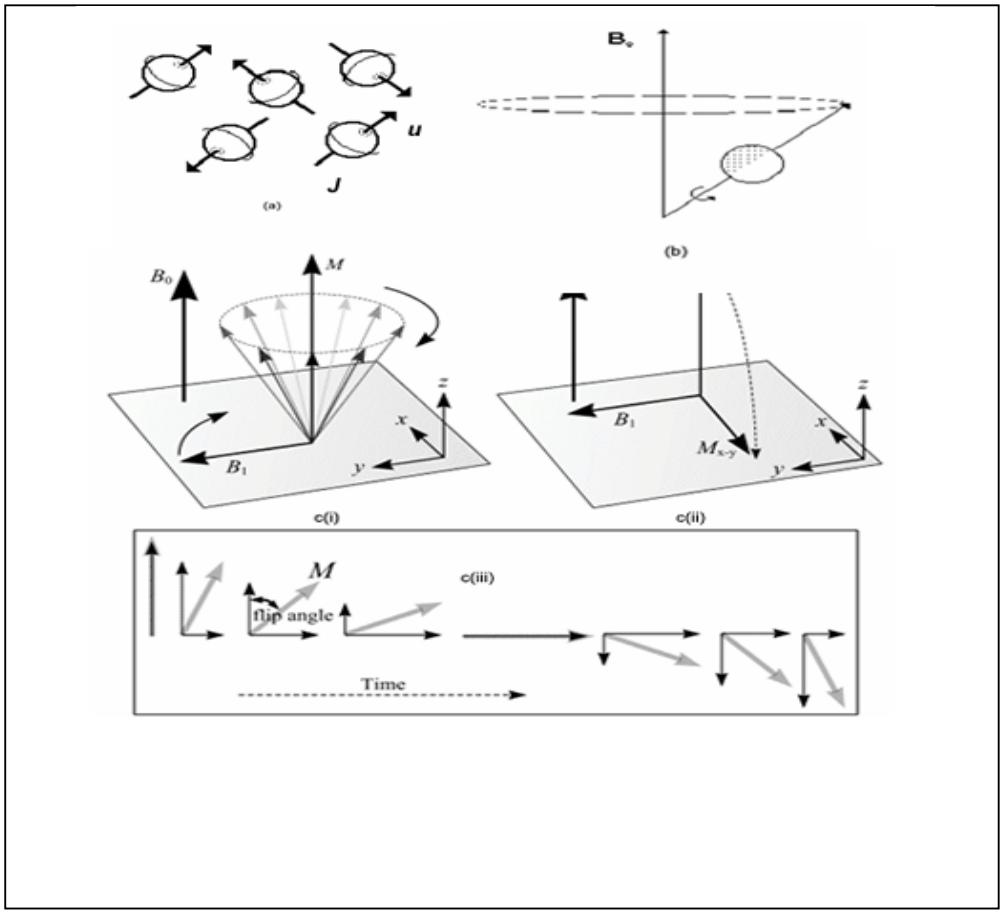

Figure 2.2: Stages of nucleus during image formation

Under normal condition, the direction of magnetic moment ($\vec{u}$) is completely random, and the human tissue does not exhibit any net magnetization effect. But under the presence of external magnetic field, $\vec{B}_0$ the spinning particles, tends to align themselves parallel or antiparallel to the applied magnetic field $\vec{B}_0$ (Liang and Haacke, 1999). Since a parallel alignment to the field is the lower energy state, it is preferred and slightly more nuclei will align parallel rather than antiparallel to $\vec{B}_0$ .Individual protons do not spin exactly parallel to $\vec{B}_0$, but in an angle to it. The frequency of the rotation is described by Larmor equation, γB_0 = f, which produce sLarmor frequency of 63.855 MHz for 1.5 T MRI Scanners.

The application of $\vec{B}_0$ to human tissue will produce a net longitudinal magnetization effect ($\vec{M}$) as though an iron is placed in a magnetic field, although not as strong. The presence of $\vec{M}$ does not imply the generation of NMR signals, in fact, $\vec{M}$ is not measurable when it lies parallel to $\vec{B}_0$.

MR signals can be detected only if a transverse magnetization, which is perpendicular to $\vec{B}_0$ is created. According to Faraday Law, time varying transverse magnetization can induce a voltage in the receiver coil. Transverse magnetization is created by applying a time varying (oscillating) magnetic field $\vec{B}_1$. The RF transmitter generates $\vec{B}_1$ perpendicular to $\vec{B}_0$, which forces the protons to spin while $\vec{M}$ are rotated in an angle known as flip angle from $\vec{B}_0$ axis. $\vec{B}_1$ is applied perpendicularly at the level of radio frequency at Larmor frequency, which will tip of the longitudinal magnetization into transverse magnetization.

Upon termination of RF pulse, the nuclei return to their original alignment, that is parallel to $\vec{B}_0$ and energy is emitted in the form of weak RF signal. The return of nuclei to its original position causes the magnetization processes about $\vec{B}_0$. The processing of transverse magnetization is detected as time varying electrical signal (weak RF signal). The induced voltage has the characteristic of damped cosine and also called free induction decay (FID).

When a RF pulse is applied, the signal is at its maximum intensity. This time varying MR signal is detected by a receiver coil and the receiver systems demodulates MR signal to extract information that is digitized to create the raw data. Raw data will be utilized by the reconstructor hardware to generate images. Image contrasts and

localization are achieved through setting and timing of signal generation and by using gradient systems. This is done by radiographers through Control Console.

2.4 DATA ACQUISITION AND RECONSTRUCTION

There are many ways to acquire MRI data. The requirement is simply that enough of spatial frequency space or k-space be sampled to allow an image to be reconstructed. MRI acquisition methods are most often described by pulse sequence diagram (PSD) that shows timing of RF pulses, gradient waveform at different axes and the data acquisition. MRI pulse sequence plays a central role in MR Imaging. Important concept and design are realized through PSD. Till now, PSD remains an active research area to extend the versatility of MRI.

Basically, a PSD illustrates hardware activities during scanning and data acquisition. Sequence execution time is indicated along the horizontal axis. Each line in PSD belongs to a different hardware component. One line is needed for the radio frequency transmitter and also one for each gradient (G_x = slice selection gradient x, G_y = phase encoding gradient y, G_z = frequency encoding gradient z, also called readout gradient). PSD has two different element, the slice selection excitation and acquisition gradients. An example of PSD is illustrated in Figure 2.3 below.

2.4.1 Spin-Warp Acquisition

The most common way to sample k-space data is with a rectilinear raster scan. Spin warp is also known as 2D DFT acquisition because image is reconstructed by directly applying the 2D DFT on the acquired data. Figure 2.3 shows a PSD for spin warp. It consists of 2 stages; where the first stage is the slice selection stage and the second stage is data encoding and acquisition stage. The slice selection process begins with

gradient lobes (G_x, G_y) movements which will initialize k-space position to the beginning of the raster lines. G_x is fixed area negative lobe called de-phaser moves the k_x position to same initial value for each line .

While the constant gradient G_y , is applied to x-gradient to scan along the initiated line, where at the same time signal is captured by RF receiver. This step is repeated till enough data is collected, i.e. 128 or 256. It is also a common practice to repeat the reading (different number of echoes) and to over sample the either x-direction or the y-direction during data acquisition.

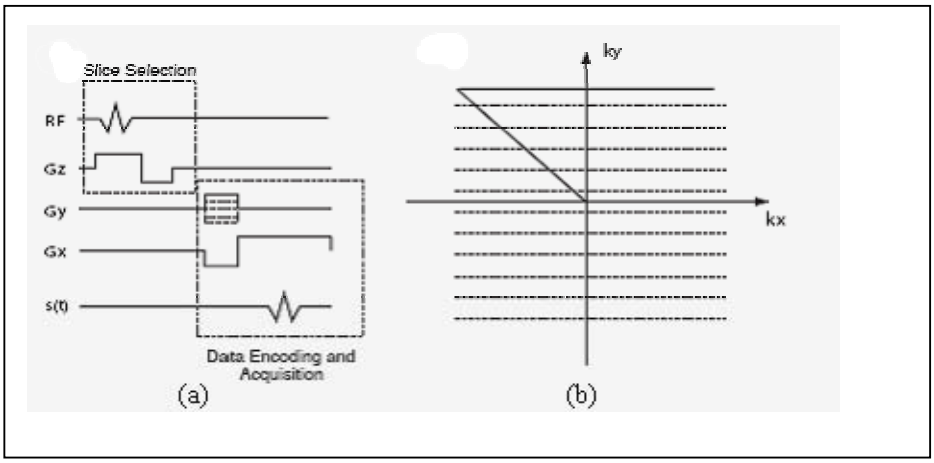

Figure 2.3: PSD diagram for Spin-Warp Acquisition

2.4.2 Spiral Acquisition

Acquisition starts at the origin of k-space and spirals outwards as been indicated in Figure 2.3(a). This can be achieved in single acquisition or in multiple rotated acquisitions so as to cover k-space uniformly. The main advantage of spiral acquistion is imaging speed and good flow properties but has a poor image quality.

2.4.3 Projection Acquisition

Projection acquisition methods are the earliest methods used for MRI based on CT's technology. Originally proposed by P.Lacterbur (1973) and was a great achievement for MR Imaging. Although this method is abandoned after advancement of spin-warp but in some cases it is still revived and maintained for specific application such as 3D angiography. The main advantage is to allow tremendous undersampling while maintaining resolution for high contrast objects. But the main disadvantage is image blurring. Figure 2.4 shows trajectory of a typical projection acquisition.

2.4.4 Echo Planar

It is considered to be an extended version of spin warp, where multiple lines in k-space are acquired after single excitation. This can be done in a single shot or multiple interleaved acquisitions. The main advantage is high speed imaging, allowing direct 2DFT reconstruction but produces image ghost for motions. It is introduced by Masfield in 1977 (Bernstein et al, 2004) and enable to produce one complete image in 30 – 100 ms.

Modern MRI Scanners which utilizes parallel acquisition techniques uses echo-planer as their base acquisition technique. Figure 2.4 shows trajectories of a spiral, projection and echo planar acquisition technique.

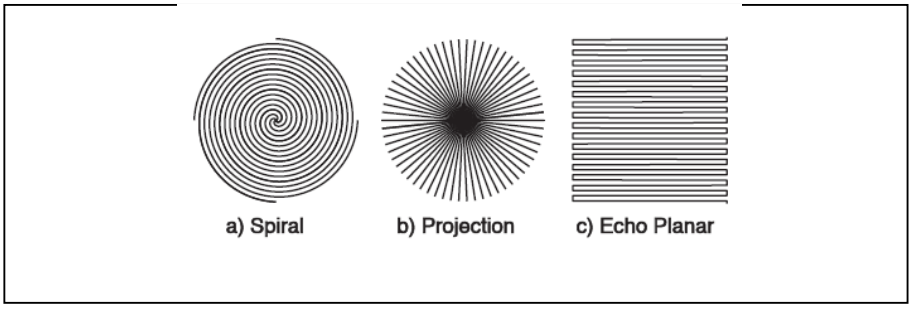

Figure 2.4: K-space trajectories

2.4.5. Parallel Imaging Techniques (PIT)

Time is an important factor in MR Scanning. Reduction of acquisition time without diminishing the signal to noise ratio is a challenging task. The conventional techniques discussed above could take long scanning hours and further improvement might not be possible as those techniques already operating at their limits of potential imaging speed. Their limitation is because of the technical and physiologic problems associated with rapidly switched magnetic field gradients. Perhaps greatest progress in increasing the imaging speed is with the development of Parallel Imaging Techniques (PIT), which has been already employed in modern MRI Scanners. . By employing PIT, Philips® MRI scanner Achieva 3.0T is able to reconstruct 860 to 1230 images of 256 X 256 per-second.

Reduction of data acquisition timing in high speed imaging using PIT is achieved by under sampling k-space and recording images simultaneously from multiple imaging coils. Under sampling reduces the acquisition time and the use of multiple RF coils eliminates the wraparound caused by the under sampling. This principal can be applied to any imaging sequence and k-space trajectories. The multiple array coils do still use the conventional techniques of echo planner or spin wrap, but each coil is doing it separately. Over the last 10 years, great progress in the

development of parallel MRI methods has taken place, thereby producing a multitude of different parallel imaging reconstruction techniques and strategies.

The most well known are Simultaneous Acquisition of Spatial Harmonics (SMASH), Sensitivity Encoding for fast MRI (SENSE) and Generalized Auto calibrating Partially Parallel Gcquisitions (GRAPPA). Currently k-t-blast , k-t-Sense , are techniques which is recently introduced by Dr. Jeffrey Tsao.

Among the schemes listed above, the latest technique is the k-t-blast designed by Philips Medical System jointly with Dr. Jeffrey Tsao from Zurich IBTZ/ETH, Zurich, Switzerland has been introduced in mid 2006. SENSE was the early technology designed years back developed by Philips® in partnership with Peter Boesiger (Blaimer et al, 2004). Although multiple array coils are been employed in PIT, their reconstruction technique is still based on the standard FFT Reconstruction. A complex pre-processing step is employed to read the data produced from different coils into image matrix before applying FFT. Further discussion ofPFIT is beyond this thesis.

2.5 GENERAL ISSUES IN MR RECONSTRUCTION

The objective of this section is to introduce issues which are of central importance in MR reconstruction. These issues are commonly encountered and lead to image errors, images with poor quality such as presence of unwanted elements or low resolution.

Un-wanted elements such as noises, artifacts and Gibbs phenomena which need to be minimized or removed during reconstruction are presented. Great concern is the question of how these substances are being generated in imaging systems and how to handle them. The first aspect is mostly related to hardware while handling it would be typically mathematical and processing by using any filters which is suitable

to scanned object. Neither is discussed in this section, but rather background for each issue is presented. Terms, causes and its effects on image are presented as well, but leaving out deeper analysis on mathematics which is lengthy and beyond the scope of this thesis.

2.5.1 Gibbs Phenomena

Gibbs ringing is a common image distortion that exists in Fourier images, which manifests itself as a spurious ringing around sharp edges as illustrated in Figure 2.5. Gibbs ringing is due to Gibbs phenomenon, which is an overshoot or ringing of Fourier series occurring at discontinuities. It is shown the maximum overshoot of the spurious ringing is about 9% about the intensity discontinuity and is independent of data points used in reconstruction.

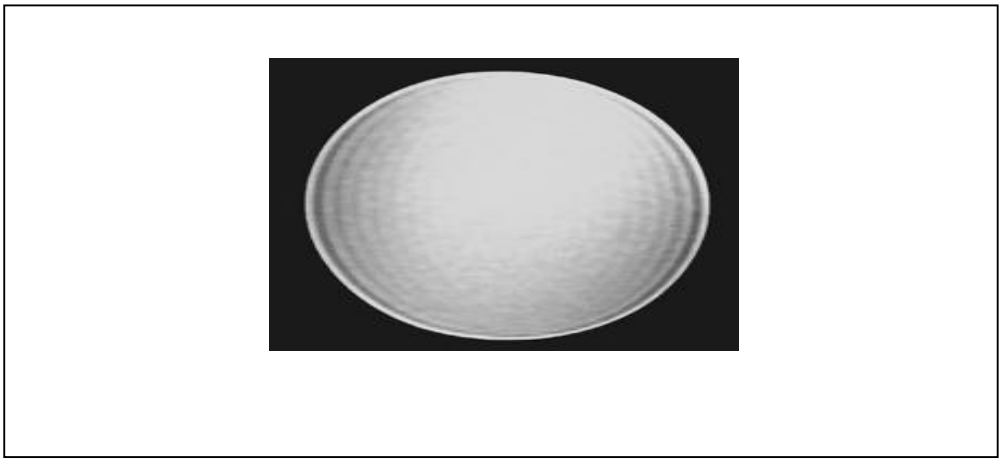

Figure 2.5: Gibbs Ringing

However, the frequency of oscillation increases with number of data points. When a large number of data points is used, the spurious ringing does not cover an

appreciable distance in the reconstructed image and this became 'invincible' (Liang and Lauterbur, 1999).

Basically, the Gibbs ringing artifact is a result of truncating the Fourier series model to finite sampling. It is related to the convergence behavior of Fourier series. When the real image data, $I(x)$ is a smooth function, the Fourier reconstructed image data, $\hat{I}(x)$, given in equation 1.7, uniformly converges to $I(x)$ as $N \to \infty$ for $x \in FOV$. For discontinues, the convergence behavior in the neighborhood of a point of discontinuity will be 'anomalous'. The overshoot at discontinuity points does not tend to zero but tend to produce a finite number. The existence of this finite, nonzero limiting value of the overshoot is due to the non uniform convergence of $\hat{I}(x)$ to $I(x)$, which is called Gibbs phenomena.

Obviously, Gibbs ringing can be reduced by collecting high frequency data, but this not possible due to constraints in MR data acquisition. It can be suppressed by properly applying suitable window function. However, this leads to a trade off in spatial resolution and suppression of tiny pathological information such as tiny tumor images.

2.5.2 Resolution limitation

In section1.2.2, it has been shown that the resultant of Fourier Reconstruction formula is the true image convolved with a periodic sinc function. This is expressed in equation 2.1:

$$\hat{I}(x) = I(x) * h(x) \tag{2.1}$$

The convolution kernel function *h(x)* is known as the Point Spread Function (PSF), since $\hat{I}(x)$ =*h(x)* for $I(x) = \delta(x)$; where $\delta(x)$ is the minimum separation between 2 discrete data point for the two points to remain resolvable in the resultant image (Liang and Lauterbur,1999). If *h(x)* deviates from $\delta(x)$, the resultant $\hat{I}(x)$ will be blurred. The amount of blurring introduced can be quantified by the width of *h(x)* such creating a resolution limitation to $\hat{I}(x)$.

Recalling equation 1.7, which gives a reconstruction formula for N Fourier samples:

$$\hat{I}(x) = \Delta k \sum_{n=-N/2}^{N/2-1} s(n\Delta k) e^{i2\pi\Delta kx} \quad , |x| < \frac{1}{2\Delta x} \tag{2.2}$$

By setting the image function, *I(x)* to a δ-function , which set the s(Δk) = 1, the PSF can be expressed as Liang and Lauterbur,1999) :

$$h(x) = \Delta k \sum_{n=-N/2}^{N/2-1} e^{i2\pi\Delta kx} \tag{2.3}$$

and consequently it can be further simplified to

$$h(x) = \Delta k \frac{\sin(\pi N \Delta k)}{\sin(\pi \Delta k x)} e^{-i\pi\Delta kx} \tag{2.4}$$

The effective width of *h(x)* which cover a single period of *h(x),* is given by integration of equation 2.4 which yields :

$$W_h = \frac{1}{h(0)} \int_{-(1/2\Delta k)}^{1/2\Delta k} h(x)dx = \frac{1}{N\Delta k} \tag{2.5}$$

According to equation 2.5, a resolution of limitation is set as both of W_h and N cannot be reduced simultaneously. Practically N is not huge to satisfy for a sufficient W_h, resulting in an increment of W_h which leads to low resolution Fourier images.

2.5.3 Noises

As it has been explained in previous section, the MR Images are generated from measurement and processing of activated signals of human body. Practical measurements always contain undesirable components that are uncorrelated with the desired signals. This unwanted component is referred as *noise*. There are two main categories of image noise, (1) statistical or random noise and (2) systemic or non-random or structured noise (Hendricks, 2000).

Statistical noise is pixel to pixel variation in signal intensities, caused by random signal fluctuations measured during signal sampling. Most of this kind of noise is result of eddy current set up in patient's body (due to external magnetization) which produces spurious background signal. This background signal may add or subtracted from the true signal. Practically, random noise is reduced by increasing slice thickness, number of data acquisition, etc.

Systemic noises are more confusing to image interpretation. It consists of non-random signal variation that arises from a number of possible sources such as patient movement, respiration, vascular flow, gradient coil motion, data truncation artifacts. Both types of noises tend to mask the detection of low-contrast lesions which could be misinterpreted for abnormalities in MR Images.

Noise is represented as random variable x(n), thus describing it as a function is not very useful and uniformly distributed throughout the image. One way of measuring the effect of noise is to calculate the signal-to-noise ratio (SNR). In the case of MRI, the SNR can be measured by computing the mean signal intensity over a certain region of interest (ROI) and dividing this by the standard deviation of the signal from a region outside the image (Hendricks, 2000).

There are many definitions to define the signal to noise ratio i.e. in terms of relaxation time or in term of signal intensities. SNR can be also computed separately for FFT reconstruction, zero-padded FFT reconstruction, filtered backward projection or any other data acquisition techniques. As for FFT reconstruction, SNR per pixel of a FFT image is inversely proportional to $\sqrt{N}$ (Liang and Lauterbur, 1999). A general SNR definition that can be applied for all images is the ratio *of the mean pixel value to the standard deviation of the pixel values* (Hendricks, 2000).

Another property which yields image noise is image noise variance (NV). NV is calculated from single magnitude images, but alternative methods are also been proposed to compute NV, namely double acquisition method (Sijbers, 1998). In single image acquisition method NV are estimated from σ^2 , which can be estimated in few ways. While in double acquisition method, the same object is scanned twice and NV is estimated by subtracting the expected values (E).

A low SNR also could be due to hardware or improper parameter setting during scanning. Proper parameter setting for TR, TE, slice thickness, FOV, FOI, etc has been defined by manufacturers for each type of scanning. Violating this values could lead to a low SNR, which will produce a blur, low resolution and low contrast images. Figure 2.6(a) and Figure 2.6(b) are examples for improper parameter settings. Parameters such as number of signal averages, number of images, TR, TE, FOV number of echo is set to minimum level to acquire a simple raw data file. Practically, SNR can be improved during scanning process by increasing NSA, number of signal averages, that is repeating signal acquisition sequences. Regardless of which noise estimation parameter is used, the objective is to reduce the noise and increase the image contrast.

2.5.4 Artifacts

Image artifacts are any features which appear in an image which are not the real representation of the original image. Compared to noise, where noise is distortion of data either in raw data or reconstruction data, artifacts are image distortion. Therefore, image artifacts can result in false negatives and false positives which lead to incorrect medical diagnosis by identifying the artifacts as pathological.

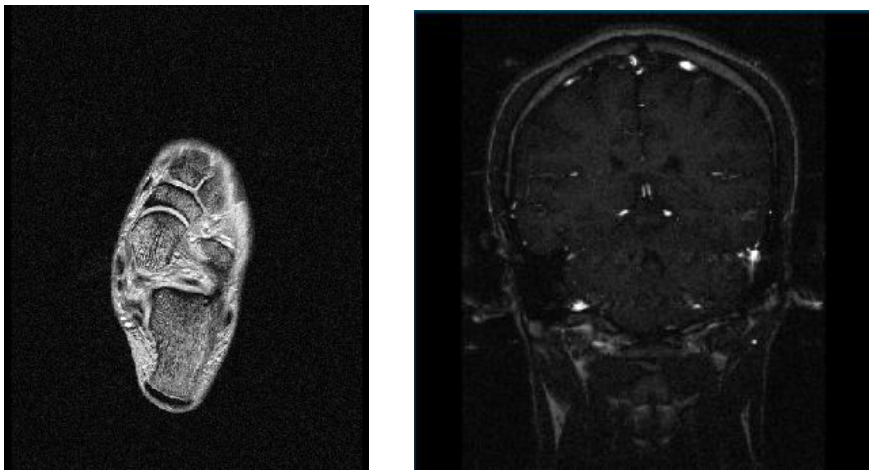

(a) Foot (b) Cranial images

Figure 2.6: Low SNR images
(Note : Parameters : NSA = 1; echo =1, TR= 100ms, Te=50ms)

An image artifact sometime is a result of improper operation of MR Scanner and other times a consequence of natural processes or properties of the human body. It is impossible to eliminate every artifact, from MR images, and new artifacts emerge regularly from new imaging techniques, such as making the reconstruction analysis a dynamic and continuous process in parallel of advancement of MR scanners.

There are dozens of image artifacts, where each has its own cause of effect. Some are obvious and easy to deal while many others are complex and require careful analysis. Classification of artifacts is by their source of origin. Some of the artifacts are listed below together with their cause, effect, removal and example. Samples of each artifact are displayed in Figure 27.

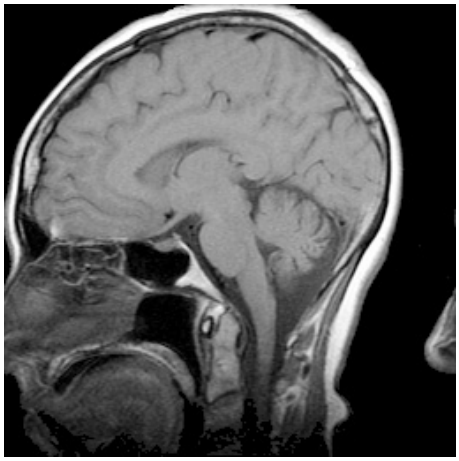

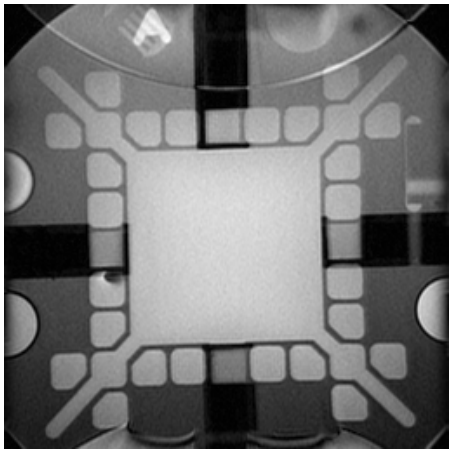

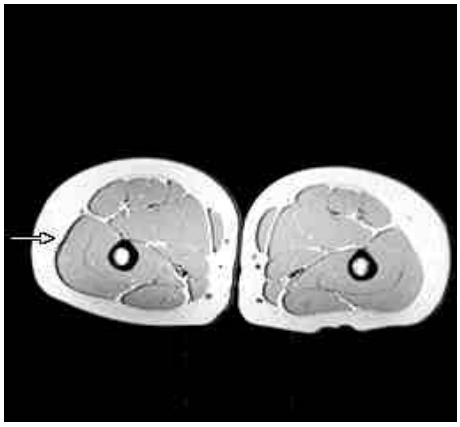

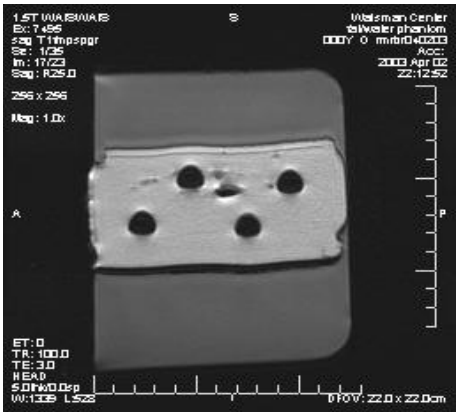

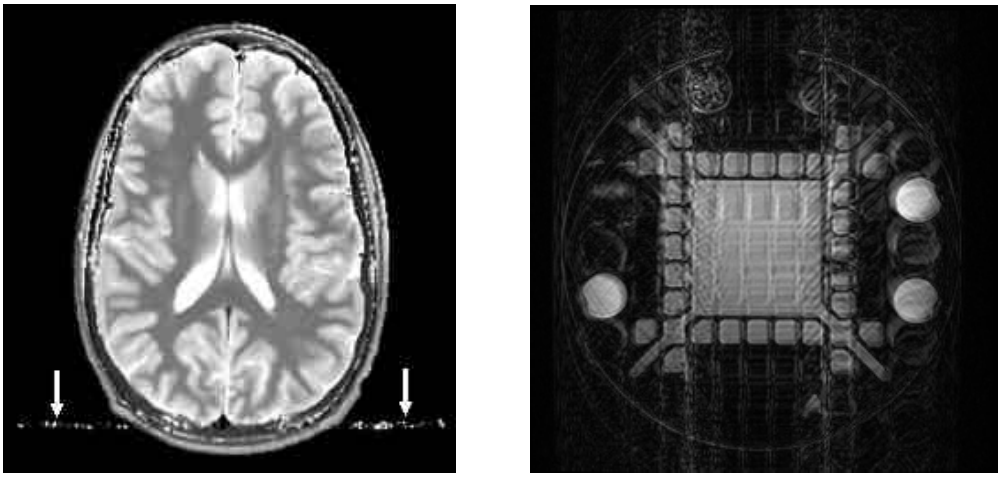

Figure 2.7: Example of MRI Artifacts

i. Aliasing or Wrap Around Artifact

A wrap around artifact is the appearance of a part of the imaged anatomy, which is located outside of the field of view, inside of the field of view. In the image of the head in Figure 2.7, the nose extends beyond the field of view on the left, and its imaged position is wrapped around and appears on the right of the image. The appearance of aliasing artifacts is dependent on how the samples are taken from a continuous signal. This happens when the MR sampling rate is lower than twice the maximum frequency of the image features. The out of field data are represented at the wrong frequency, and after Fourier transformation, end up inside Field of View (FOV). Aliasing artifacts can be prevented in the data acquisition stage by properly choosing the sampling rate or limiting the measured signal bandwidth or increase the FOV (Liang and Lauterbur, 1999).

ii. Chemical Shift Artifact

The term chemical shift refers to the shift in the resonance frequency of nuclear spins in different chemical environment. A chemical shift artifact

is caused by the difference in chemical shift (Larmor frequency) of fat and water. The artifact manifests itself as a misregistration between the fat and water pixels in an image. Chemical shift artifacts can be reduced by using a strong readout gradient or using solvent suppression techniques (Liang and Lauterbur, 1999).

iii. Motion Artifacts

Motion artifacts are presented in a variety of forms depending on the nature of the objects motion and type of acquisition system. The most problematic physiology motions are blood flow, respiratory motion, cardiac motion or movement of the patient. While other source could be hardware related such as mechanical vibration of receiver coils or gradient magnet.

Common artifacts manifest from movements are image blurring and ghost artifacts (unknown origin). There are many other types of artifacts such as Data corrupted artifacts, noisy spike artifacts, ripples artifacts, RF coils artifact etc. Each has its own cause that can be reduced by varying imaging parameter or with a good hardware design.

2.6 SUMMARY

In this chapter, basic principles of MRI such as a view from historical perspective, physics of image formation and data acquisition methods were presented. One must understand that image reconstruction algorithms vary according to the data acquisition techniques which have been presented in Section 2.4.

Important issues such as limitation in resolution, Gibbs phenomena, noises and artifacts have been presented as well. These issues are the main focus in any

image reconstruction algorithm. The main objective of any reconstruction algorithm is to minimize the noises and to produce an image which is full of useful information for clinical diagnosis.

Analysis of these reconstruction techniques is presented in the next chapter.

CHAPTER THREE

REVIEW OF MRI RECONSRUCTION TECHNIQUES

3.1 INTRODUCTION

During the data acquisition process, spatial information such as spin density, relaxation parameters and chemical shift information is encoded with free-induction decay (FID) signals from decaying neutrons. This data is called raw data. It is a time-domain data. Depending on how spatial information is encoded, the image reconstruction technique varies. Practical acquisition technique as discussed in Chapter 2, leads to two general acquisition types, i.e. rectilinear or radial. Cartesian grid acquisitions such as Echo Planar Imaging (EPI) are rectilinear acquisitions; while spiral, radial and 'rose' acquisition techniques, are radial types.

Data acquired in Cartesian grid are uniformly sampled and their corresponding reconstruction is simply by applying direct 2D DFT. Data acquired from radial samples are not uniform and their reconstruction varies according to the type of acquisition. Techniques for both types are reviewed and presented in this chapter.

Generally image reconstruction is solving mathematical equation created by data acquisition. It is a dynamic field which evolves from time to time since the discovery of MRI Scanners. Motivation for this is to comply with new hardware inventions and to produce better quality images in short period of time. The first reconstruction algorithm proposed was Iterative Backprojection (IBP) by P.C. Lauterbur (Kumar et al,1975 ; EMRF,2003) or also known as *zeugmatogram*. Images of bottle were demonstrated in 1973 using IBP, followed by image of clam and thoracic image of rat in 1974 (EMRF, 2003). In 1975, Fourier imaging technique was

proposed by Kumar (Kumar et al,1975) which became the basic of MR Imaging today. This method is cheap, computational less complex, reliable and fast compared to the earlier reconstruction method, iterative back projection reconstruction.

Consequently, following this success, more reconstruction algorithm were proposed and analyzed by reducing noises and removing artifacts to produce clearer images. Improvements to Fourier imaging were proposed (Wood and Henkelman, 1985; Gottlieb et al,1992) while other attempts were made to introduce new algorithms such as Least Square Method (Barrowdale and Erickson,1980), Autoregressive methods (Yang and Smith, 1996), Singular Value Decomposition methods and Autoregressive Moving Average methods (Smith, 1992). Generally, the reconstruction algorithms fall in two categories: non-parametric techniques and parametric techniques.

In this chapter, technical details of non-parametric techniques and parametric technique algorithms are presented. In non-parametric technique, FFT Reconstruction is discussed in more depth compared to other technique as FFT is method of choice for current MRI Scanner. After discussing Parametric Technique, limitation of those techniques is examined and presented at the end of this chapter.

3.2 NON PARAMETRIC TECHNIQUES

3.2.1 Projection (Radon Transform) Techniques

Projection reconstruction is also known as Radon Transform Reconstruction (RTR). RTR which is based on projection acquisition, was the fist MRI k-space trajectory proposed by P.C. Lauterbur in 1973 (Liang and Lauterbur, 1999). The projection acquisition fills in k-space data with radial spokes, where analysis of projection data can be done on radon coordinates (polar coordinates) or equivalent normal Cartesian

coordinates as shown in Figure 3.1 (Liang and Lauterbur, 1999). If P(r,**μ)** denotes the measured projection in polar coordinates , a general polar reconstruction equation is described as (Liang and Lauterbur, 1999):

$$P(r,\boldsymbol{\mu}) = R\{I\} = \int_{R^n} I(\mathbf{r})\delta(p - \boldsymbol{\mu}.\mathbf{r})\, dr \qquad (3.1)$$

where,

$P(r,\boldsymbol{\mu})$ is measured data on a polar coordinate system

$\boldsymbol{\mu}=(\cos\phi,\sin\phi)$

$r=(x,y)$

$dr = dxdy$

δ is the unit impulse

$I(r)$ is the desired image function.

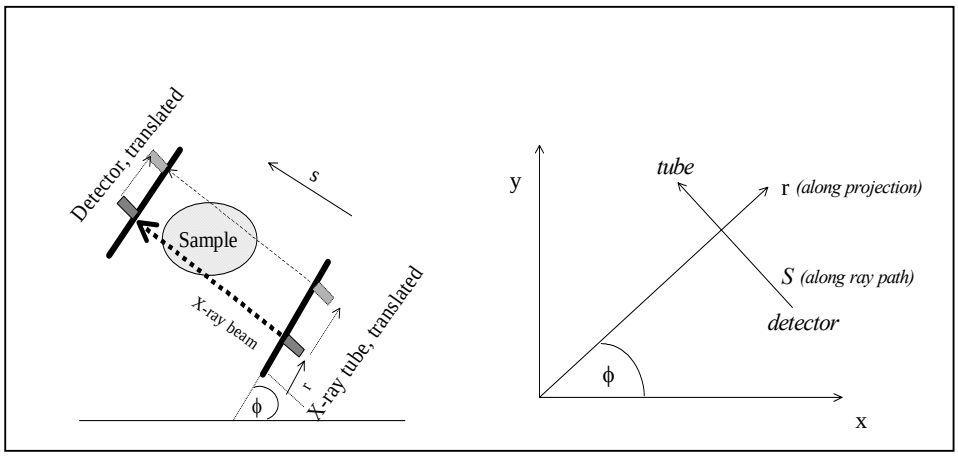

Figure 3.1: Coordinate Position for Projection Technique

As equation 3.1 shows, for data directly sampled from Radon projection space, image $I(\mathbf{r})$ can be determined by simply applying inverse Radon transform on

measured $P(r,\boldsymbol{\mu})$ data. But practically applying direct integration on $P(r,\boldsymbol{\mu})$ is not possible.

Several reconstruction algorithms are available to solve for $I(\boldsymbol{r})$, such as Algebraic Reconstruction (AR), Direct Backprojection Reconstruction (DBR), Filter Backprojection Reconstruction (FBR) and Gridding Reconstruction (GR), to name few popular computational practical methods. The mathematical foundation for backprojection reconstruction is provided by the Radon transform which computes 1-D projections of a 2-D data at different view angles.

3.2.1.1 Direct Backprojection Reconstruction (DBR)

DBR is the simplest method used to compute the inverse Radon formula by utilizing backward technique. This technique uses a backprojection operator, ß which is defined as (Liang and Lauterbur, 1999; Bernstein et al, 2004):

$$ß\{ P(r,\boldsymbol{\mu}) \} = P(\boldsymbol{\mu}.\boldsymbol{r}, \boldsymbol{\mu}) \quad (3.2)$$

In 2D Cartesian coordinate, $ß$ can be rewritten as

$$ß\{ P(r,\boldsymbol{\mu}) \} = P(x\cos\phi + y\sin\phi, \phi) \quad (3.3)$$

which, leads to the general reconstruction formula:

$$I(r) = \int_{|\mu|=1} ß\{ P(r,\boldsymbol{\mu}) \, d\boldsymbol{\mu} \quad (3.4)$$

From equation. 3.3 and equation 3.4, backprojection reconstruction formula for 2D Cartesian coordinate is given by:

$$I(x,y) = \frac{1}{2}\int_{0}^{2\Pi} P(x\cos\phi + y\sin\phi) d\phi \quad (3.5)$$

Practically, projection measurements are discrete both angularly and radially. Therefore equation 3.5 is implemented in discrete form. Also for 2 D discrete points, *P(r, ϕ)* is available for following points:

$$r = n_p \Delta p \qquad \mathrm{n_p} = -\frac{N_p}{2} \ \ldots\ , \ \frac{N_p}{2} \ \text{-1}$$

$$\phi = n_\phi \Delta\phi \qquad n_\phi = 0,1,\cdots \mathrm{N}_\phi - 1$$

Then, the image data *I (x, y)* can be expressed as:

$$I(x,y) = \Delta_\phi \sum_{\mathrm{n}_\phi}^{\mathrm{N}\phi\text{-}1} \mathrm{P}(\mathrm{r_n}, n_\phi \Delta\phi) \tag{3.6}$$

where $r_n = x\cos(n_\phi \Delta\phi) + y\cos(n_\phi \Delta\phi)$. As r_n may not exactly fall on the sampling points along *r*-axis; it is necessary to perform signal interpolation along *r*-axis. Again, there are varieties of signal interpolation algorithms ranging from direct methods (such as nearest-neighbor algorithm) to higher order algorithms.

Basically due to low SNR ratio of projection technique, DBR method produces low resolution images (Liang and Lauterbur, 1999). To overcome this low resolution issue in DBR, improvements such as Filtered Backprojection Reconstruction (FBR) were proposed.

3.2.1.2 Filtered Backprojection Reconstruction (FBR)

Similar to the previous algorithm, FBR is also a method which directly implements the inverse Radon formula using backward technique. But in FBR, data are filtered before back projected to reconstruct the image.

Generally, FBR formula is expressed as:

$$I(r) = \int_{|\mu|} B\{\overline{P}(r,\mu)\}d\mu \tag{3.7}$$

For Cartesian data, FBR has the following reconstruction formula (Liang and Lauterbur, 1999):

$$I(x,y) = \int_{0}^{\pi} B_2\{\overline{P}(p,\phi)\}d\phi \tag{3.8}$$

where $\overline{P}(p,\phi)$ is the measured projection data, given by :

$$\overline{P}(p,\phi) = \int_{-\infty}^{\infty} S_p(k,\phi)|k|e^{i2\pi kp}dk$$

Finally, the 2D Cartesian filtered data $\overline{P}(p,\mu)$ is obtained by applying a 1 D filter, *H(k):*

$$\overline{P}(p,\mu) = F_k^{-1}\{S_p\{k,\mu)H(k)\} \tag{3.9}$$

There are many filters choices available for *H(k)* such as Ramp filter, Ram-Lak Filter, Shepp-Logan Filter , Low-Pass-Cosine Filter and Generalized Hamming Filter.

Although FFT technique supersedes Projection techniques for image reconstruction in MRI, the study of FBP is still active. Some MRI Scanners such as Philips® 1.5T Intera do provide FBP as an optional reconstruction method. This technique is largely employed for image reconstructions in CT Scanners.

Currently, there are few new improvements suggested for FBP, such as parallel geometry FBP and their performance has been studied in detail (Pispatsrisawat et al, 2005). Fast Hierarchical Backprojection method (Basu and Bresler, 2000) is another technique which uses FBR and had shown remarkable

improvement by achieving the same 'cost' of performance as Fourier Transforms but this method is targeted for CT Scanners.

Although, improvements can be made for MRI data set, practically, data acquisition system puts a limitation on its usage. Modern MRI Scanners are focusing on improving imaging speed by applying parallel beams for data acquisition and each beam are treated separately to produce multiple images at the same time. Design for projection system hardly achieves these parallel imaging techniques.

3.2.2 FOURIER TECHNIQUE

3.2.2.1 General Fourier Signal Equation

Fourier Transform (FT) algorithm has wide application in science and engineering, such as in bio-medicine, telecommunication signal processing and spectrum analysis. Other than application in MRI, it is also implemented in other areas such as CT scanner, Ocean imaging, Aerospace imaging and currently in digital imaging.

Problem of reconstruction from Fourier transforms of a phase encoded data can be formulated as below (Liang and Lauterbur, 1999):

$$\text{Given} \qquad S(k_n) = \int I(r) e^{-i2\pi k_n \cdot r} dr \quad \text{, determine } I(r) \tag{3.10}$$

Where $S(k_n)$ is the measured k-space signal and reconstruction is the process of finding the desired image function *I(r)* for $k_n \in D$ in which *D* contains the set of k-space points.

It is widely known that DFT is the natural computational tool used for any image reconstruction. As the image data is a 2D data, equation. 3.10 can be written as

$$S(p_n, q_n) = \int_{-\infty}^{\infty} \int_{-\infty}^{\infty} I(x, y) e^{-i2\pi p x} e^{-i2\pi q y} dxdy \tag{3.11}$$

It is assumed that k-space is uniformly sampled such that

$$p_n = n\Delta p, n = ...-3,-2,-1,0,1,2,3....$$
$$q_n = n\Delta q, n = ...-3,-2,-1,0,1,2,3... \quad (3.12)$$

Equation 3.11 can be carried out as two sequences of 1D Fourier Transform, by performing a 1D Fourier transform on x-axis followed by another 1D Fourier transform on y-axis.

$$S(p_n, q_n) = \int_{-\infty}^{\infty}\left[\int_{-\infty}^{\infty} I(x,y)e^{-i2\pi px}\mathrm{dx}\right]e^{-i2\pi qy}dy \quad (3.13)$$

To formulate an exact reconstruction equation, there are two factors which need to be considered from equation 3.13. The first factor is that the equation is defined for an infinite sampling while practically the data is acquired on finite sampling. The second factor is the data is sampled at evenly spaced internals in time as shown in equation. 3.12 or in another word, the data is *discrete*.

Considering equation 3.13 for 1D Fourier transform, for sampling interval of $t_n = n\Delta t, n = ...-2,-1,0,1,2...$ the integration over infinite samples can be approximated by discrete sum (Liang and Lauterbur, 1999 ; Press et al, 1992) :

$$\sum_{-\infty}^{\infty} S[n]e^{i2\pi n\Delta tx} = \frac{1}{\Delta t}\sum_{n=-\infty}^{\infty} I\left(x - \frac{n}{\Delta t}\right) \quad (3.14)$$

By defining a FOV, W_x to eliminate any periodic replicas, (Liang and Lauterbur,19999) formula for image function on infinite sampling can be rewritten by taking the inverse Discrete Fourier transform:

$$I(x) = \Delta t\sum_{n=-\infty}^{\infty} S[n]e^{i2\pi n\Delta tx}, \ |t| < \frac{1}{\Delta t} \quad (3.15)$$

And by considering the discrete data of *D*,

$$D = \{n\Delta t, \frac{-N}{2} < n < \frac{N}{2})$$

where N is the total number of data , the image function can be concluded as :

$$I(x) = \Delta t \sum_{n=-N/2}^{N/2-1} S[n] e^{i2\pi n\Delta t x} \quad , \ |x| < \frac{1}{\Delta t} \tag{3.16}$$

Since $I(x)$ is frequency band limited function due to finite sampling, equation. 3.16 must satisfy Nyquist criterion to avoid the loss of image information. Nyquist criterion states $I(x)$ can be uniquely recovered as long as $\Delta t \le 1/N\Delta t$. Therefore, the largest acceptable pixel size for $I(x)$ is $\Delta t = 1/N\Delta t$, which is called Fourier Pixel Size. Substitute $\Delta t = 1/N\Delta t$ in equation. 3.16 and treating $\Delta t = 1$, the Direct Discrete Fourier Transform Reconstruction formula is expressed as:

$$I[m] = \sum_{n=-N/2}^{N/2-1} S[n] e^{i2\pi nm/N} \qquad -N/2 \le m < N/2 \tag{3.17}$$

3.2.2.2 Direct FFT Reconstruction (DFR)

The MRI data is complex-valued data and defined for a finite sequence as $d_n = 0,1,2,.....N-1$. Discrete Fourier transform of this complex data is described by

$$D_m = \sum_{n=0}^{N-1} d_n e^{-i2\pi mn/N} \qquad for \ \ m = 0,1,...N-1 \tag{3.18}$$

By denoting the raw data as D_m, the image data, d_n can be recovered using inverse discrete Fourier transform as in equation 3.16:

$$d_n = \frac{1}{N}\sum_{n=0}^{N-1} D_m e^{i2\pi mn/N} \quad for \ \text{n} = 0,1,...N-1 \tag{3.19}$$

Direct evaluation of the Discrete Fourier Transform (DFT) is time consuming and computationally expensive. Practically, DFT is computed using Fast Fourier Transform (FFT) algorithm which reduces the number of computations needed for N points from $2N^2$ to $2N \lg N$. There are few approaches in applying FFT, but the most common choice is Cooley and Tukey Algorithm ([Press et al, 1992). Matlab® 'fft' command utilizes this algorithm. Using '*fft*' or '*fft2'* can be used directly on re-arranged raw data to produce reconstructed image.

Standard FFT algorithms such as Cooley and Tukey algorithm are implemented as in equation 3.19. Using such routine to evaluate MRI Fourier Reconstruction Formula as in equation. 3.17, some pre and post processing of data is necessary.

3.2.2.3 Implementation

Figure 3.2 shows flow chart on how DFR algorithm is applied in this thesis. Raw data are stored in a binary file which is read using a Converter programme. Data format and data converter programmes are discussed more detail in Chapter 5. Basically, the function of a converter programme is to read the binary hexadecimal data ordered in IEEE Single Precision Byte format and re-arrange into Matlab®'s 2D image matrix i.e. *I(m.n).* Each *I(m,n)* represent a single pixel which denotes intensity of signal in greyscale. The horizontal pixel location indexed from left to right by integer , *n* and the vertical locations indexed from top to bottom by integer , *m* .

Normally, the complex-valued frequency signal (raw data) is truncated in one direction to reduce acquisition time. Data truncated is performed to reduce scanning time or to fit the biggest possible FOV to avoid aliasing effects.

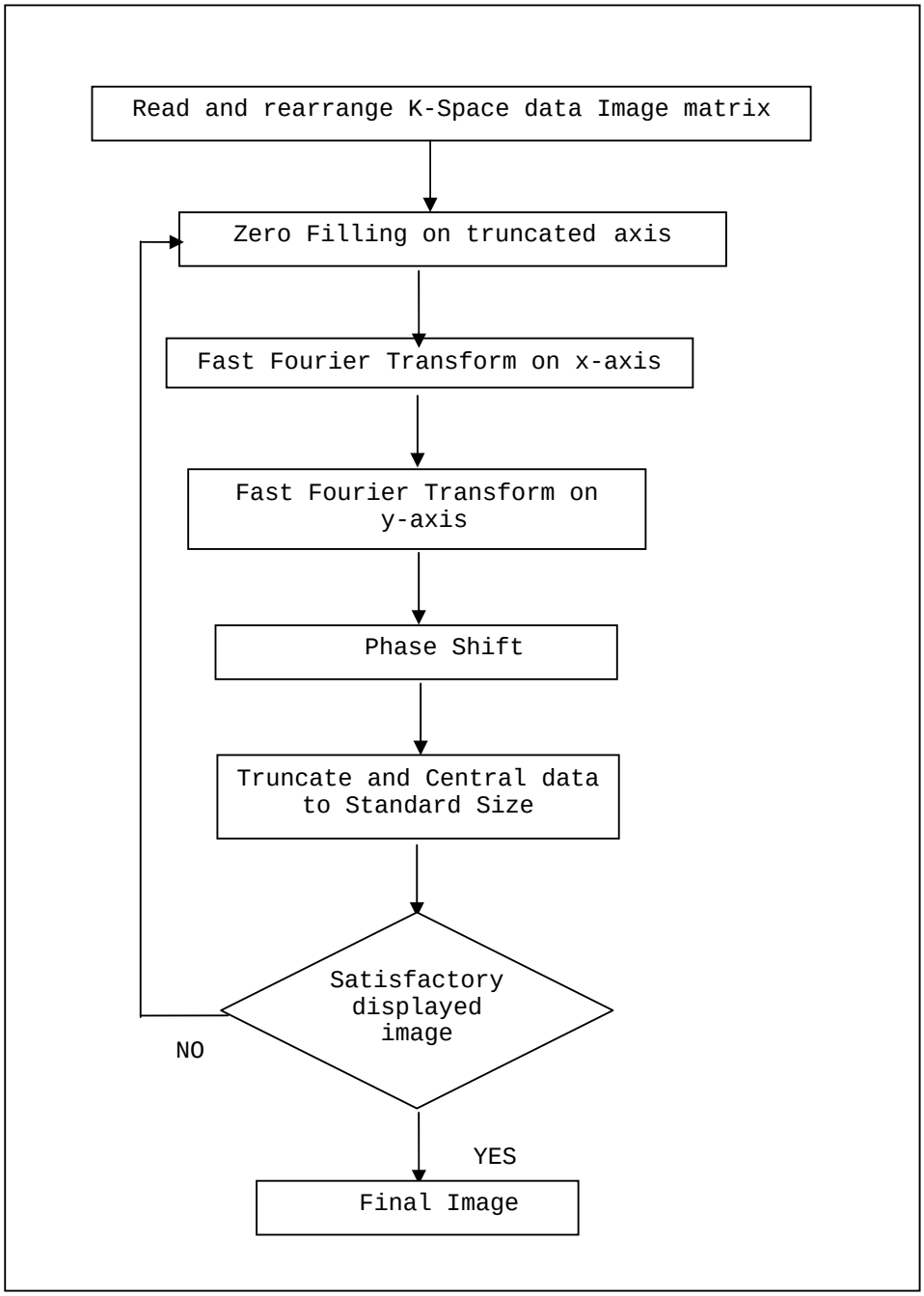

Figure 3.2 : Flow Chart of FFT Algorithm

Truncated axis might not have number of data samples which is equals to integer power of 2. When N is not in integer power of 2, radix-2 FFT algorithm cannot be used efficiently (Press et al, 1992). This truncated data axis can be padded with zeros (zero padding) to achieve N^2. Zero padding produces no artifacts and has no effect on SNR, in some cases it improves appearance of images (Liang and Lauterbur, 1999; Bernstein et al, 2004).The only drawback is increased reconstruction time, and can increase the appearance of truncation artifacts although zero filling itself does not contribute to any artifacts. On the positive site, apart from completing N^2, zero padding also can be used for increasing digital resolution and for zooming. It is customary to centre the data in the 2D view. As the image will placed in the centre, zero fillings are done symmetrically

In Matlab® FFT algorithm is implemented using a built-in function '*fft*' or '*fft2*' which utilizes the Cooley-Tukey algorithm. The execution time for '*fft'* depends on the length of the transform. It is fastest for powers of two. Function (subroutine) '*fft2*' works by performing a 1D *'fft'* on x axis and followed by another *fft* on y-axis.

The FFT algorithm as in equation 3.19 describes when a sequence of numbers, $D_0, D_1, D_2, D_3 \ldots\ldots D_{N-1}$ is an input to FFT, the algorithm assumes the zero time point, k_x, k_y = 0, is the initial point D_0. The zero and positive spatial frequency values are assumed to be $D_0, D_1, \ldots\ldots D_{N/2-1}$ while negative spatial frequency values $D_{N/2}, D_{N/2+1}, D_{N/2+2}, \ldots\ldots D_{N-1}$.

But MRI data are not acquired in the same input order expected by FFT routine. The data is measured in a single readout of a full echo and are ordered from negative to positive values with zero-point k_x, k_y = 0 falling in the middle. When MRI

raw data is feed into FFT routine, the raw data must be or-ordered before feeding or the output data array should be reordered accordingly. This is known as phase-shift

The common approach is to apply phase shift after FFT routine. Phase shift in Matlab® is implemented using *'fftshift'* which rearrange the outputs of *fft, fft2*, by moving the zero-frequency component to the centre of the array. Mathematically, phase shift is sign alternation before and after FFT of each pixel (Liang and Lauterbur, 1999; Bernstein, 2004).

MRI data is also over sampled to remove fold over (aliasing) and to achieve a flatter filter response. To eliminate the over sampled data, the image data is truncated after FFT routine. As the data is accumulated in the centre, the desired new image size can be obtained from copying the data in the centre of the image view.

This algorithm is applied on downloaded data (see Chapter 5) and images as in Figure 3.3 are produced. These images are further evaluated in Chapter 6.

Basically, FFT is a basic reconstruction technique which requires filtering and scaling. Filtering is performed to enhance low contrast, remove Gibbs phenomena or any artifacts that might occur in an FFT image. An ideal filter is not possible but range of filter selections are applied on FFT images based on the imaging sequence. Different filters are used for different anatomical section. Filters for cranial imaging might be different from filter for an angiography or thorax sequence as the later involves moving particles such as blood flow and movement of heart, hence produce movement artifacts as sign of mobility.

While, the brain sequence might need a medium filter as too many electrical activities occur in brain. On top of filter, additional algorithm such edge detection algorithm also may be needed to identify edge of images as some sequences such as

gastrointestinal and cardiac imaging will display thickening of edges due to movement.

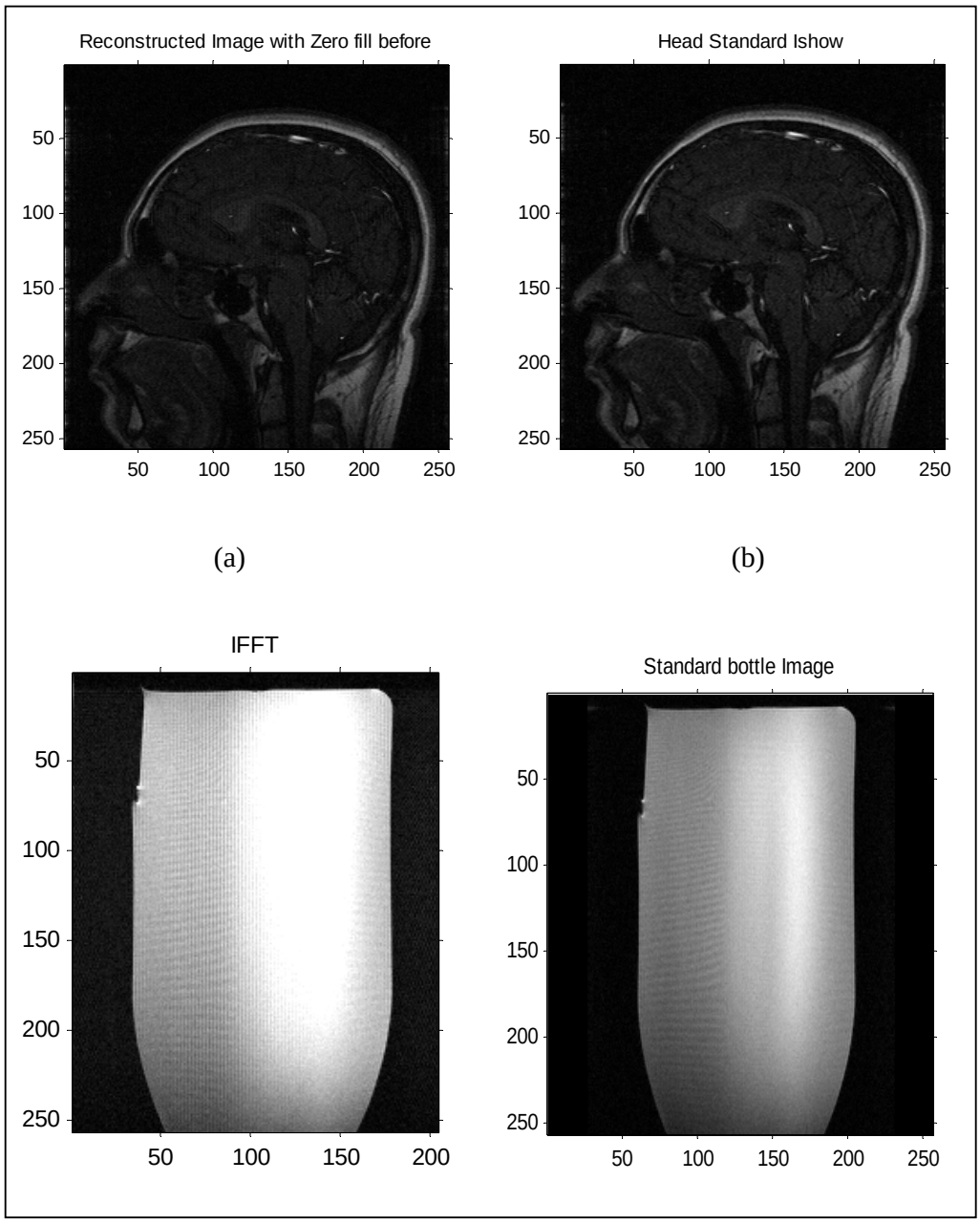

(a) (b)

(c) (d)

Figure 3.3: Images reconstruction using 2D FFT Algorithm

Note: (a) Cross Section of human cranial reconstructed using 2D FFT
(b) Cross Section of human cranial (Standard Image)
(c) Cross section of phantom image, reconstructed using 2D FFT
(d) Cross section of phantom image (Standard Image)

Generally, FFT reconstruction method is the preferred technique compared to other techniques. Easy hardware implementation, easy and fast computational is the motivating factors. Shortcomings of this method have been presented in Section 1.2.2 and have been explored in detail in Section 2.5. Close examination of reconstructed bottle image shows stripy appearances vertically which are not part of actual image. Such reconstruction using FFT needs further process such as edge detection algorithm or windowing to produce better images.

Windowed FFT reconstruction with edge detection algorithm is not applied in this thesis as it is not the objective of this thesis.

3.2.3 Gridding Reconstructions (GR)

The DBR and FBR are transform based techniques which utilize property of inverse Radon to obtain the image data. However, it is possible to use direct FFT methods on radial projection data by interpolating (resampling) the acquired Radon data to Cartesian data. This technique is called Gridding Reconstruction. GR is method of choice compared to FBR. It provides more accurate image data and computationally effective and inexpensive compared to FBR.

Problem of resampling the discrete radon data set (projection data) were studied extensively and many methods were developed (Bernstein et al, 2004). A straightforward interpolation results in high level of artifacts, while application of a sophisticated interpolation leads to computational complex algorithms.

A convolution based method is widely used for resampling. This technique uses a convolution in k-space to convert the input data to a uniform Cartesian data. It gives high accuracy of interpolation and processing time compared to other methods. The natural choice of convolution function is to convolve the k-space data with a

SINC function as stated by Sampling Theorem (*k-space value at any location can be calculated exactly by SINC interpolation of the measured value*) as demonstrated by O'Sulivan (Jackson et al, 1991). Practically, convolving the SINC function with projection data at every point requires long computational time therefore, the SINC function is replaced with a grid kernel, or also known as convolution function (Beatty et al, 2005, Bernstein et al,2004).

Many works have been done to determine the optimal grid kernel such as zero-order Prolate Spherical Wave Function (PSWF), Two-term cosine, three term cosine, Gaussian Kernel and Kaiser-Bessel function. Kaiser-Bessel function gives nearly optimal results in the sense that the final image is closest to the ideal image using parameters such as least-squares differences with efficient computational time. (Jackson et al, 1991).

Generally GR algorithms can be divided into 3 main steps: the convolution, direct 2D FFT and De-apodization.

Before convolution, the discrete data is multiplied by a Density Compensation Function (DCF). DCF is performed as the data is not uniform around the k-space data. Convolution as explained earlier is data after DCF is convolved with gridding kernel. This followed by FFT and finally the resultant data goes through de-apodization where the result of FFT is divided by an ideal de-apodization function. De-apodization is to remove the apodization effect which was introduction as additional smoothness at discontinuation points during convolution. Apodization introduces artifacts at the edge of FOV. The ideal apodization function would be a rectangular function.

Practical approach is the image data (FFT data) is divided by Fourier transform of the convolution function. (Beatty et al, 2005; Bernstein,2004; Schomberg and Timmer, 1995).

If S*(u,v)* is denoted as non-Cartesian sampling function, *M(u,v)* is the data function of proton density signal *m(x,y)* , III(u,v) as comb function ,

$$M(u,v) = \int_{-\infty}^{\infty} \mathrm{m(x,y)}\, \mathrm{e}^{[-2\pi i(ux+vy)}\, dxdy \tag{3.20}$$

The *S(u,v)* consists of P two dimensional delta function at positions u_j, v_j :

$$S(u,v) = \sum_{j=1}^{P} {}^{2}\delta(u - u_j, v - v_j) \tag{3.21}$$

The sampled data is then given by:

$$M_s(u,v) = M(u,v).S(u,v) \tag{3.22}$$

Gridding is the sampled data convolved with a grid kernel or convolution function, *C(u,v)*.

$$M_{SCS}(u,v) = [M_s(u,v) * C(u,v)].III(u,v) \tag{3.23}$$

where the comb function , *III* is defined

$$III(u,v) = \sum_i \sum_j {}^{2}\delta(u - i, v - j) \tag{3.24}$$

The final image *I(x,y)* is the Fourier transform of equation. 3.23. This is followed by a deapodization function to remove shading effect. The entire process is shown in Figure 3.4

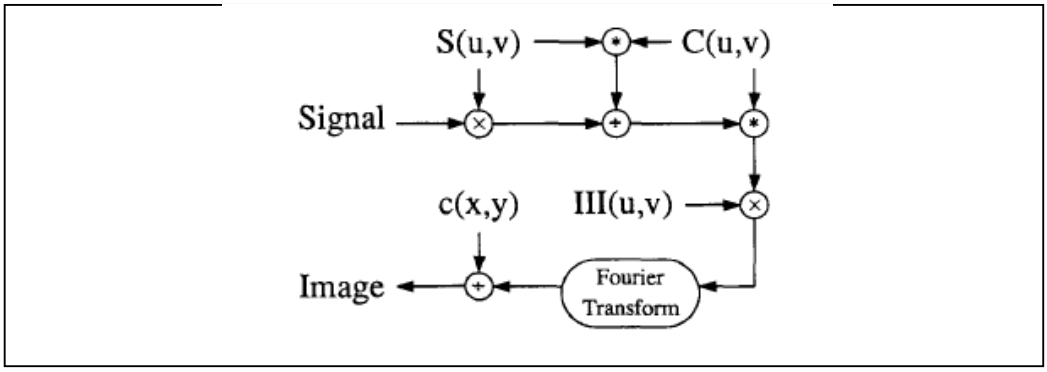

Figure 3.4: Flow Chart of Gridding Reconstruction

3.3 PARAMETRIC TECHNIQUES

The techniques described earlier are classical methods started with the invention of MRI. Few assumptions are made regarding the origin of data such as data are assumed to be infinite. The waveforms (signals) outside of the data windows, FOV are assumed to be zero. A more efficient way is to predict prior information of input process and use this parameter to model the output data. This is known as parametric technique; the prior data prediction is an attempt to eliminate need for filtering or windowing in conventional techniques.

Parametric methods make use of linear process or models to estimate the data sequence. Models are assumed to be driven by white noise. The output of this model is compared with the input waveform and the model parameters adjusted for the best match between model output and the wave form of interest. After the best match has been obtained, the model frequency characteristic provides the best estimate of the waveform spectrum from given constraints. This can be used to solve the spectrum analysis.

Different model types are used in this approach. They are differentiated by the nature of their transfer function. Three popular model types are autoregressive (AR),

moving average (MA) and autoregressive moving average (ARMA). These models are also known as all-pole (AR), all-zero (MA) or pole-zero (ARMA).

The model selection requires some knowledge about shape of spectrum that MRI Data exhibits (Semmlow, 2004). Research and studies has been done to implement AR and 1D ARMA model and proven to produce better image then Fourier Reconstruction. The nature of MA model is such that it cannot model well narrow banded spectrum such as MRI data which makes it not a high-resolution spectral estimator. This shortcoming limits its usefulness in bio-signals.

The input signal, *u(n)* and output signal, *y(n)* of AR and ARMA models can be described respectively by equations 3.25 and 2.26:

$$y(n) + \sum_{k=1}^{p} a(k)y(n-k) + u(n) = b(k)u(k) \qquad (3.25)$$

$$y(n) + \sum_{k=1}^{p} a(k)y(n-k) = \sum_{k=1}^{q} b(k)u(n-k) \qquad (3.26)$$

where *a(k)* represents the AR coefficients and *b(k)* represents the MA coefficients, while *p* and *q* represent the model order of AR and MA respectively.

Typically both AR and ARMA are IIR filters. From equations 3.25 and 3.26, obviously estimating the unknown model orders (*p* and *q*) is first step towards parametric estimation. . One way to determine the model orders is to plot the residual error or prediction error variance E_f, against model order. When E_f exhibits a sharp decline, the correct model is attained. Other schemes in estimating the model order are Likelihood Ratio Test (LRT), Final Prediction Error (FPE), Minimum Description Length (MDL), Eigenvalues of Covariance Matrix, Singular Value Approaches (SVD)

etc. A random search on IEEE Xplore for model order simply returns an enormous return of 987 research papers on this problem. Generally, model order determination techniques are mostly based on FPE, AIC or MDL, where these techniques are modified to suit the application of interest. .

Basically, the objective is to estimate appropriate value for model orders (p and q) as the model orders have significant role in modeling. It determines the number of parameters to be estimated, and hence the computational complexity of the algorithm. Fitting the data is more to a 'recursive' algorithm, where p and q are computed first , by using this estimated p and q, parameters, a and b are estimated under the more recursive it is, the more 'expensive' the computation is.

Another effect is that the model orders affect the quality of the spectrum. If a lower model is estimated, the resulting spectrum will be smooth and displays poor resolution while the noises will be suppressed totally (Davila and Chiang, 1995). While using a high model will over fit the data and generate spikes in reconstructed images. Over fitting data leads to a spectrum with spurious peaks (or spikes). Both over fitting and under fitting is not desirable while estimating model orders. The maximum value for p is suggested to be N/2 while it is suggested p is to be chosen in the order of N/2 (Liang and Lauterbur, 1999). While q depends on algorithm used to solve the ARMA equation.

Once the model orders p and q are obtained, AR and MA parameters are estimated through various algorithms. To name few algorithms available to estimate AR parameters are: the Yule-Walker, the Burg, Marple's Least square Algorithm, the Covariance, the modified covariance method, SVD method , Barrowdalle Method, etc.

Solving for ARMA is more complex. As ARMA consists of AR and MA filters, some algorithm attempts to solve them separately. AR parameters are

estimated and the results from AR parameter are used to estimate MA parameters. This is known as suboptimal method while optimal methods are more complex with attempt to solve both AR and MA filter at same time. Maximum Likehood Method (MLM) is one of complex optimal methods which have been proved not beneficial when applied to MRI data. Optimal methods also are computationally complex and expensive.

M.R. Smith proposed a solution for ARMA method using Transient Reconstruction Approach (Yang and Smith, 1996; Smith et al, 1986). Smith applied FFT on data rows while on column data; he applied TERA algorithm. This produces a significant positive result, except lengthy reconstruction time. Other approaches would be Improved Cadzow Method (Salami, 1983). Although Improved Cadzow Method produces good estimates of ARMA parameters, it often requires a too high AR model order before desirable results are obtained. Furthermore, computing MA parameters is also complicated (Nichols et al ,1985). This leads to complexity in computation which is not computationally cheap (time constraints).

Parametric techniques which have been investigated for MRI reconstruction are AR model, ARMA model and AR model with SVD estimation. Comparing AR model and ARMA model, the later provides better result when reconstructed using TERA approach. While the Burg Method is proved to be not suitable due to nature of its algorithm that forward and backward prediction which gives incorrect amplitude and closer to the unit cycle which produce high spikes in reconstructed images. (Smith, et al,1986).

Smith et al estimate AR Model by using Modified AR Transient Error Method, which estimates the Fourier transform of the signals (Smith et al, 1986). This method is proved to reduce both noises and truncation artifacts. Anyhow, the best result was

obtained by applying on rows of MRI data, while TERA approach is applied on column data. Each column is treated separately. The algorithms are summarized in following steps :

1 By assuming the column data is a subset of Kronecker Delta function , each column is split into Hermitian and anti Hermitian component. Series to account for data symmetry.

2 Each Series in then modeled as output of IIR . AR and MA portion is estimated separately. Model orders are determined by using FPE utilizing E_f. AR parameters are estimated from Barrowdale and Erickson combined with Cholesk's method . Upon determination of AR parameters, MA coefficients are determined (assuming MA coefficient = input error sequence)

3 Finally data sequence is estimated from Step 2.

This algorithm will be explored in detail in Chapter 4, while presenting the 2D ARMA. Another attempt of parametric estimation is using SVD to estimate AR parameters. Although studies proves and exhibits the advantage of using ARMA method, practically it is not been applied in any practical algorithms.

3.4 EXTRAPOLATION RECONSTRUCTION

Extrapolation Reconstruction is proposed to replace FT when usage of FT is not desirable especially when the data is low. The goal of data extrapolation is to use appropriate constraints to recover some of unmeasured high frequency components on that the MRI data , *S[n]* New algorithms have been proposed , which are defined for a bigger frequency range. With this new range, image function is often reconstructed with Fourier Method.

Two popular constraints are been studied: the finite spatial support and the maximum entropy constraints which lead to Band limited Extrapolation Reconstruction and Maximum Entropy Reconstruction. Maximum Entropy is widely used in various areas of science and engineering. Lately, this methods are been considered for speech analysis and reconstruction. Usage of Maximum Entropy has been studied extensively, but its usefulness is not well established. And its suitability on MR image data is doubtful (Liang and Lauterbur, 1999).

3.5 EVALUATION OF MRI RECONSTRUCTION TECHNIQUES

Generally, as we discussed above, we can categorize the reconstruction techniques into 4 categories, namely, Backprojection Reconstruction, Fourier Transform Reconstruction, Parametric Reconstruction and Extrapolation Based Reconstruction. Application wise, only Fourier reconstruction has been implemented while Backprojection reconstruction is no longer applied in MRI. In case of Parametric Reconstruction, very few studies are conducted to denote their clinical usage in comparison to FR .The reconstruction time is the bottleneck of their usage.

While the Extrapolation Based Reconstruction is time consuming and although represent the data, but not in-consistent with the data. There is high possibility for important low frequency signals such as a tumour signal would be averaged away.

In some imaging sequences, backprojection acquisition has proved to produce better images. In recent studies attempts are made to directly implement BR taking the advantage of modern processor speed. By using high end computing facilities , T. Pipatsriswat and his colleagues from Carnegie Mellon University, Pittsburg, USA (Pispatsrisawat et al, 2005) proves that Hierarchical Backprojection Method (HBR) could produce results in same ‘cost’ of FFT methods while attaining the advantages

of FBP method. But successful implementation of this technique also depends on parametric choice. Furthermore, due to its practical limitations, HBP is not employed by MRI Manufacturer.

In case of non-Cartesian acquisition, Gridding Reconstruction is the method of choice. Gridding means to interpolate the acquired radial data to Cartesian k-space data where FT can be applied directly without any hassle. Accuracy of estimating a gridding kernel is the key point to successful implementation of gridding. Gridding could be simple and robust and has parameters which are the grid over sampling ratio and the kernel width. Typical or conventional grid over sampling ratio is two, but lately J. M. Pauly proves high accuracy result with reduction in computing time can be achieved by using a ratio is between 1.125 to 1.375 (Beatty et al, 2005). Kaisser-Bessel convolution kernel is optimized for this range and 3D reconstruction was exhibited.

Entropy reconstruction also leads to FT Reconstruction. Although there are many studies on usage of wavelet reconstruction and neural network approach, practically all these methods were not found suitable when clinically tested. These new techniques fail gracefully due to medico-legal reasons. Although these new techniques (wavelet, maximum entropy, neural network) provide image consists with the data acquired, but not necessarily representative of data and this leads to mis-interpretation of images. This is clear indicative of failure.

Considering this fact, and as Backward Reconstruction is being replaced by Gridding which is based on Fourier Transform, the techniques are now streamed down to two comparative methods: the Fourier transforms and Parametric Method

As mentioned earlier, Fourier transform is been the method of choice for more then 20 years since it is introduced by Ernst and Kumar in 1973. Advantages of

Fourier transform is mainly because of speed and hardware simplicity. The algorithm, acquisition techniques, pre-processing and post processing is fast compared to other method. Fourier transform applied through FFT algorithm is fast, reliable and simple. The acquisition technique for FT is also fast and easily implemented while wide range of post-processing techniques suited well the output of Fourier Transform. In parallel imaging, Fourier Transform is used to reconstruct 1200 (256 X 256) images by using parallel acquisition and pipelining in reconstruction hardware (Blaimer et al,2004; Haacke and Liang (2000)].

Another advantage of Fourier Transform is that this technique proved to represent the data. While other techniques might be consistent with the data such as neural network, maximum entropy technique, they do not actually represent the data. If we consider an extreme case of processing several images together with motion and a small tumour (i.e. abdomen images), the image will look clean as though there is no motion or movement of structures, but the tumour also will be averaged away. This clearly indicating a mode of failure and such these techniques are not employed and considered in clinical application.

Compared to case of FT, the image might exhibit artifacts indicating effect of motions, but the tumour is not averaged away. The artifact creates a lack of trust in image, but not failing the imaging method.

Although currently Fourier Transform gives the best solution to MR Image Reconstruction, it has inherent limitation. The limitation of Fourier Transform leads to artefact formation, loss of resolution and Gibbs ringing artifacts.

As data acquisition is time consuming, one way to reduce the acquisition time is to partially collect the data. When reconstructed with FT, the truncated data leads to resolution loss and the SNR is highly reduced. This problem is reduced by

correcting phase angle and post processing is done. But it is time consuming. Furthermore, applying window or filters will either suppress fine images or further introduce spikes in images.

The efficiency of Fourier also depends on smoothness of image function, unfortunately, practically acquired data is discrete which creates discontinuity. Spurious oscillation is often found at the discontinuities in the image function, which leads to Gibbs ringing artefact. This is true for any number for data points, but as the data size increases, resolution also increase, the oscillation are squeezed close to discontinue point which suppress the presence of Gibbs phenomenon. This can be overcome by applying exponential filters, but using this kind of filter, could deflate the image and hide the features of fine images which could be a useful pathological indication.

To overcome issues related to FT reconstruction, parametric techniques were proposed. One efficient and successful implementation was 1D ARMA by Smith. Smith demonstrates by using TERA algorithm, MR Images can be successfully reconstructed. One limitation to this model is model order determination which seems to an interactive process. Smith in his research fixed the values of model orders to N/2 and test for multiple of model order. An appropriate model order provides the best solution. Unfortunately, this techniques has not been tested clinically where later on, not been considered further.

3.6 SUMMARY

In this chapter, signal processing view of image reconstruction has been presented. Image reconstruction depends on data acquisition technique, which explains why different reconstruction technique emerges in early days. But due to its significant

advantages, images are often reconstructed using Fourier transform in FFT algorithm. FFT do represent the actual data, fast and less complex. In 3.0T Philips MRI Scanner, parallel acquisition provides 1200 of 256 by 256 images. Because of this, non-Cartesian acquisitions are interpolated to Cartesian k-space data to apply FT as FT is only applicable on rectilinear sampled data.

Practically, MRI data are often truncated to reduce imaging time. Also MRI data are finite and small. When this data is applied for reconstruction using FT, they exhibit artifacts, resolution loss, low SNR, hiding of fine images and spikes. Although a certain percentage of these effects can be corrected using filters, usage of filters itself introduce limitation which could lead to misinterpreted medical diagnosis.

Parametric Modelling is an attempt to address these issues. Parametric Reconstruction is introduced in this chapter, while details of proposed 2D Autoregressive Moving Average will be detailed in Chapter 4.

.

CHAPTER FOUR

PROPOSED 2D ARMA ALGORITHM USING MODIFIED TERA

4.1 INTRODUCTION

Fourier transform is the standard algorithm for reconstructing MR images. Fourier transform is applied through FFT routine and has proven to be clinically reliable for decades. Attempt to replace this algorithm ends with no success although research have proven that some algorithms could be implemented successfully. For example, research analysis proves that Neural Network approach has shown positive results, but unfortunately, this method fails during clinical test. It averages away tiny tumor in a gastrointestinal images. Hence it leads to a misguided diagnosis.

However, one good possibility is to adopt parametric based reconstruction techniques such as AR or ARMA models. Usage and analysis of ARMA model for MR image reconstruction has been discussed in section 3.4.

There are many algorithms available to solve ARMA. TERA is one such method. TERA is simple and direct and particularly, TERA has been successfully implemented to reconstruct MR images. However, despite of this success implementation, there are still some limitations in the original TERA. Model orders are not been computed dynamically, but fixed to a value of N/2. Different tests have been done for a range of N/2 to N/3. This fixation is due to the complexity in model order determination and this tends to increase the reconstruction time in old processors.

Taking advantage of current microprocessor speed and as the FT is reaching the bottleneck in reconstruction time; a modified TERA algorithm is proposed and tested in this thesis.

In this chapter, technical details of ARMA and its estimation techniques are briefly introduced and followed by discussion of TERA and the proposed algorithm, modified TERA to reconstruct MRI images.

4.2 INTRODUCTION TO ARMA MODEL

An ARMA filter is described by the following linear difference equation in term of excitation and responses for any linear system:

$$x_n = -\sum_{i=1}^{p} a_i x_{n-i} + \sum_{i=0}^{q} b_i \varepsilon_{n-i} \tag{4.1}$$

ε_n, x_n	are the excitation and response;
a_i, b_i	are the model parameters;
p, q	are the model orders;

x_n is the output of the linear system , whose transfer function for is given by :

$$H(z) = \frac{B(z)}{A(z)} = \frac{\sum_{i=0}^{q} b_i z^{-i}}{\sum_{i=1}^{p} a_i z^{-i}}$$

where $a_0 = 1$ and z = $e^{j\omega}$ (4.2)

The equation 4.1 consists of 2 parts namely Autoregressive (AR) and Moving Average (MA). ARMA model which can be also expressed in pole-zero terms. Pole-zero filters are defined as:

a. $H(z) = B(z)$: all zero model; q^{th} order MA filter; p =0
b. $H(z) = 1/A(z)$: all pole model; p^{th} order AR filter; q = 0
c. $H(z) = B(z)/A(z)$: pole –zero model ARMA(p,q) filter

One great advantage of these modeling techniques is that very accurate results can often be obtained for short data lengths as in MRI Data, provided model order and model coefficients are determined accurately. A quick look at equation 4.1 and equation 4.2 reveals when $p = 0$, the ARMA model reduces to conventional Fourier model and to a strict AR model when $q = 0$. Fourier series model is effective for representing smooth function, but becomes inefficient to represent spiky image features, while AR model lend itself to represent spiky features because AR model will produce sharp peak by poles located near the unit circle in the z-plane. Combination of these models, endows ARMA model with the capability to represent variety of image features efficiently. The widespread usage of ARMA model in various areas of data analysts is motivated by this property.

4.2.1 ARMA Estimation Techniques

The key step in using ARMA model for image reconstruction is to determine all the model parameters (the AR coefficients and MA coefficients) and the model orders p and q accurately. Fitting an ARMA model to MR raw data series is a challenging computational problem and direct solution is often avoided in practice. Several methods have been developed for estimating ARMA parameters and these can be classified into two groups, namely optimal and suboptimal techniques. Optimal techniques are attempted to solve ARMA at gross. It is a single stage process based on the knowledge of the statistics of ε_n. Among the popular optimal techniques are the Direct Method, the Maximum Likelihood Method, the Prony Method, the Durbin Method, the Pade Approximation and many more. Computational complexity and instability of system responses limit their practical application. Methods such as direct method and MLM lead to solving non linear equation that must be solved by iteration

or some other numeric technique which has high computational requirements (Wilkes, et al ,1995). While Pade Approximation is not much of practical useful as the total the data point, N supposed to be exactly $p + q + 1$, which is not possible to achieve in practice. A modification which states N > $p+ q + 1$ is Prony's Method which is also not suitable for MRI Data. One inherent difficulty with optimal methods is modeling MA coefficients which lead to iterative, repetitive and complex algorithms. Methods such as Durbin's Method, Reverse Order Levinson Recursion or Shanks Method are developed from an attempt to propose alternative MA approximation. Durbin Method turns MA modeling problem into set of two AR modeling problem where each can be solved separately. Second AR parameters are approximated from the first AR parameter. Neither of optimal techniques was studied in this thesis due to their practical limitation or instability of system response.

Sub-optimal methods are developed to overcome the computational difficulties which are associated with optimal techniques. Estimation of ARMA parameters by sub-optimal procedures is a two-stage procedure where AR parameters are estimated first and then followed by MA parameters. Popular techniques determine p and q , estimates AR parameters by solving linear least-squares problem and use outcome of these estimations in deriving the MA parameters. Such, a clear definition of relationship must be established before relating these AR and MA coefficients; this depends on the nature of the data analyzed.

Once the AR parameters are obtained, then MA spectra can be derived by various means. But not all the methods are suitable for fitting the investigated signal. For example Kay and Marple proposed modified MA coefficient method, but this method is inconsistent for most of the data studied (Wilkes et al, 1995). Other approaches are Cadzow method which was later modified by Salami (Salami, 1986),

but it is computationally expensive (Nichols et al, 1985). TERA is one technique developed by Smith (Smith et al, 1986) which is proven successfully implemented on MRI data.

Smith utilized ARMA model with the TERA approach where each row of 2D image data is splitted into Hermitian and Anti Hermitian series. Each series is then treated as a single ARMA series. Model order were fixed to N/2 (and tested for various values) and AR parameters are determined by using modified Barrowdale algorithm. Output of AR is response and with the known excitation, ε_n is equated to MA portion. By using inverse filter, ε_n is determined. Later Fourier Transform of the series is approximated from Fourier transform of AR coefficients divided by Fourier Transform of ε_n.

4.3 TERA ALGORITHM

Transient Error Reconstruction Approach (TERA) was first introduced by Smith in 1986, as been explained in previous chapter. TERA is the algorithm used to model ARMA filters in particularly to reconstruct MR images. This section discuss in detail the steps in TERA algorithm as been proposed by Smith (Smith et al, 1986).

4.3.1 TERA Algorithm

The transfer function of ARMA filter is as expressed in equation 4.2. The process is schematically shown in Figure 4.1. From Figure 4.1, the TERA approach the data as deterministic ARMA model. The algorithm consists of number of definite steps. Following are the main steps in this proposed method.

a. Step 1: Re-labeling the raw data

The finite data set $s_0, s_1, s_2, \ldots, s_n$ of each row and column of the MR data matrix is considered to be a subset of the output s_0, s_1..... of an Infinite impulse Response filter (IIR) excited by Kronecker delta function. The transfer function is defined as in equation 4.2 and linear equation as expressed in equation 4.1. The calculation starts with re-ordering the data from –L to L through 0 , from original sequence which range from 0 to N , where N is the total number of data and L = N/2.

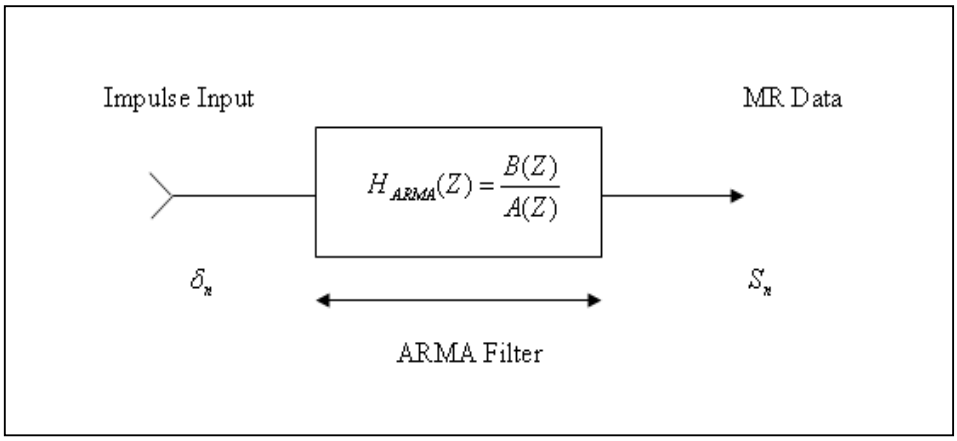

Figure 4.1 Schematic Diagram of ARMA filter

b. Step 2: Splitting into Hermitian and anti-Hermitian Series

Each row and column of the raw MR data is split into Hermitian, x_n and anti-Hermitian component y_n series to account for the data symmetry..

$$\begin{aligned} x_n &= (s_n + s^*_{-n})/2 \qquad 0 \le n \le L-1 \\ y_n &= (s_n - s^*_{-n})/2 \qquad 0 \le n \le L-1 \end{aligned} \tag{4.3}$$

The need for splitting into Hermitian and anti-Hermitian series is discussed in more detail in next section.

c. Step 3: Modeled as ARMA filter

Each series is modeled as the output of IIR filter. This requires estimating of transfer function from the finite data set generated from Step 2.

Linear equation of an IIR filter can be expressed as:

$$x_n = -\sum_{i=1}^{p} a_i x_{n-i} + \sum_{i=0}^{q} b_i \varepsilon_{n-i} \tag{4.4}$$

$$y_n = -\sum_{i=1}^{p} a_i y_{n-i} + \sum_{i=0}^{q} b_i \varepsilon_{n-i}$$

Solving for transfer function as in equation 4.4 involve approximating model orders, AR parameters and MA parameters. Model Order is fixed to N/2 and AR coefficients are estimated from Barrowdale Least Square Algorithm

d. Step 4: Applying the inverse transient

By applying TERA block, each series from Step 3 can be re-written as:

$$x_n = -\sum_{i=1}^{p} a_i x_{n-i} + \varepsilon_n \tag{4.5}$$

Where the transient error is

$$\varepsilon_n = x_n + \sum_{i=1}^{p} a_i x_{n-i} \tag{4.6}$$

And the Fourier Transform of equation 4.5 is estimated as:

$$S(x_n) = FT(x_n) = \frac{\sum_{i=0}^{L-1} b_i z^{-i}}{\sum_{i=1}^{p} a_i z^{-i}} = \frac{\sum_{i=0}^{L-1} b_i e^{(-j2\pi kx)}}{\sum_{i=0}^{p} a_i e^{(-j2\pi kx)}} = \frac{FT(\varepsilon_n)}{FT(\sum_{i=0}^{p} a_n)} \tag{4.7}$$

e. Step 5

The final image data is obtained by applying:

$$S(e^{j\omega}) = 2\,\mathrm{Re}[X^S(e^{j\omega})] - \mathrm{Re}[s_0] + j\{2\,\mathrm{Im}[Y^S(e^{j\omega})] - \mathrm{Im}[s_0]\} \qquad (4.8)$$

where $X^S(e^{j\omega})$ and $Y^S(e^{j\omega})$ are the Fourier Transform of data sequence x_n and y_n respectively for all $n \geq 0$ as in Step 4.

4.3.2 Data Symmetry

When original raw data are relabeled from –L to L-1 through 0, where L=N/2, ideally the corresponding positive and negative indexed data samples should exhibits Hermitian symmetry, which means that one is complex conjugate of the other. Practically, experiment imperfection may alter this symmetry to a certain level

Raw data symmetry can be observed by plotting an intensity graph,(intensity versus data number). As the maximum intensity is accumulated at the center of data, an interesting shape can be observed. The raw data will display a quasi-exponential increasing and decreasing from center of data. This is due to property of Fourier transform.

Figure 4.2 is one example of intensity graph plotted from an actual raw data (RAW_DATA2000.DATA) Figure 4.2 (a) shows amplitude graph for row number 256, slice number 3 and the echo sequence is 0. The horizontal line represents data points while the vertical line represents the amplitude. Note the maximum amplitude is at center. While Figure 4.2(b) shows amplitude graph for column number 96 of slice number echo sequence 1. Clearly both graphs decays quasi-exponentially from the center point towards both ends.

Modeling such signal character will lead to inaccurate model order approximation and coefficient approximation. Any modeling parameter calculated from the first half (increasing) of data will not fit for the second half (decreasing) of data. The use of only half of data would lower the Signal to Noise ratio of the image and also cause artifact in the final image.

While fitting each data individually, that is solving for –L to 0 (the center point) and 0 to L-1 separately would only increase the complexity of the problem besides it would not fit the modeling coefficients, AR and MA parameters. Fitting both wings of the data simultaneously would force the roots of AR filter onto the unit cycle and this leads to instability of the model.

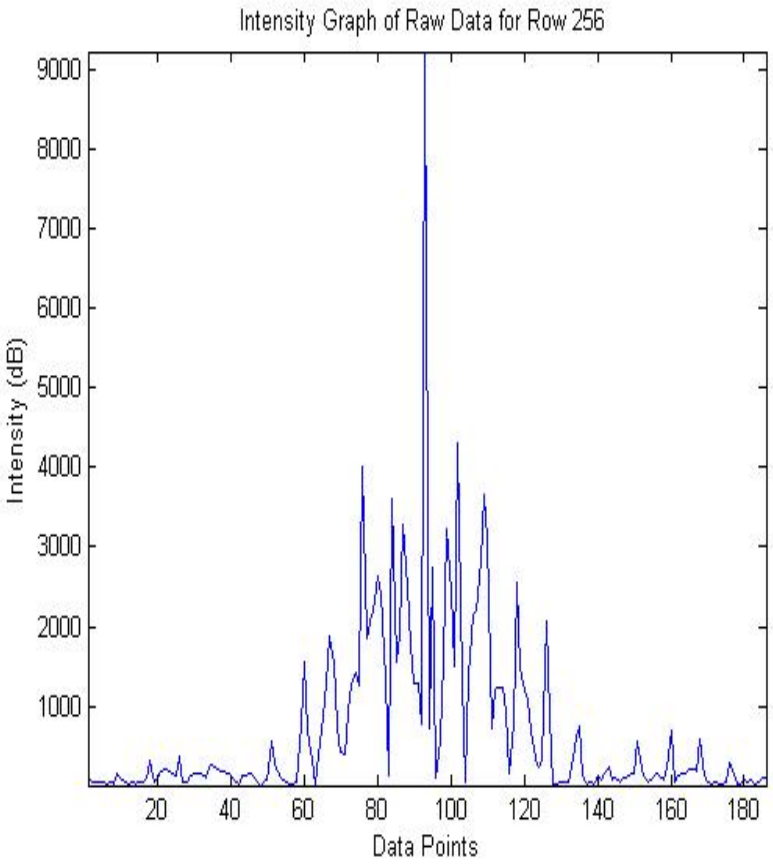

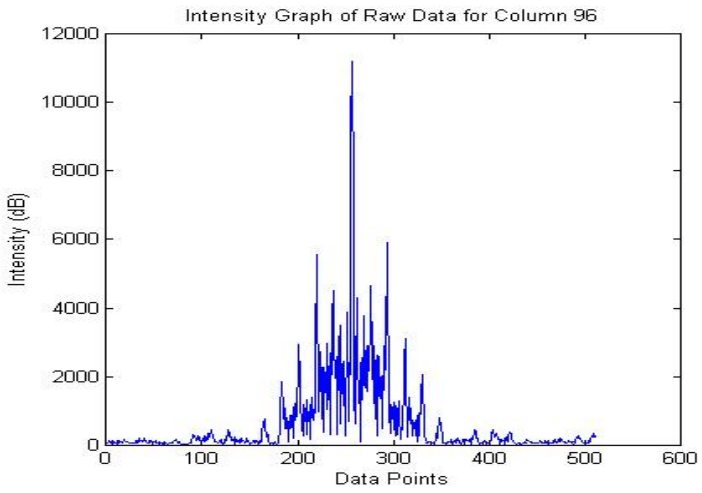

Figure 4.2: Quasi-exponential decay of MRI Raw Data

TERA method attempts to solve this problem by decomposing the data array into a Hermitian and an anti-Hermitian subarray as in equation 4.3. Such decomposition is useful because of the properties of the Fourier Transform.

The Hermitian series are an average of positive data number with conjugate of its corresponding negative data number. While the anti-Hermitian series are difference between positive data number from conjugate of its corresponding negative data number and divided by two. Ideally when this series are plotted separately, they will display the increasing and decreasing part of original raw data

When generating this series, the actual data is reduced to N/2. The original data number, N can be recovered by zero padding.

4.3.3 Modeling Technique

The original MR data is now rearranged into two data series, each following a single decaying train. Their difference equations are described in equation 4.4, while the transfer function in z-domain is:

$$X(z) = E(z)\frac{B(z)}{A(z)} \tag{4.6}$$

where, $\frac{B(z)}{A(z)}$ is the transfer function of ARMA filter while $X(z)$ and $E(z)$ are the final data and excitation process respectively. The IIR filter (Figure 4.1) can be redrawn as cascade of an MA filter with an AR filter as shown in Figure 4.3. The IIR filter is considered as the cascade of q^{th}-order MA model followed by p^{th} order AR model. The MA portion is described by $B[z] = \sum_{i=0}^{q} b_b z^i$, while AR portion is $A[z] = 1 + \sum_{i=0}^{p} a_i z^{-i}$. The combination of cascaded filter has the order of ARMA (*p*,*q*).

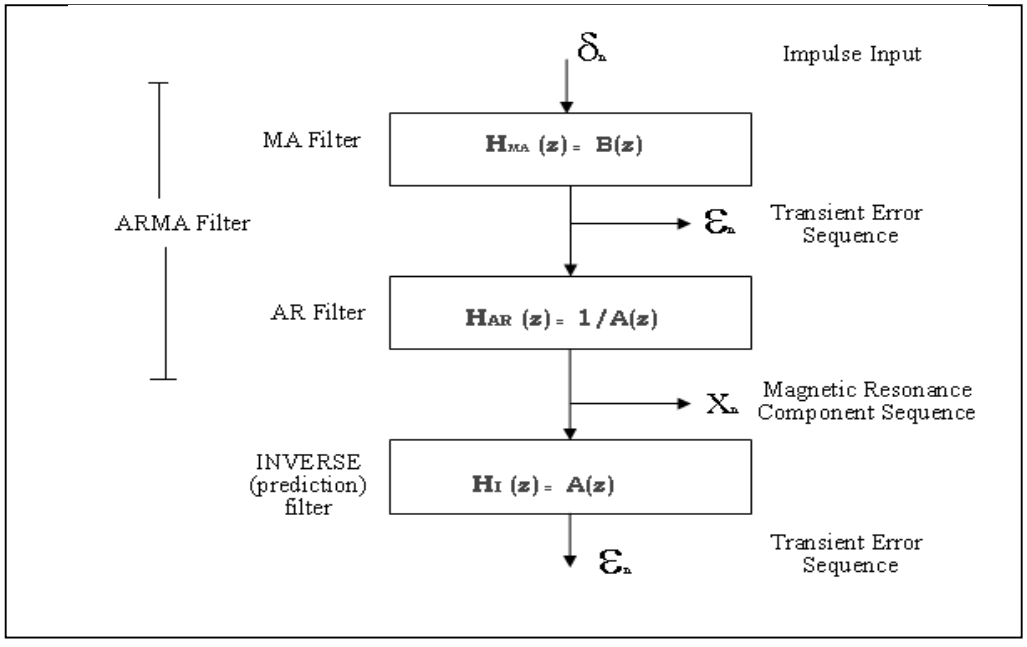

Figure 4.3 Basic Filter block structure of TERA.

In the basic TERA algorithm, the simplest excitation of ARMA filter is a Kronecker delta function as shown in Figure 4.3. Such Equation 4.4 can be re-written as:

$$x_n = -\sum_{i=1}^{p} a_i x_{n-i} + \sum_{i=0}^{q} b_i \delta_{n-i} \tag{4.7}$$

The MR data series, x_n is modeled as output of a p^{th} order AR filter excited by this sequence The excited MA filter produces a response series, ε_n. This is illustrated in Figure 4.3, hence,

$$x_n = -\sum_{i=1}^{p} a_i x_{n-i} + \varepsilon_n \tag{4.8}$$

$$\varepsilon_n = x_n + \sum_{i=1}^{p} a_i x_{n-i} \tag{4.9}$$

Once the AR coefficients are determined, the application of an inverse AR filter to MR data allows ε_n being determined. From equations 4.8 and 4.9, the MA coefficients, b_i are equivalent to ε_n which ends with an ARMA (*p*, *L*) model.

Finally, using the fact that MR component series is produced by exciting the total IIR by a single impulse, the total ARMA filter can be calculated using AR and MA coefficients (a and ε_n). Finally image function for Hermitian and anti-Hermitian series, $S(x_n)$ and $S(y_n)$ can be obtained through estimation of Fourier transform of ε_n and a as :

$$S(x_n) = \frac{\sum_{i=0}^{L-1} b_i z^{-i}}{\sum_{i=0}^{p} a_i z^{-i}} \Big| z = e^{(-j2\pi kx)}$$

$$= \frac{\sum_{i=0}^{L-1} b_i e^{(-j2\pi kx)}}{\sum_{i=0}^{p} a_i e^{(-j2\pi kx)}} = \frac{FT(\varepsilon_n)}{FT(\sum_{i=0}^{p} a_n)} \tag{4.10}$$

Provided the model is accurate, there are a finite number of AR coefficients (a) and transient error of MA terms (ε_n), which can be zero padded to an appropriate length, N power of 2. The padding with zeros introduces absolutely no errors since the coefficients following the highest order of (p, q) are supposed be zero, if the model is applicable. The image function for anti-Hermitian series, $S(y_n)$ can be found from similar expression.

The final image data is obtained by combining the Hermitian and anti-Hermitian series as in equation 4.5.:

$$S(e^{j\omega}) = 2\,\mathrm{Re}[X^S(e^{j\omega})] - \mathrm{Re}[s_0] + j\{2\mathrm{Im}[Y^S(e^{j\omega})] - \mathrm{Im}[s_0]\}$$

$$S_n = 2*\mathrm{Re}(x_n) - \mathrm{Re}(s_0) + j(2*\mathrm{Im}(y_n) - \mathrm{Im}(s_0)) \tag{4.11}$$

Since Hermitian and anti-Hermitian series are half of the actual data, the original data size is recovered by zero padding, absolutely without violating the data or decrement in SNR or resolution. Implementation of this TERA modeling technique will be discussed in Chapter 5.

4.4 MODIFIED TERA ALGORITHM

Work of Smith on TERA is further extended in this research. Fixed model orders in previous algorithm is changed to dynamic computation of model order each Hermitian and anti-Hermitian series. Furthermore, different AR parameter estimation technique is employed, Yule-Walker Method compared to Barrowdale method employed by Smith. Yule-Walker method is proven to be more stable. Finally, the final image data

is estimated directly from the prediction error of Hermitian and anti-Hermitian series, unlike TERA, which estimates the final data from a division of Hermitian and anti-Hermitian series prediction error with AR coefficients as in equation 4.11.

4.4.1 MTERA Algorithm

Following is the major steps in MTERA algorithm

a. Step 1: Re-labeling the raw data

The original raw data is relabeled temporarily as in TERA. The finite data of MR data is considered to be subset of an IIR filter excited by Kronecker delta function. The calculation starts with re-ordering the data from –L to L through 0 , from original sequence which range from 0 to N , where N is the total number of data and L = N/2.

b. Step 2: Spliting into Hermitian and anti-Hermitian Series

Each row and column of MR data is split into Hermitian, x_n and anti-Hermitian component y_n series to account for the data symmetry as in equation 4.3. The need for splitting into Hermitian and anti-Hermitian series is discussed in previous section

c. Step 3: Each series in Step 2 is modeled as an ARMA filter

Each series is modeled as the output of IIR filter. Linear equation as in equation 4.4 applies. By applying TERA block as in Figure 4.3, each series from equation 4.4 is re-written as:

$$x_n = -\sum_{i=1}^{p} a_i x_{n-i} + \varepsilon_n \tag{4.12}$$

Where the transient error is

$$\varepsilon_n = x_n + \sum_{i=1}^{p} a_i x_{n-i} \tag{4.13}$$

There are two major steps in determining the transient error, ε_n which are estimating the model order, p and determining AR coefficients. Success of mTERA depends on correct and accurate computation of both values. As explained earlier, high model orders tends to produce spikes in final image while a very low model order bends to normal FFT technique.

Varieties of algorithm are available to determine both model order and AR coefficients, but not all algorithms are suitable to apply on MR data. However, despite of any algorithm chosen, the computation of model order and AR parameters are intrinsic and nested.

First a range of suitable model order i.e. from 1 to N/3 is selected. For each of this proposed model order, AR parameters are computed. By using this model order and AR coefficients, a criterion to determine the best model order is selected. Finally, by using the best model order, AR coefficients are re calculated and used in equation 4.13.

Proposed algorithm for selecting best model order is Total Prediction Error while Yule-Walker algorithm is proposed for AR coefficient determination. These algorithms are discussed in detail in next section.

d. Step 4 : Approximation of Image Function

The image function of Hermitian, $S(x_n)$ and anti-Hermitian series, $S(y_n)$ is approximated from the Fourier Transform of ε_n :

$$S(x_n) = \sum_{i=0}^{L-1} b_i z^{-i} \mid z = e^{(-j2\pi ix)}$$
$$= \sum_{i=0}^{L-1} b_i e^{(-j2\pi i)} \qquad (4.14)$$
$$= \mathrm{FT}(\varepsilon_n)$$

TERA estimated the image function by adopting $\frac{FT(\varepsilon_n)}{FT(\sum_{i=0}^{p} a_n)}$. A simulation test using this TERA image function estimation results in distorted image.

e. Step 5: Final Image Data

The final image data is obtained by applying:

$$S(e^{j\omega}) = 2\,\mathrm{Re}[X^S(e^{j\omega})] - \mathrm{Re}[s_0] + j\{2\mathrm{Im}[Y^S(e^{j\omega})] - \mathrm{Im}[s_0]\} \qquad (4.15)$$

where $X^S(e^{j\omega})$ and $Y^S(e^{j\omega})$ are the Fourier Transform of data sequence x_n and y_n respectively for all $n \geq 0$ as in Step 4 above

Improvements for TERA method as proposed above, where made on 3 aspects. First the model orders were proposed to be computed dynamically using TPE for each Hermitian and anti Hermitian series compared to TERA where model orders are fixed due to limitation of computing facilities. An advantage of using dynamic computation of model orders is each series can be approximated using model orders which suit them best. Thus this modification eliminates using unsuitable fixed model orders for generated data series. Moreover, model order fixed for a raw data set, for example for a scan might not be the same for second scan. Research shows that normally the model order does not goes beyond than N/2 and selected on the range of N/3 , but does not give an exact model order. This range can be used to test model orders , i.e. start from 1 to N/2 for each generated series.

Second difference is determination of AR coefficients using Yule-Walker method. In old algorithm, least square method Barrowdale was adopted. Yule-Walker method is more stable compared to Barrowdale, although the small trade-off is Barrowdale produces images with higher resolution than Yule-Walker. But this issue is not significant as the difference of resolution is negligible when a constant, $\alpha = 0.99$ is multiplied by AR coefficients. Using Yule-Walker also decreases the computation timing as Barrowdale has more intrinsic computation (Barrowdale and Erickson, 1980)

Third aspect is approximating the final image data. TERA approximate the image data for Hermitian and anti-Hermitian series as in equation 4.11. Image data is computed from division of TERA prediction error, ε_n over AR coefficients, a_n. The ε_n contains data computed from TERA as in equation 4.9. Since the data is intensity representation in grayscale level, this is not more than an attempt to reduce the intensity of final image data. In MTERA, the final data is proposed to be computed from the ε_n only as in equation 4.14.

Implementation of m-TERA is discussed and presented in Chapter 5.

4.4.2 Model Order Determination

One major step in MTERA modeling technique is to estimate the AR parameters; in fact, this is major goal in all system identification and modeling applications. Obviously selecting the model order, *p* is first key step before estimating the AR parameters. The success of any AR coefficient determination algorithm depends on accuracy of estimated model order.

Several techniques are available to estimate model orders, namely Akaike Information Criterion (AIC), Final Prediction Error (FPE), Minimum Description Length (MDL), Criterion Autoregressive Transfer (CAT), Covariance Eigenvalues Method (Liang and Wilkes, 1993) , Modified MDL Approach (Wilkes et al, 1992) and etc. Due to wide usage and efficient results obtained in previous computations, FPE is selected as model order algorithm in this thesis. FPE utilizes Total Prediction Error, E_f , where E_f is calculated as :

$$E_f = \sum_{n=p}^{L-1} \left| x_n + \sum_{i=1}^{p} a_i x_{n-i} \right|^2 \tag{4.16}$$

One way to determine the correct order, p is to monitor the E_f as the model order increases. When E_f exhibits a sharp decline, the correct model order is attained. Or E_f also can be calculated by using the FPE method .FPE is based on function (for mean subtracted data):

$$FPE(p) = \frac{L+p}{L-p}\sigma_p^2 \tag{4.17}$$

σ_p^2 is the modeling error or variance of the residual of the estimated AR(p) model. σ_p^2 is obtained from Total Prediction Error (or Total Square Error) for no windowing method

$$\sigma_p^2 = \frac{1}{L+p} E_f = \frac{1}{L+p} \sum_{n=p}^{L-1} |x_n + \sum_{i=1}^{p} a_i x_{n-i}|^2 \tag{4.18}$$

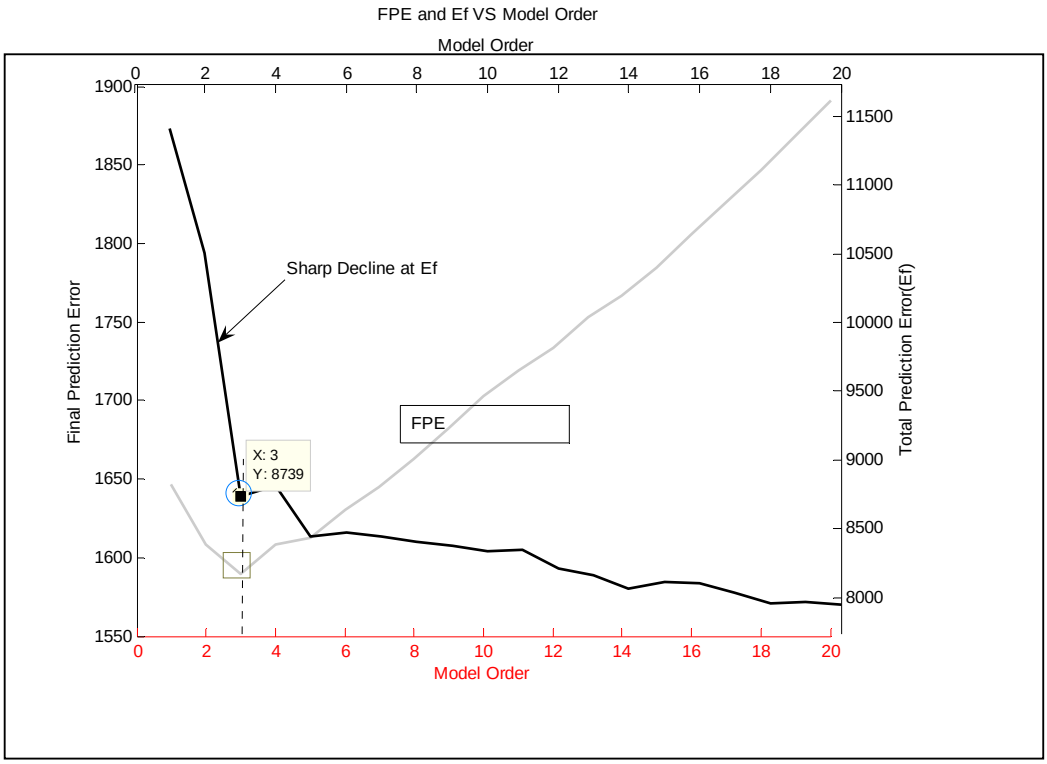

Figure 4.4 Model Order using FPE and Ef
(*Note:* TPE is exhibiting a sharp decline while FPE function is minimized when the correct model order is attained. Data is plot from RAW DATA 2000 and from real data. Simulation can be seen in mulittest12b.m file)

To determine the correct AR model order, for each increasing model order, FPE (*p*) is determined. The fractional term is monotonically increasing so that FPE becomes a function with a defined minimum at the best model order.

If FPE(p) and E_f is plotted against model order , p , at best model order, FPE(p) will be minimum point while E_f will display a sharp decline. This is demonstrated in Figure 4.4. Simulation results are discussed in Chapter 6. Data for

As mentioned earlier, model order determine success of ARMA algorithm. Too high orders will over fit the data and generate spikes in final image while a low

data order will lead to resolution loss and makes no different from non-parametric method.

4.4.3 AR Coefficient Determination : Yule-Walker method

There are several methods to estimate the AR coefficients $(a_0, a_1, a_2, ...a_p)$ such as Least-square Methods, Yule-Walker, Burg Method, Barrowdale Method, Modified Covariance method, neural network methods etc. But not all the methods are suitable to be applied on MR data. For example forward and backward minimization methods such as Burg Algorithm are proven to be unsuitable for MR data, although this algorithm is regarded as a computationally effective algorithm for AR estimation in other application. When Burg algorithm is applied for MR Data, it leads to highly spiked images (Smith et al, 1986).

The AR parameter estimation technique proposed here is Yule-Walker method (YW Method). The YW method is also called the Autocorrelation Method, where autocorrelation of the data is estimated to fit a *p*-th order autoregressive (AR) model. This formulation will lead to formation of Yule-Walker equation, which could be solved by the Levinson-Durbin recursion algorithm.

To generate a relationship between AR parameters and autocorrelation of MR data series, consider a general AR(*p*) model:

$$x_{i+1} = a_1 x_i + a_2 x_{i-1} + \ldots a_p x_{i-p+1} + \varepsilon_{i+1} \qquad (4.19$$

To generate a response that lags by 1 unit the following steps will apply:

a. Multiplying 4.19 by x_i:

$$x_i x_{i+1} = \sum_{j=1}^{p} (a_j x_i x_{i-j+1}) + x_i \varepsilon_{i+1} \qquad (4.20)$$

b. Take the expectation :

$$E\{x_i x_{i+1}\} = \sum_{j=1}^{p} (a_j E\{x_i x_{i+1-j}\}) + E\{x_i \varepsilon_{i+1}\} \tag{4.21}$$

a_j are kept outside the expectance operator as they are deterministic variables rather than statistical .

c. As the random perturbation of ε of the current value is unrelated to previous value $E\{x_i \varepsilon_{i+1}\} = 0$

$$E\{x_i x_{i+1}\} = \sum_{j=1}^{p} (a_j E\{x_i x_{i+1-j}\}) \tag{4.22}$$

d. Divide through by (N-1) gives the autocorrelation value

$$r_1 = \sum_{j=1}^{p} a_j r_{j-1} \tag{4.23}$$

Repeating steps (a) – (d) to compute lag 2, lag k (any number not p) and for lag p, would lead to the following equations:

$$\begin{aligned}
r_1 &= a_1 r_0 + a_2 r_1 + a_3 r_2 + \ldots\ldots\ldots + a_{p-1} r_{p-2} + a_p r_{p-1} \\
r_2 &= a_1 r_1 + a_2 r_0 + a_3 r_1 + \ldots\ldots\ldots + a_{p-1} r_{p-3} + a_p r_{p-2} \\
r_{p-1} &= a_1 r_{p-2} + a_2 r_{p-3} + a_3 r_{p-4} + \ldots\ldots\ldots + a_{p-1} r_0 + a_p r_1 \\
r_p &= a_1 r_{p-1} + a_2 r_{p-2} + a_3 r_{p-3} + \ldots\ldots\ldots + a_{p-1} r_1 + a_p r_0
\end{aligned} \tag{4.24}$$

By considering r_0=1, equation 4.24 can be represented in matrix form as [Manolakis, Ingle & Kogon (2000)]:

$$\begin{bmatrix} r_1 \\ r_2 \\ \vdots \\ r_{p-1} \\ r_p \end{bmatrix} = \begin{bmatrix} 1 & r_1 & r_2 & \cdots & r_{p-2} & r_{p-1} \\ r_1 & 1 & r_1 & \cdots & r_{p-3} & r_{p-2} \\ \vdots & \vdots & \vdots & \vdots & \vdots & \vdots \\ r_{p-2} & r_{p-3} & r_{p-4} & \cdots & 1 & r_1 \\ r_{p-1} & r_{p-2} & r_{p-3} & \cdots & r_1 & 1 \end{bmatrix} \begin{bmatrix} a_1 \\ a_2 \\ a_3 \\ a_4 \\ a_5 \end{bmatrix} \tag{4.25}$$

Or succinctly in vector form as

$$\vec{R}\vec{a} = \vec{r} \tag{4.26}$$

where $\vec{R}_x$ is the autocorrelation matrix, $\vec{a}$ is the vector model parameters, and $\vec{r}$ is the vector of autocorrelation. Further, $\vec{R}_x$ is full rank and symmetric, such inevitability is guaranteed to find $\vec{a}$, $\vec{a} = \vec{r}\vec{R}^{-1}$.

Equation 4.25 and 4.26 is known as the Yule-Walker equations. Because of its Toeplitz structure and nature of right hand, this linear system can be solved recursively by using Levinson-Durbin Algorithm. Another way of representing the matrix form of equation 4.25, is in term of noise as :

$$\begin{bmatrix} R_x[0] & R_x[-1] & \dots & R_x[-P] \\ R_x[1] & R_x[0] & \dots & R_x[-P+1] \\ \vdots & \vdots & \vdots & \vdots \\ R_x[P] & R_x[P-1] & \dots & R_x[0] \end{bmatrix} \begin{bmatrix} 1 \\ a_1 \\ \vdots \\ a_p \end{bmatrix} = \begin{bmatrix} \sigma^2 \\ 0 \\ \vdots \\ 0 \end{bmatrix} \tag{4.27}$$

Levinson or Levinson-Durbin recursion is an algorithm proposed to speed up the recursive computation involving Toeplitz matrix. It expects input of autocorrelation sequence of M size, calculates the coefficients of the m^{th} step coefficient using those obtained in $(m-1)^{th}$ step for inputs *r(0),r(1),……r(m).* The algorithm begins with initialization of constants, can be

$$\begin{aligned} &P_0 = r(0) \\ &\beta_0 = r^*(1) \\ &k_0 = -r^*(1)/r(0) \\ &a_1 = k_0 \end{aligned} \tag{4.28}$$

The second step is recursive calculation for *m=1, 2 …. M-1:*

$$\begin{aligned} &P_m = P_{m-1} + \beta_{m-1} k_{m-1}^*; \vec{r}_m = [r(1)r(2)\cdots r(m)]^T \\ &\beta_m = \vec{a}_m^T J \vec{r}_m^* + r^*(m+1); k_m = -\frac{\beta_m}{P_m}; \vec{a}_{m+1} = \begin{bmatrix} \vec{a}_m \\ 0 \end{bmatrix} + \begin{bmatrix} J\vec{a}^* \\ 1 \end{bmatrix} k_m \\ &\text{for final data, M :} \\ &P_M = P_{M-1} + \beta_M k_M^* \end{aligned} \tag{4.29}$$

One great advantage of using Matlab® is the entire algorithm discussed above, can be implemented using built-in function, *'aryule'* which utilizes Levinson-Durbin algorithm to compute the AR coefficients. Certainly, this reduces the burden of re-writing codes. Implementation is discussed in next Chapter

4.5 IMPLEMENTATION OF 2D ARMA USING MODIFIED TERA

As been explained earlier, the motivation for this new approach is based on successful implementation TERA for 1D ARMA Parametric modeling technique which was initiated by Smith in 1986. For ID parametric modeling, one axis (either rows or columns) of MR data is reconstructed using IFFT while the other axis is modeled with TERA. There is no definite rule on which direction to be modeled as both shows the two sided quasi-exponential decay from center of data since the highest intensity is accumulated at center of data. But the general understanding is to reconstruct the truncated axis using modeling technique while the non-truncating axis by normal FFT.

For 2D reconstruction, obviously it may appears such the inverse Fourier transform for both directions should be estimated via ARMA modeling using the MTERA algorithms directly, but this does not work. A direct modeling of rows followed by columns generates a distorted image as in Figure 4.5.

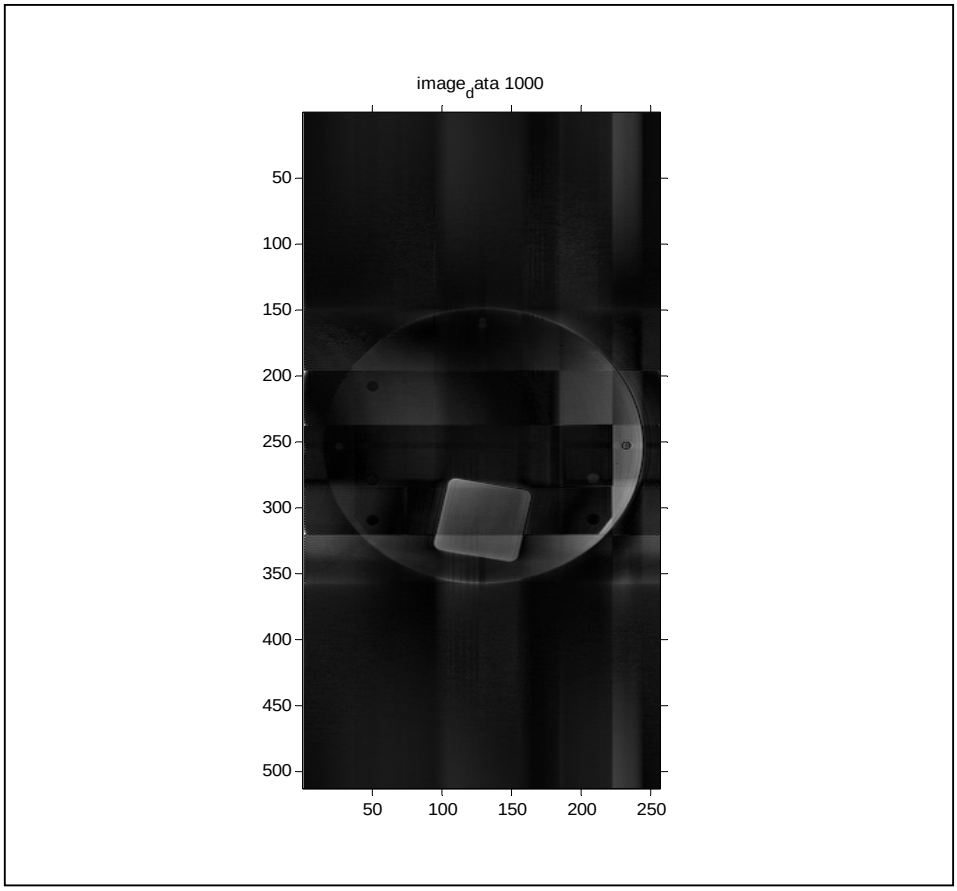

Figure 4.5: Image reconstructed by applying direct application of 2D m-TERA

One possible solution for 2D implementation was suggested by Smith and Nicholas (Smith and Nicholas, 1989) is to reconstruct columns with IFFT and the data rows to be modeled using TERA. Then the data columns are unreconstructed using FFT and modeled again. By applying this method, TERA is successfully implemented on rows and columns for a 2D modeling reconstruction. This is preconditioning ARMA modeling.

Considering this fact, 2D ARMA using MTERA can be achieved by:

a. Reconstruct rows (or columns) using IFFT
b. Reconstruct the column data (or row data) using MTERA
c. Unreconstructed the row data (or column data) using FFT

d. Reconstruct the row data (or column data) using MTERA

Reconstruction can begin with any dimension, either row or column but generally modeling technique requires additional computation time.

4.6 SUMMARY

In this chapter, a modified algorithm for solving ARMA technique for MRI reconstruction is proposed. The technique proposed is modified TERA or m-TERA, which can be used to solve for ARMA filters. Basically ARMA is an IIR filter and it is assumed that the process is stationary random process.

Modified TERA consists of 5 major steps as been introduced in section 4.4. The algorithm begins with temporarily re-labeling the original MR data so the data range is extended from –L to L-1 through 0, where L is N/2. Re-labeled data is then splitted into Hermitian and anti-Hermitan series as in equation 4.3. Each of this data series are solved individually as an IIR filter as been described in Figure 4.3 and the transient error is computed as in equation 4.9. This involves estimating model order and AR coefficients repeatedly which is computationally expensive, but taking advantage of current microprocessor speed, it is not a limit anymore.

The final data is generated by approximating the Fourier transform of transient error as described by equation 4.14 and equation 4.15.

MTERA method differs from original TERA method from three aspects where the main aspect is the determination of model order dynamically using TPE whereas in original TERA method, model orders are being fixed. Other differences are determination of AR coefficients and calculation of data for final image. Using dynamically computed model orders, AR parameters are estimated using YW method. YW method estimates the autocorrelation of MR Data and generated YW equation is

solved using Levinson-Durbin algorithm to find AR coefficients. Determination of model order plays a major role in successful implementation of the m-TERA method, same with determination of AR coefficients. Both have been discussed in detail in Section 4.4.

And finally 2D implementation of MTERA has been presented. Application and implementation of this algorithm is presented in Chapter 5.

CHAPTER FIVE

IMAGE DATA ANALYSIS AND RESULTS

5.1 INTRODUCTION

The implementation of the proposed 2D ARMA using MTERA algorithm as been proposed in chapter 4 is presented in this chapter. Raw data for simulating m-TERA is obtained from Philips® 1.5 Intera MRI scanner which is available at Department of Diagnostic Imaging at Hospital Tunku Ampuan Afzan , Kuantan , Pahang.

This chapter begins with the introduction to concept of k-space followed by the raw data acquisition procedure, discussion of raw data formats and how it is organized in a data file. MRI k-space raw data is a complex data in binary format and currently there are no publicly available documents to explain its data arrangement and organization. It is as internal knowledge to Philips®.

Understanding the raw data format and how the data sequence is arranged is essential and important milestone in this thesis. Data mismatch is not tolerable as this will cause incorrect representation of intensity at certain point; which could lead to an inaccurate image.

The converter program is a program to read binary raw data file according to given description and re-arranged into an image matrix format. Computational needs, implementation and results of executing 2D ARMA and 2D IFFT is finally presented at end of this chapter.

5.2 K-SPACE

As explained earlier in chapter 2, raw data composed of signal emitted due to release of energy when the Hydrogen molecules back to its original position during free precession period. This signal is captured by RF receivers which feed the signal into Analog-to-Digital Conversion System which digitizes the signal and transfer to the computer system for reconstruction.

Signals are in the space, released from the human body or scanning objects. Signals are collected at discrete set of k-space points; meaning captured data is stored into k-space plot. K-space is the space or plot of all possible wave numbers (captured signals). The 'k' refers to the fact that there are k-number of waves forms encoded into the plot. It is simply an array of complex numbers, representing certain type of data with some important properties. One interesting properties is the data has relationship to image via Fourier Transform. K-space is square and divided into vertical and horizontal axes and the center contains the frequencies with highest signal and is responsible for image contrast. Basically the k-space composes information of high and low frequency of spatial information.

K-space trajectory defines how the k-space is filled. Its path can be denoted by $\vec{k}(t)$. This path illustrates the acquisition strategy, influences on which type of artifacts can result and determines the image reconstruction algorithm to be employed.

The x-axis of k-space represents Frequency encoding while the y-axis represents the phase encoding. Data is collected after each phase and frequency encoding and sampled directly at each TR (Relaxation time between demagnetization). It is sampled such the k-space center contains frequencies with highest signal which is responsible for image contrast. The outer k-space is filled with other frequency signals which are responsible for image contrast. K-space matrix data

is then plotted on a text file to be read by the computer system to reconstruct the image. This text files are the raw data files.

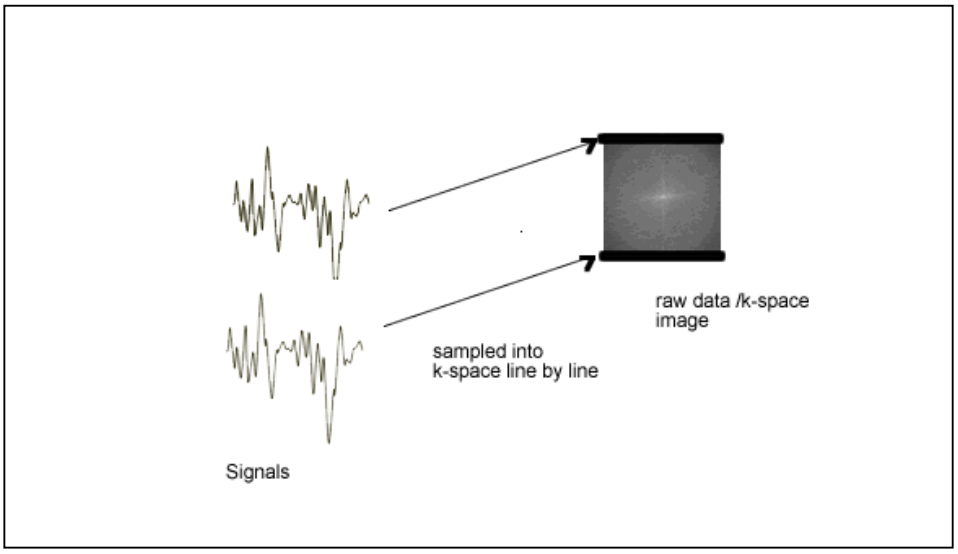

Figure 5.1: Filling k-space line by line

The k-space matrix or raw data matrix can be seen as a grid of points to reconstruct an image. A 256 X 256 image should have 65,636 data points. Nevertheless, this point does not indicate its position in the reconstructed image. Each signal measured in MRI is a mixture of the signals from every pixel sample. The task is to separate or decompose the signal to extract the grey scale information and this is done but applying FT (in this research, we are approximating the FT of the signal by applying 2D ARMA rather than direct 2D FFT) on the image.

There are many k-space matrix trajectories defined and employed. Basically they fall in two broad categories: the rectilinear and circular, which can be extended into echo planar, spiral or Cartesian. These trajectories have been shown in section 2.4 (Data acquisition techniques). As it has been explained earlier in Chapter 2 , 3 and 4,

different trajectories leads to different reconstruction algorithm and the most simple of them is rectilinear or echo planner which leads to direct implementation of Fast Fourier Transform.

5.3 RAW DATA

5.3.1 Clinical Research Agreement

Data for this research work were obtained from Philips® 1.5T Gyroscan, a 1.5T MRI scanner which is available at Department of Diagnostic Imaging (DDI) at Hospital Tengku Ampuan Afzan, Kuantan (HTAA). Data is downloaded with permission from Philips® Medical Systems Sdn. Bhd. and Director of Diagnostic Imaging Department, Dato Dr. Hjh Zainon whom co-operated well and was highly interested in this research title.

The entire process for data download took more than one year. The first visit to DDI, HTAA were not successful as the radiographers and radiologists were not aware of raw data downloading process or format. Philips® MRI engineers who were present for a maintenance service confirmed that raw data has not been downloaded before in this region.

Later on after an enquiry with Philips® global support center, we were informed raw data from Philips® MRI Scanner is available only for researchers after signing a contract known as 'Philips® Clinical Research Agreement', CRA . CRA is to protect Philips® right and copyright over raw data. Raw data files are treated confidential as it reveals the hardware property of the scanner. This CRA contains information related to the research work and to protect Philips® right on raw data as raw data is considered to be confidential. Philips® also generously offered some assistance from Philips® experts and local engineers to operate the MRI Scanner

during data downloading. Any findings should be reported to Philips® as well. Upon signing the CRA, a software key (which costs more than Rm30, 000) were generated and sponsored. This software key will enable the administrator of MRI system to access, scan and download raw data.

The software key is valid and to be used only at certain location and MRI scanner which has been specified in CRA. It has a validity period of 1 year and can be extended upon request after expiry.

The second visit to HTAA to download the raw data were not successful either. The documentation only specifies the raw data scanning procedures without detailing the raw data format, its file extension or in which directory the raw data was saved. Once the option for saving raw data is selected, the MRI system generates and saves different raw data format files. Lack of understanding the raw data format and unavailability of publicly available documentation for raw data format, leads us to download only part of sets of raw data file. On the third visit and fourth visit, raw data were downloaded successfully with different objects, scanning parameters and with multiple images and slices.

5.3.2 Types of Raw data

The raw data file format and organization varies with different MRI Scanner manufacturers. Although the same signals are captured and recorded, however how the data is arranged in a file differs. As for Philips® MRI Scanners, there are 4 different sets of data files which are made available for researcher to download. Each set of data consists of pair of files which are collected at different stages during a scanning process. Below is the list of the data sets and when they are collected.

1. ***Unprocessed raw data***

   This is the 'typical' raw data or k-space data where signals are recorded as soon as it comes out from the Analog to Digital Circuit. During the AD processing those signals also goes through DC offset correction, girding and reversals. Signals are still rich with noises as filter is not applied yet to filter any unwanted noises. These files are available under the extension of .LIST and .DATA. The LIST files specify the scanning parameters, noise information and the data arrangements of DATA file. While the DATA files consists the actual data in binary format.

   More on these files will be explored in next section.

2. ***Processed Raw Data Files***

   The second set of data files available and still can be considered as a raw data file are CPX (Complex) file. CPX means complex files and certainly this convention is misleading as image data either typical raw data or processed raw data are in complex format.

   CPX data are data available after the 2D FFT applied on the typical raw data. Although it has been processed to some extend, but CPX data files are not ready for image production as zero filling and scaling is yet to be done.

   Again, CPX data comes as pair of files as CPX_100.LIST and CPX_100.DATA

3. ***Image Data File***

   It is a completely processed image data files. It is the final data after been processed (filtered) and scaled for display appropriate with acquired k-space data. Image data represent the actual image and its properties; such

as size, grayscale contrast and filtered. Their file extension is .PAR and REC.

4. ***PAR/REC Format***

   This data type are made easy for spectroscopy analysis and not meant for image production. Available with file extension of .SPAR and .SDAT

5.3.3 Raw data downloading procedure

Scanning an object for raw data requires double of normal scanning time as the object is scanned twice, once for raw data and once for imaging. This is time consuming and in addition to this timing issue, the raw data files are huge files. A simple, one slice image file will have 30- 40 M of raw data file. Transferring the raw data from MRI computer to workstation via local connections took a lot of time; such each downloading session will last for 4 -5 hours. As the MRI Scanner can be operated only by the engineers, all visits are made possible only with the presence of Philips® MRI Engineers. Such, frequent and long visits are not possible. Each visit took about a month for appointment and only 1 day visit to download raw data files.

To download raw data, one must be have super-user login privileges. Raw data can be obtained on the MRI Scanner through 'delayed reconstruction mode'. During the parameter settings, two additional parameters are activated and need to be set manually are:

a. On 'POSTPRO' page, set the 'save raw data' parameter to 'yes'
b. And use a 'delayed recon' mode

Once the other parameters are set and the scan is initiated, the system will scan twice. The first time is for image production and this image will be stored image data in control panel workstation. Second scanning is to scan for raw data; which is not

stored in workstation. After the scan is complete, the raw data is transferred via ftp before continuing with other scans as the raw data will be deleted after each scan. This is not the same for image data which was reconstructed by the system. The reconstructed image data will be pushed to Control panel workstation for storage.

After the scan is completed, in the console, 'Add Recon' button will appear. Selecting this will prompt 'Raw Export', where the system will ask for an ID. After a choice, for example "123", the 'proceed' button is pressed and scan list will be listed. Export of raw data will be performed when the scan list is started by pressing the start scan. Navigate to system's TEMP directory by FTP from any machine connected directly to MRI Scanner, browse for file with extension: RAW_123.DATA and RAW_123.LIST.

Depending on scan request, the file size varies. For a simple one slice, one echo, 128X128 scan, the data file could be 30 – 40 M while for a complete scan of 16 images, 2 echo scans might have 100M file. Total of 15 raw data sets were downloaded. Downloaded data files are summarized in the Table 5.1 and Table 5.2.

5.4 STRUCTURE OF RAW DATA FILES

As been explained above, the raw data files come in pair: .LIST files and .DATA files. There is little printed information on the data file formats as they are considered self-documenting. Technical documentations are not available for public or external researchers. This is due to the raw data are propertied and reveal some hardware properties, which can be used to re-engineer the entire system.

The self-documenting, text file is the .LIST files which can be read by opening it with any text editor such as notepad. The LIST file is ASCII text file describing everything about the corresponding raw data such acquisition, scan properties, data

arrangement, reconstruction etc while the data itself contained in a .DATA file. DATA file are binary files which requires “gateway” functions to read the data. The ‘gateway’ functions can be written in any high level languages such as Matlab®, C, C++, etc. Its objective would be to open the DATA file, identify number of data, its sequence in k-space plan and re-arrange into a format which can be plotted and processed further.

Table 5.1
Parameters for Scanned Raw Data Images
Location: HTAA Time/Date: 9/22/2005 6:05:19 PM

No	Parameters	200	300	301	302	400	401	500
1	Scan matrices	256	256	256	256	512	512	288
2	Reconstruction Matrices	256		256	256	512	512	512
3	Field of View(mm)	230	230	375	530	230	180	na
4	Rectangular Field of View (%)	80	80	80	100	80	70	na
5	Coil Selection	QHead	QHead	Qbody	Qbody	Qhead	qhEAD	Syn-Sgi
6	Te (ms)	15.0	20	13	15	20	9.2	13
7	Tr (ms)	100	shtst	525	100	shorterst	na	525
8	Half scan	NO	NO	NO	NO	NO	NO	NO
9	Number of Signal Averages	1	1	1	1	2	1	1
10	Slices	1	1	1	1	1	1	32
11	View	Sagittal	Sagittal	Coronal	Sagittal	coronal	Axial	Transverse
12	Sense	NO	NO	NO	NO	NO	NO	NO
13	Clear	NO	NO	NO	NO	NO	NO	NO
14	Technique	T1W/SE	Tw2/SE	tse	tse	T1w/se	T1w/FFE	TSE
15	Scan Percentage	100	100	100	100	100	100	70
16	Flip angle(◦)	69	90	90	90	90	90	90

ID No	Image Description
100	Bottle Sagittal (no images)
200	Bottle II Sagittal (t1w/se)
300	Rahman Head (Mr. ra)
301	Rahman's Abdomen
302	Rahman's Lower Extrimity
400	Joshua's Head (test)
401	Joshua's Feet (test)
500	Siti Nur Sahimi diagnosed : Acute Transverse Myelities (T1w)

Table 5.2
Parameters for Scanned Raw Data Images on 23rd Feb 2005

No	Parameters	901	900
1	Scan matrices	384	384
2	Reconstruction Matrices	512	78
3	Field of View	210	230mm
4	Rectagular Field of View	80%	95%
5	Coil Selection		Head
6	Te (ms)	100	100
7	Tr (ms)	4052	shortest
8	Half scan	no	NO
9	Number of Signal Averages	3	3
10	Slices	20	16
11	View		Transeverse
12	Sense	No	NO
13	Clear	no	NO
14	Technique		T2w/tse
15	Scan Percentage	80	80
16	Flip angle(◦)	90	90deg

Note: RAW_900.DATA is scanned on 11 months old patient

As mismatching the data to k-space graph is not tolerable, the gateway program must be very accurate in reading the DATA file and for this, understanding how the data is organized became essentially important to write the gateway functions.

In the LIST file, comments are represented by '#' sign, while each information line begins with a dot (.). First information is about the scan itself, the scan name and software versions as seen in Table 5.3 below.

The general information is the next information. Table 5.4 shows general information, where we could identify that there are 3 slices (number of locations) and 2 echo scans (number of echoes) making a total of 6 two-dimensional (number of encoding dimensions) images in total.

Table 5.3
Extract from RAW_789.LIST; Part 1

```
# === DATA DESCRIPTION FILE ==========================================================
#
# CAUTION - Investigational device.
# Limited by Federal Law to investigational use.
#
# Scan name   : REC B10:MS,S
# Dataset name: RAW_789
#
# Gyroscan SW release           : 9.1-1
# Reconstruction Host SW Version :   3
# Reconstruction   AP SW Version :  23
#
```

Table 5.4
Extract from RAW_789.LIST; Part 2

```
# === GENERAL INFORMATION ============================================================
#
# n.a. n.a. n.a.  number of ...                          value
# ---- ---- ----  ---------------------------------   -----
.    0    0    0  number_of_mixes                   :     1
#
# mix  n.a. n.a.  number of ...                          value
# ---- ---- ----  ---------------------------------   -----
.    0    0    0  number_of_encoding_dimensions     :     2
.    0    0    0  number_of_dynamic_scans           :     1
.    0    0    0  number_of_cardiac_phases          :     1
.    0    0    0  number_of_echoes                  :     2
.    0    0    0  number_of_locations               :     3
.    0    0    0  number_of_extra_attribute_1_values :     1
.    0    0    0  number_of_extra_attribute_2_values :     1
.    0    0    0  number_of_signal_averages         :     1
```

The image size, range of k-space coordinated and range of actual image are detailed next. The k-space coordinates starts from -256 to 255 for x axis and -128 to 127 for y axis. Meaning the k-space plot is 512 X 256 points for both echo sequence 0 and echo sequence 1. X axis in k-space data is over sampled to accommodate the real and imaginary data separately. Considering real and imaginary data for each point will lead to a 256 X 256 final image size with image coordinate ranges from -128 to 127 on x-axis and -256 to -1 on y axis. Therefore, final image size would be 256 X 256. This information also reveals that there are 512 data points for each column in the DATA file.

Table 5.5
Extract from RAW_789.LIST; Part 3

```
#
# mix  echo n.a.  k-space coordinate ranges          start  end
# ---- ---- ----  ---------------------------------  -----  -----
.    0    0    0  kx_range                        :  -256    255
.    0    0    0  ky_range                        :  -128    127
#
.    0    1    0  kx_range                        :  -256    255
.    0    1    0  ky_range                        :  -128    127
#
# mix  echo n.a.  k-space oversample factors        value
# ---- ---- ----  ---------------------------------  ---------
.    0    0    0  kx_oversample_factor            :    2.0000
.    0    0    0  ky_oversample_factor            :    1.0000
#
.    0    1    0  kx_oversample_factor            :    2.0000
.    0    1    0  ky_oversample_factor            :    1.0000
#
# mix  n.a. n.a.  reconstruction matrix             value
# ---- ---- ----  ---------------------------------  -----
.    0    0    0  X-resolution                     :   256
.    0    0    0  Y-resolution                     :   256
#
# mix  echo loca  imaging space coordinate ranges   start  end
# ---- ---- ----  ---------------------------------  -----  -----
.    0    0    0  X_range                          :  -128    127
.    0    0    0  Y_range                          :  -256     -1
.    0    0    1  X_range                          :  -128    127
.    0    0    1  Y_range                          :  -256     -1
.    0    0    2  X_range                          :  -128    127
.    0    0    2  Y_range                          :  -256     -1
#
.    0    1    0  X_range                          :  -128    127
.    0    1    0  Y_range                          :   256      1
.    0    1    1  X_range                          :  -128    127
.    0    1    1  Y_range                          :   256      1
.    0    1    2  X_range                          :  -128    127
.    0    1    2  Y_range                          :   256      1
#
```

From Table 5.6, the LIST file further describes the DATA as complex data vectors of different types, namely STD, REJ, PHX, FRX, NOI and NAV, where each of the type is been detailed. It appears that the data of our interest belongs to STD. Furthermore, this data are complex data vectors; represented as binary data in little endian single precision IEEE float format.

Table 5.6
Extract from RAW_789.LIST; Part 4

```
#
# Complex data vector types:
# --------------------------
# STD = Standard data vector (image data or spectroscopy data)
# REJ = Rejected standard data vector#       (only for scans with arrhythmia rejection)
# PHX = Correction data vector for EPI/GraSE phase correction
# FRX = Correction data vector for frequency spectrum correction
# NOI = Preparation phase data vector for noise determination
# NAV = Phase navigator data vector
#

#
# The complex data vectors are represented as binary data in little endian single precision IEEE float format.

|
```

Table 5.7
Extract from RAW_789.LIST; Part 5

```
# Identifying attributes of complex data vectors:
# -----------------------------------------------
# The next table specifies the identifying attributes for each type of complex data vector:
#
# typ mix   dyn   card  echo  loca  chan  extr1 extr2 ky    kz    aver  sign  rf    grad  enc   rtop  rr    size   offset
# --- ----- ----- ----- ----- ----- ----- ----- ----- ----- ----- ----- ----- ----- ----- ----- ----- ----- ------ ------
#
# STD   *     *     *     *     *     *     *     *     *     *     *     *     *     *
# REJ   *     *     *     *     *     *     *     *     *     *     *     *     *     *
# PHX   *                 *     *     *                                       *     *     *
# FRX   *                 *     *     *                                       *
# NOI                     *     *
# NAV   *     *     *     *     *     *     *     *     *     *     *     *     *     *
#
# === START OF DATA VECTOR INDEX ======================================================
#
# typ mix   dyn   card  echo  loca  chan  extr1 extr2 ky    kz    aver  sign  rf    grad  enc   rtop  rr    size   offset
# --- ----- ----- ----- ----- ----- ----- ----- ----- ----- ----- ----- ----- ----- ----- ----- ----- ----- ------ ------
#
  NOI     0     0     0     0     0     0     0     0     0     0     0     1     0     0     0     0     0 159744 0
  FRX     0     0     0     0     0     0     0     0     0     0     0     1     0     0     0     0     0   2048 159744
  FRX     0     0     0     1     0     0     0     0     0     0     0     1     0     0     0     0     0   2048 161792
  FRX     0     0     0     0     1     0     0     0     0     0     0     1     0     0     0     0     0   2048 163840
  FRX     0     0     0     1     1     0     0     0     0     0     0     1     0     0     0     0     0   2048 165888
  FRX     0     0     0     0     2     0     0     0     0     0     0     1     0     0     0     0     0   2048 167936
  FRX     0     0     0     1     2     0     0     0     0     0     0     1     0     0     0     0     0   2048 169984
  STD     0     0     0     0     0     0     0     0   127     0     0     1     0     0     0     0     0   4096 172032
  STD     0     0     0     1     0     0     0     0   127     0     0     1     0     0     0     0     0   4096 176128
  STD     0     0     0     0     2     0     0     0   127     0     0     1     0     0     0   333     0   4096 180224
  STD     0     0     0     1     2     0     0     0   127     0     0     1     0     0     0   333     0   4096 184320
  STD     0     0     0     0     1     0     0     0   127     0     0     1     0     0     0   666     0   4096 188416
  STD     0     0     0     1     1     0     0     0   127     0     0     1     0     0     0   666     0   4096 192512
  STD     0     0     0     0     0     0     0     0   126     0     0     1     0     0     0     0     0   4096 196608
  STD     0     0     0     1     0     0     0     0   126     0     0     1     0     0     0     0     0   4096 200704
```

The Institute of Electrical and Electronics Engineers, Inc (IEEE) has defined standards for floating point representations and computational results. Floating points either REAL numbers or COMPLEX number are categorized into 3 precisions as follows:

a. Single Precision contains 4 consecutive BYTES of binary numbers

b. Double Precision contains 8 consecutive BYTES of binary numbers

c. Extended Precision contains 16 consecutive BYTES of binary numbers

While LITTE ENDIAN and BIG ENDIAN describes the byte ordering of octets. If the integer format is big-endian, the octets of the representation are ordered in the octet stream from the most significant octet to the least significant octet. If the integer format is little-endian, the octets of the representation are ordered in the octet stream from the least significant octet to the most significant octet. In another word, in BIG ENDIAN, the most significant byte (MSB) value is stored at the memory location with the lowest address; the next byte value in significance is stored at the following memory location and so on. While in LITTLE ENDIAN, the least significant byte (*LSB*) value is at the lowest address. The other bytes follow in increasing order of significance.

The IEEE single precision floating point standard representation requires a 32 bit word, which may be represented as numbered from 0 to 31, right to left. The 31st bit is the sign bit, *S*, the next eight bits are the exponent bits, 'E', and the final 23 bits are the fraction 'F':

Complex single precision data is 8 contiguous bytes containing a pair of 4 bytes of REAL. The higher order 4 bytes contain REAL (4) data that represents the imaginary part of the complex number as shown in Figure 5.2.

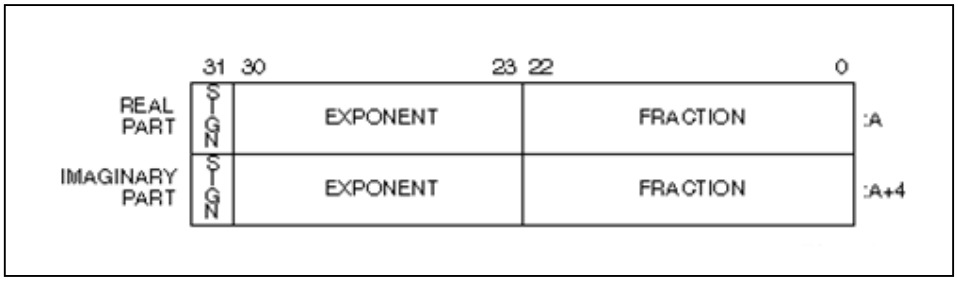

Figure 5.2: Complex Single Precision IEEE Format

Generally, the complex data inside DATA file are ordered sequentially as (real0, imag0, real1, imag1, real2, imag2 …. real N, imag N). It is consequent array of binary numbers representing k-space data points. Total number of data expected can be calculated from x range and y range given. Each data points are identified by byte offsets.

Table 5.8
Extract from RAW_789.LIST; Part 6

```
# === START OF DATA VECTOR INDEX ================================================
#
# typ mix   dyn   card  echo  loca  chan  extr1 extr2 ky    kz    aver  sign  rf    grad  enc   rtop  rr    size   offset
# --- ----- ----- ----- ----- ----- ----- ----- ----- ----- ----- ----- ----- ----- ----- ----- ----- ----- ------ ------
#
  NOI     0     0     0     0     0     0     0     0     0     0     0     1     0     0     0     0     0 159744 0
  FRX     0     0     0     0     0     0     0     0     0     0     0     1     0     0     0     0     0   2048 159744
  FRX     0     0     0     1     0     0     0     0     0     0     0     1     0     0     0     0     0   2048 161792
  FRX     0     0     0     0     1     0     0     0     0     0     0     1     0     0     0     0     0   2048 163840
  FRX     0     0     0     1     1     0     0     0     0     0     0     1     0     0     0     0     0   2048 165888
  FRX     0     0     0     0     2     0     0     0     0     0     0     1     0     0     0     0     0   2048 167936
  FRX     0     0     0     1     2     0     0     0     0     0     0     1     0     0     0     0     0   2048 169984
  STD     0     0     0     0     0     0     0     0   127     0     0     1     0     0     0     0     0   4096 172032
  STD     0     0     0     1     0     0     0     0   127     0     0     1     0     0     0     0     0   4096 176128
  STD     0     0     0     0     2     0     0     0   127     0     0     1     0     0     0   333     0   4096 180224
  STD     0     0     0     1     2     0     0     0   127     0     0     1     0     0     0   333     0   4096 184320
  STD     0     0     0     0     1     0     0     0   127     0     0     1     0     0     0   666     0   4096 188416
  STD     0     0     0     1     1     0     0     0   127     0     0     1     0     0     0   666     0   4096 192512
  STD     0     0     0     0     0     0     0     0   126     0     0     1     0     0     0     0     0   4096 196608
```

From Table 5.8, the first 169984 are header files which can be ignored. Reading for data starts from bit 169984. For y axis number 127, there are 4096 bytes which corresponds to 512 data of 8 byte (4 byte for Real and 4 bytes for Imaginary part). Such consequence 2 of 4 bytes makes one complex number. This data can be read 8 bytes or 4 bytes in 'Converter' program.

DATA file, RAW_789. DATA as in Table 5.8 is simple as it contains only 6 images. From Figure 5.8 the *ky* of 127 repeated 6 times, each for 1 image. First 2 lines are for first and second echo of Slice number 0. Data for slices (images) are arranged as:

Line 1: Y=127, Data for x= 1…512 of Image for Slice 0 echo 0
Line 2: Y=127, Data for x= 1…512 of Image for Slice 0 echo 1
Line 3: Y=127, Data for x= 1…512 of Image for Slice 2 echo 0

Line 4: Y=127, Data for x= 1…512 of Image for Slice 2 echo 1
Line 5: Y=127, Data for x= 1…512 of Image for Slice 1 echo 0
Line 6: Y=127, Data for x= 1…512 of Image for Slice 1 echo 0

Using this information provided in LIST file, a gateway function or converter program is written to read the binary complex data in an image matrix. The slice sequence as shown above must be understood clearly before writing a converter program. Not in all cases the slices are arranged sequentially.

5.5 CONVERTER PROGAM

As we have seen in previous section, the DATA file is a sequence of binary data file representing the complex k-space data. Different data points are identified by offsets. Data from raw data file are in scrambled order; such the converter program objective is to read data line by line and re-arrange it in the natural order which suits readable image format. For example, Matlab® expects the image data in a 2 dimensional matrix format, so the data is re-arranged as I(row, column). The complexity of this program depends on number of images, number of echo scans and their arrangement in the DATA file.

Two versions of converters were written in Matlab® in this thesis. The first one is to read a simple DATA file which consists of a single slice, conventional spin echo, scan percentage of 100%, reconstruction matrix equals to acquisition matrix, no sense and no clear. Writing codes to read this simple sequence is direct, provided one knows how to it via programming languages or applications such as Matlab®. File associate commands such as '*fopen*','*fread*','*fseek*','*frewind*' and '*fclose*' are used to open and read the DATA file.

Algorithm below shows implementation of Converter Program for a simple 1 slice file:

I. Input parameters such as *headerbyte*, *matrix size*, *reconstruction matrix size*, are defined.

II. Open raw data file; specify the file format as 'little endian format'.

III. Navigate to start of data , ignoring header bytes from beginning of file

IV. Read the entire data into one single matrix , *A*=[1,total data]; where total data is x-range X y-range

V. Reorder *A* into size of [*x_range* , *y_range*]

VI. Matrix *B_real* reads Real values from *A* and Matrix *B_imag* read Imaginary values from *A* (the next 32 bit data).

VII. Matrix *C* as complex of *B_real* and *B_imag.*

The single slice raw data files are straight forward, but unfortunately, setting for simplest parameters as above would lead to a distorted or heavily blurred images. Such files can be used to verify the understanding of raw data format and organization. A true scan will have more complex data files.

The second converter program was written to read a complete scan file. RAW_900.DATA (scanned on patient) has 16 slices with 2 echo sequence; total to 16 images. The data arrangement is not in order (slice 0 echo 0, slice 0 echo 1, slice 1 echo0 …) but in an interleaved sequence as: Slice 0, Slice 2, Slice 4, Slice 6, Slice 8, Slice 10, Slice 12, Slice 14, Slice 1, Slice 3, Slice 5, Slice 7, Slice 9, Slice 11, Slice 13 and Slice 15. Each slice data were repeated twice; once for each echo sequence. So the data sequence must be identified accurately, for example, selecting data related to slice 3, echo 0. To identify slices, the sequence is re-numbered according to its position: Slice 0 echo 0 -> Position 1, slice 0 echo 1 -> position 2 etc. This position is used to 'navigate' through the binary raw data file, RAW_900.DATA. The algorithm to read RAW_900.DATA is as below:

I. Input parameters such as *headerbyte, matrix size, reconstruction matrix size, image number (slice sequence), echo number* are defined.

II. Determine the *slice_position* using *if-statement* , *switch* statement or mathematical equation

III. Open raw data file; specify the file format as 'little endian format'.

IV. Define *start_of_data* = *headerbyte+(slice_position*offset_to_silce_position)*

V. Use *for-loop* to read rows of each column of the image matric, navigate to respective *bit_position* . In each column, read the entire row, and rearrange to form complex matrix

```
For ( i from 1 to y_range)
{
      Define bit_position as start_of_data*col_num;
     Navigate to bit_position
       For(j from 1 to x _range)
       {
         read '32' bit data into A_real;
         read next '32' bit data into a_image;
         }
      Rewind data file
}
```

VI. Matrix *A_real* and *A_imag* is reformed into a complex-value matrix

5.6 COMPUTATIONAL REQUIREMENTS

5.6.1 Software

Matlab®, a high-performance language for technical and scientific computing is used as platform for algorithm implementation. Programs were written in Matlab® -m file format to read the raw data, FFT Reconstruction, 2D ARMA and to display reconstructed images. Matlab® is fast, reliable with many built-in-functions; it integrates computation, visualization, and programming in an easy-to-use environment

5.6.2 Hardware

Following is the workstation information used in this thesis which resembles reconstructor workstation used in Philips® MRI Scanner:

Model: Dell Precision 670

Processor: Dual Processor of Intel® Xeon™ CPU 3.2GHz

Memory: 4GB of DDR2 533 Mhz

Graphics: 256M External Graphic Card: NVDIA Quadro FX3400

Display: 19in TFT Flat Panel

5.7 IMPLEMENTATION

Simulation of MRI reconstruction from raw data in this thesis was implemented in 4 stages, namely:

a. Implementation and testing the Converter programme.
b. Implementation and testing of MRI Reconstruction using 2D IFFT.
c. Implementation and testing of MRI Reconstruction using 2D ARMA, solved with proposed MTERA.
d. Graphical and Statistical analysis of reconstructed images

The Converter function or 'gateway' function is written to read the binary (IEEE Single Precision format) raw data file into 2 dimensional matrix formats. The converter function opens the raw data file, navigates to data points and rearrange into a Matlab® image matrix. CP is implemented according to algorithm explained in Section 5.5.

If the data is arranged in an ascending order, i.e. *data1, data2 …. Data N*, then reading and re-arranging are simple and direct. Data can be read into a single array of 1 X T, and later re-arrange into M X N matrix representing the image size. But this is

not always true in Philips® raw data, especially for scans with more than 1 image. The data is arranged in an interleaved fashion, such it is shown in Table 5.9:

Table 5.9
Data arrangement in a raw data file

Slice 1 Data 1, Slice 2 Data 1 …. Slice K, Data1 *Slice 1 Data 2, Slice 2 Data 2 …. Slice K, Data2* *Slice 1 Data 3, Slice 2 Data 3 …. Slice K, Data2* *Slice 1 Data N , Slice 2 Data N, …. Slice K, Data N*

To read this kind of data arrangement, the file pointer is set to start and read the first data of selected slice. To read consequent data bytes, file pointer is repositioned to start of file and data offset is recalculated based on total byte in each sequence. Each line in Table 5.9 is defined as a sequence, which has data for a one row of image matrix. A *slice-sequence* variable is defined if slices are not arranged in sequence as in Table 5.9 . For example for row 1, slices are arranged 1, 3, 5, 7, 9, 11, 15, 2, 4, 6, 8, 10, …, Slice K . This type of arrangement is seen in raw data file, RAW2000.DATA shown in Table 5.11.

In raw data set raw_2000, odd numbered slices are arranged first and followed by even numbered slices. To read this, the file pointer is initialed to start of file and navigate to required slice and data by computing the offset of required data. A variable called BitStartPoint is used and re-initialized as:

$$BitStartPoint=OFFSET+(SliceSequence1)*4096+((1)*OneSetDataSequenceByte \quad (5.1)$$

where,

BitStartPosition : To navigate the file pointer to this position

OFFSET : Defines noise offset which need to be ignored

SliceSequence : Slice position

OneSetDataSequenceByte : Total byte of data in the sequence

i = number of data points, $1 \le i \le N$

Some parts of converter programme' code is displayed in Table 5.10 Upon finish reading and re-arranging the raw data, a message is displayed to verify total number of data read by the program (Table 5.11).

Second part of the simulation program is 2D IFFT Reconstruction. 2D IFFT is very direct and applied according to algorithm in Chapter 3.2. A flow chart of FFT reconstruction is given in Figure 3.2. The image data is zero filled to achieve 2^n number of points in any truncating axes. Table 5.12 shows codes of IFFT implementation.

Table 5.10
Example of a converter function

```
 [fid,msg] = fopen(DATAFILE,'r',littleendianformat);
for i=1:YRANGE
    %set the offset
     BitStartPoint = OFFSET + (SliceSequence -1)*4096 + ((i-1) *
OneSetDataSequenceByte );
     ;
     fseek(fid, BSP, 'bof');
     jj=1;
     countx=0;
     for j=1:XRANGE

        % [R(j,i),count] = fread(fid, XRANGE*2, 'float','l');
       [R(j,i),count1] = fread(fid, 1, 'float','l');
      [I(j,i),count2] = fread(fid, 1, 'float','l');

     countxy=count1+count2;

     countx=countx+countxy;
     end
     BSP = BSP + OneSetDataSequenceByte ;
     starty= starty -1;
     frewind(fid)
end
```

Implementation of IFFT is direct and simple using Matlab®. From Figure 5.12, C1 is the image matrix read with a converter function. By using *ifft2*, FFT is computed and also zero-padded to 512 X 256 if C1 is truncated in any direction. Zero padding in MRI data has been proved did not produce any additional artifacts, but rather increases the resolution of image produced. The effects of zero padding have been discussed in Chapter 3.

Finally the third stage is 2D ARMA function implemented as in Chapter 4.3. There are few ways that 2D ARMA can be implemented. One way is to model directly both axes with 1D MTERA. Another approach is to perform 2D IFFT, followed by 2D FFT and 1D MTERA horizontally and vertically. Neither of this produces a clear image.

Table 5.11
Output of a converter function

```
Step1: Reading Philips Data File
-------------------------------------------------------
Raw Data file                    : RAW_2000.DATA
Header Offset                    : 225280
Data Bytes To Read               : 24375296
K-space cordinate range of X     : -255  -  256
K-space cordinate range of Y     : -93  -  92
Points at X-Vector (X-cordinate) : 512
Points at Y-Vector (Y-cordinate) : 186
Total Data Expected              : 6094848
Slaid Number                     : 13
Actual Slaid Number              : 12
Slaid Numbering                  : 1, 2, 3....16
Echo Sequence                    : 1
Position of Required Slice       : 14
Data Points For 1 Slaid          : 95232
TotalByte (R+I) for One ROW      : 4096
Total Data Sequence              : 32
OneSetDataSequenceByte           : 131072
```

Table 5.12
Code for FFT implementation

```
im = ifft2(C1,512,256);
im3 =fftshift(abs(im2),1);
%[sa,as]= size(im)

figure(1);
colormap gray;
imshow(abs(im3),[]);
title('2D IFFT Image');
axis on;
```

Another approach is to reconstruct the columns using IFFT and rows are reconstructed using 1D MTERA. These are followed by FFT the column and reconstruct again using 1D MTERA. By using the approach we have achieved 2D ARMA and this approach produces a clear image.

5.8 RESULTS

Images were reconstructed from phantom image of raw data set, raw_2000. This raw data set contains 16 different images with two different echo scan, which totals to 32 images. Although all 32 images are contained in same file, the images are different and represent different level of human tissue. Such each slice can be accessed and processed separately. Each raw data image has a size of 512 X 186 and is zero padded to 512 X256. 2D IFFT and 2D ARMA are applied as been explained in previous section and Chapters.

5.8.1 Intensity Plot

Results of intensity plot during reconstruction are presented here. All images are reconstructed from slice number 13, echo number of 1 from raw data 2000.

Figure 5.3(a) and 5.3(b) show absolute value of rows and columns of a rearranged k-space data. Since the data represents intensity of each pixel, these graphs are also known as intensity graphs. As the highest intensity is concentrated in the mid section of k-space Cartesian plot, two sided quasi-exponential decay; which is decreasing and increasing exponential form from mid point is clearly visible. This justifies the need for generating the Hermitian and anti-Hermitian Series. While, Figure 5.4 (a) and (b) show absolute values after an initial 1D FFT on columns of raw data. Before phase-shift, the reconstructed axes displays the data is diverse and placed at the beginning and end of the data. This is due to expectation of zero point, the FFT routine expects the zero point of the data is series on the beginning, that is $s_0, s_{1.}, \cdots s_n$, while the raw data contain data from –n to n-1 through 0. A phase-shift will eradicate this error. This is displayed in Figure 5.5(a) and Figure 5.5(b). From Figure 5.6, the data of reconstructed axes are in the middle, while in the non-reconstructed axes, the data still exhibits the quasi-exponential shape.

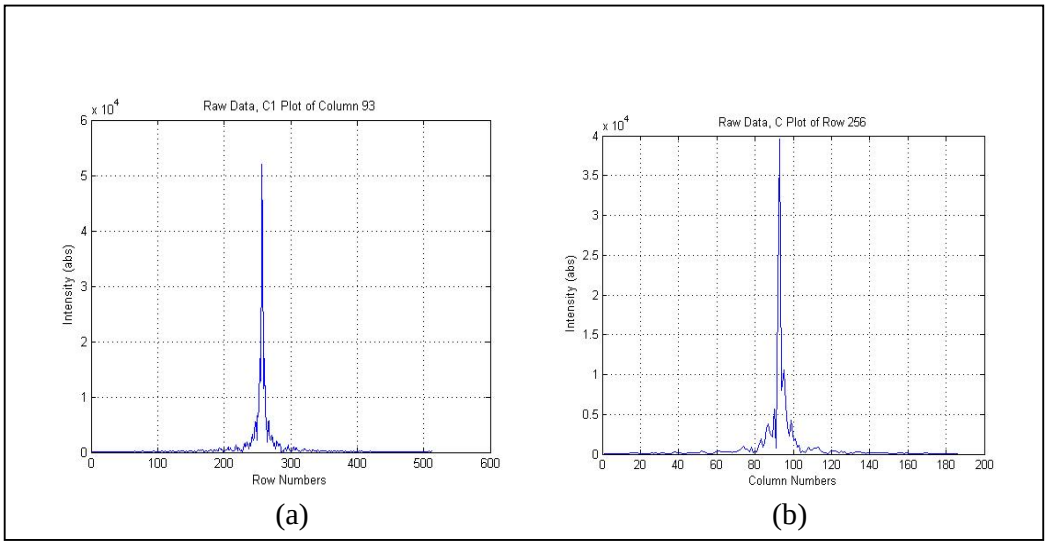

Figure 5.3 Intensity Plot of raw data (a) row column 93 and (b) row 256

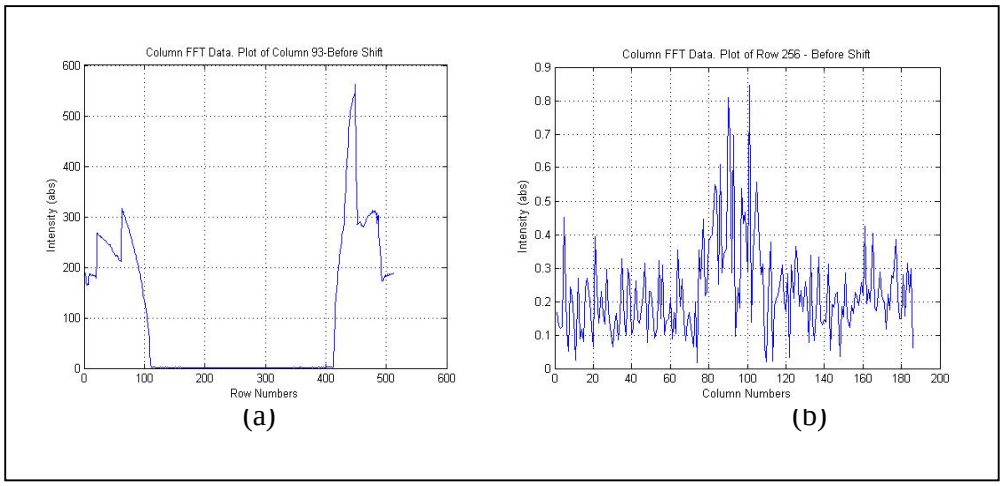

Figure 5.4: Intensity plot after 1D IFFT on columns

For a complete reconstruction, another 1D IFFT on rows are required. Figure 5.6 is plotted from image reconstructed using 2D IFFT. While Figure 5.7 shows the same raw data which is reconstructed using 2D ARMA using MTERA algorithm.

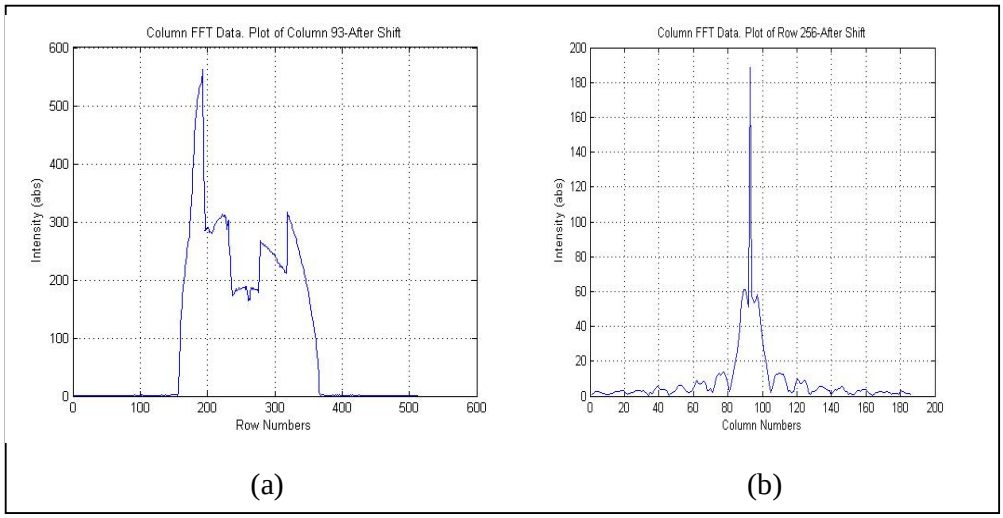

Figure 5.5 Intensity plot after 1D IFFT and phase-shift

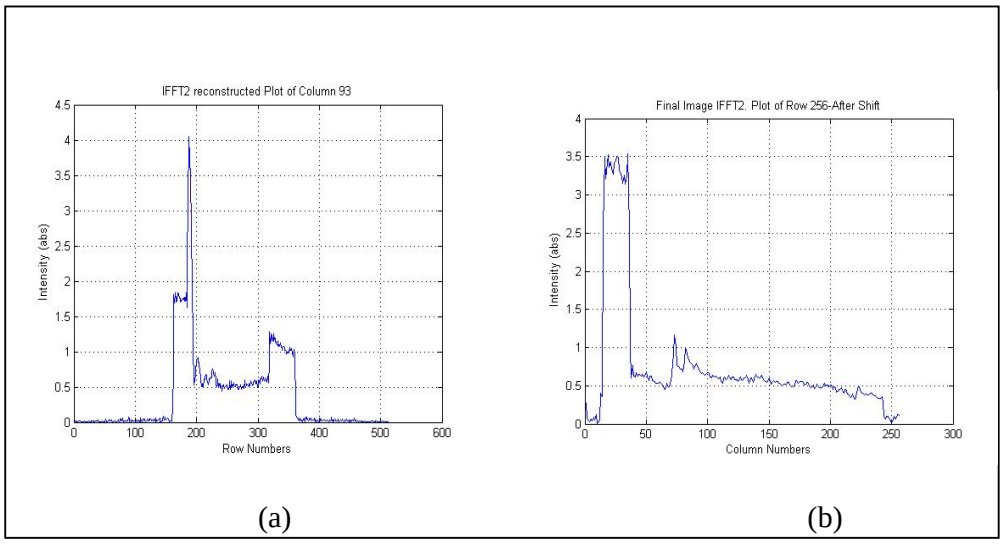

Figure 5.6 Intensity plot image reconstructed using 2D IFFT

Both Figure 5.6 and Figure 5.7 exhibits the same shape as they represents the same image reconstructed using the same data, but different method. There are some differences in Figure 5.7 and Figure 5.8, which will be discussed in next section. One question can put over here, do the Figure 5.6 exhibits the Gibbs phenomena?

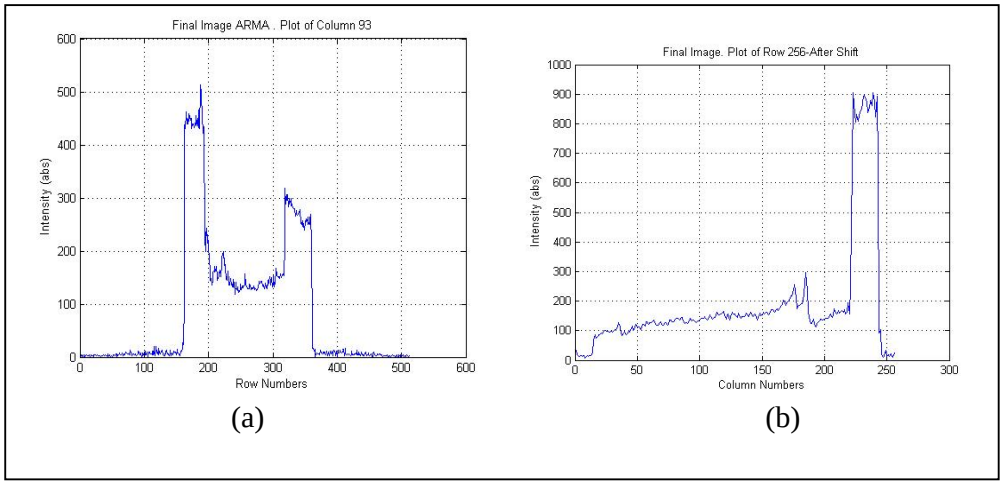

Figure 5.7 Intensity plot for image reconstructed using 2D ARMA

5.8.2 Final Image

Final images for both 2D IFFT and 2D ARMA, implemented using MTERA algorithm is shown in Figure 5.8 and Figure 5.9 respectively. Figure 5.8 shows image reconstructed for slice number 13, echo 1 of RAW_2000.DATA. While Figure 5.9 shows reconstructed images for slice number 1, echo number 1 from the same raw data set.

These images are discussed more in detail in Section 5.9.

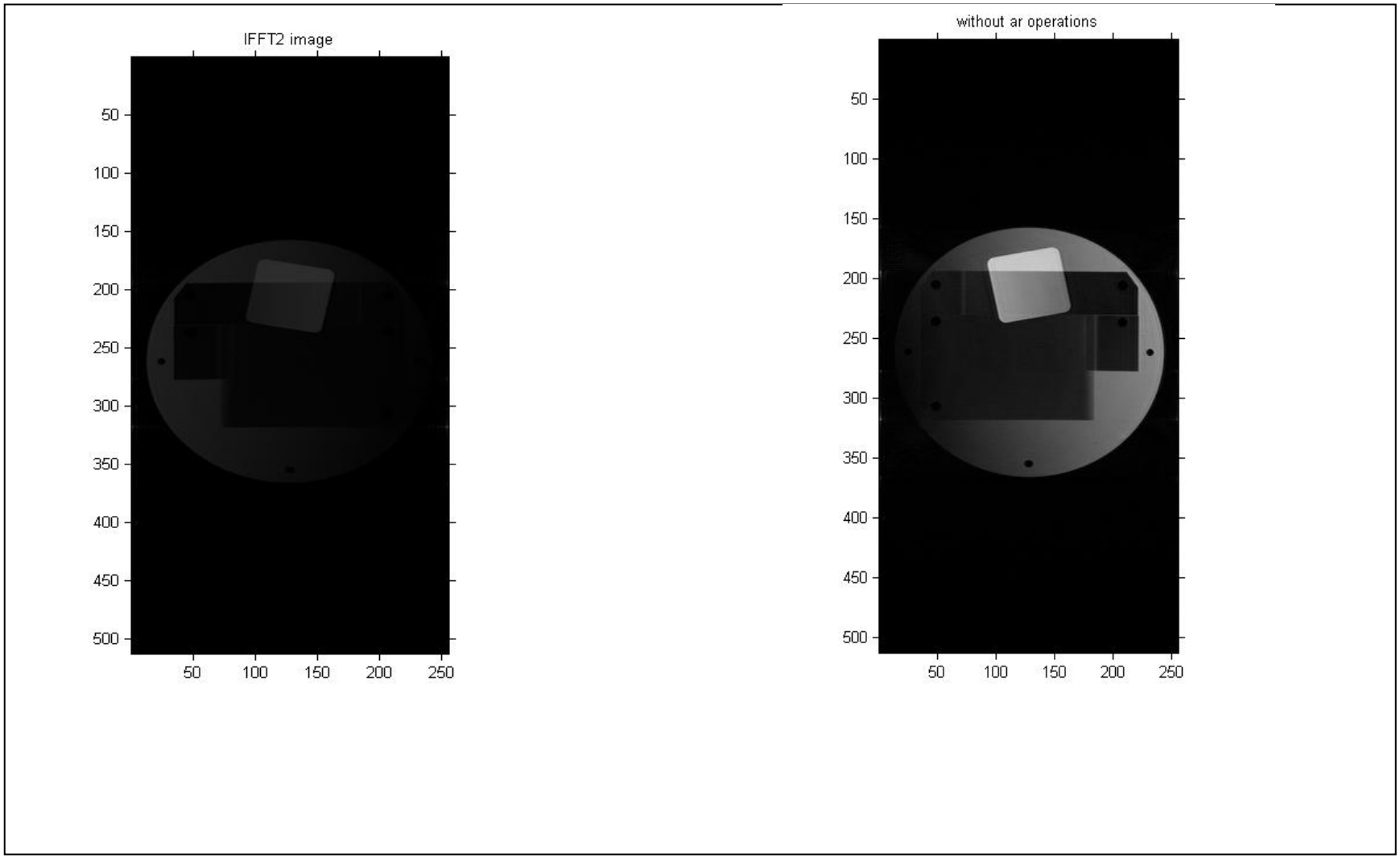

Figure 5.8: Final Image of Slice 13 for 2D IFFt and 2D ARMA

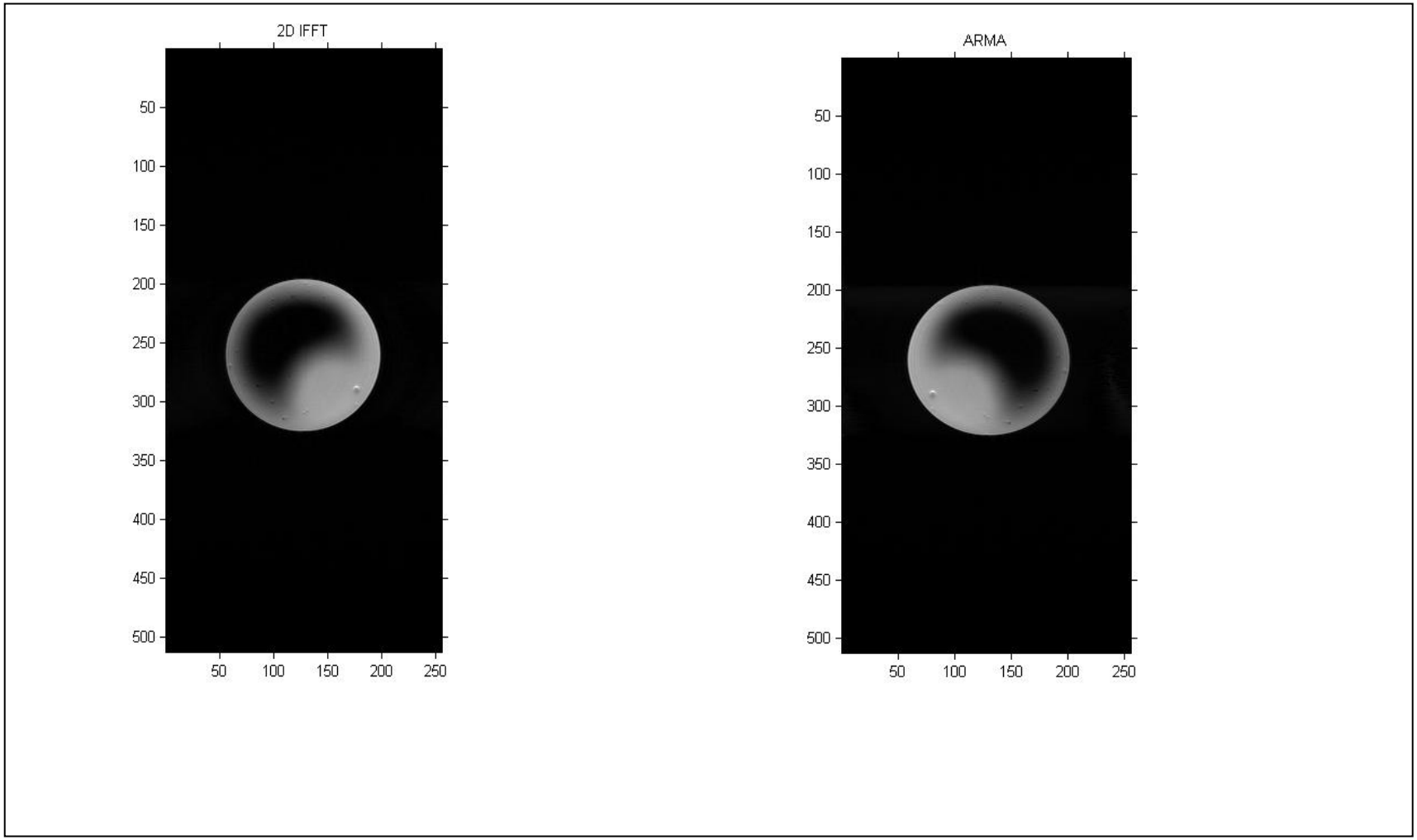

Figure 5.9: Final Image of Slice 1 for 2D IFFT and 2D ARMA

5.8.3 Performance Metrics

There are many performance criteria that we could use to generate some important properties from reconstructed images. In particularly, for MRI, Signal to Noise Ratio (SNR) and CNR would be a useful performance description. Unfortunately, both involve measurements of some hardware properties which were not obtained. For example, SNR computation for statistical noise (Chapter 2.5.3) is computed as [Hendrick, (2000)]:

$$SNR\,\alpha\,\frac{S(1)}{\sigma_o}(\sqrt{T_{tot}/TR}\sqrt{TE-T_c})V \qquad (5.2)$$

where:

S(1) are signals from a single acquisition per phase-encoding step from a pulse sequence

TR is Relaxation Time

TE is echo time

$T_{tot} = TR * N_{acquisition} * N_{phaseeencoding}$

T_c is a time constant which is defined by $TE \geq T_s + T_c$

A different approach to calculate SNR would be as a proportion of mean signal to the standard deviation of the pixel values. This definition is adopted although it does not reveal the actual content of noises, but rather describes the pixel to pixel variation of individual images.

The type of noise which is useful is systemic noise which includes Gibbs ringing which appears itself as spurious ringing in the image. Systemic noises are observed in final images rather than measured quantitatively.

Image resolution can be displayed as intensity mean. This is direct computation of signal averages. Higher intensities display images with higher

resolution. Mean, reconstruction time, pixel variance and pixel standard deviation are presented in Table 5.13 below:

Table 5.13
Statistical Measurement of Reconstructed Images

	Slice Number 13		Slice Number 1	
Parameters	2D IFFT	2D m-TERA	2D iFFT	2D m-TERA
Mean	0.429	109.44	0.2864	75.69
Mean Square	0.9462	61531.00	0.8271	53400
Variance	0.721	49550.00	0.747	46700
Standard Deviation	0.873	222.60	0.8623	216.22
Recon. Time (s)	3.43	166.76	3.36	204.98
SNR	0.4914	0.49	0.3318	0.3473

5.9 RESULTS DISCUSSION

Images were reconstructed from matrices with 512 data samples in each row and 186 data samples in each column. Before 2D IFFT and 2D MTERA applied, the data matrices were zero padded to 512 by 256. A ‘pure’ reconstruction was done, meaning no filtering, resolution increment or rotation done to image produced by both reconstruction techniques. Although IFFT reconstructed images can be processed further, this is not been done, as the objective is to compare the pure IFFT and ARMA method to exhibit the effectiveness of ARMA in removing noise.

For IFFT reconstructed images, IFFT was applied to rows, and followed by columns. While it is not the case with 2D MTERA, where columns were reconstructed using IFFT and rows were reconstructed using MTERA algorithm. Then columns were then constructed again using FFT and modeled with MTERA. Attempt to model the 2D MTERA directly, does not appear to be successful.

Results of these reconstructions were displayed in previous section. First the intensity (absolute values) during each phase of reconstruction was presented followed by comparison of images produces.

Figure 5.3 is plot of raw data. This plot verifies the accuracy of converter program as it displays the quasi exponential shape, the typical form of MRI raw data.. Note the shape of the columns and rows displays a decaying two sided quasi-exponential increment and decrement from and to the center of data. When one axes is reconstructed using IFFT, the other axes remains unchanged. This is displayed in Figure 5.4 and 5.5. Without phase-shift, the data are in distorted order due to FFT routine expectation of zero-point. It expects the data to be arranged from 0 to N while the actual raw data is arranged from $-N/2$ to $N/2-1$ through 0.

Direct comparison of the intensity of 2D ARMA using MTERA method and 2D IFFT were presented in Figure 5.6, and Figure 5.7. A spike is clearly seen in Figure 5.6(a) near row number 200. This is due to truncation artifacts or Gibbs phenomenon. These spikes are suppressed in Figure 5.7(a) in which the MTERA method was applied. Although the Gibbs ringing were seen in the intensity plot, this is not always the case as the Gibbs overshoot will be hidden when used with large data sets such as 256 points. The effect of Gibbs is only observed as loss of resolution.

Figure 5.8 and Figure 5.9 displays the final images reconstructed using 2D MTERA and 2D IFFT final images. The IFFT image are tilted and flipped, which needs to be restored to the original form. A quick look shows that there is improvement in resolution in MTERA images. This is not surprising, as it is also indicated in pixel intensity count at Table 5.13. For both images, 2D MTERA shows

remarkable improvement in image intensities, but as predicted the reconstruction times are about are 68 times slower for 2D MTERA. Again, this is due to huge computation of model orders and AR parameter estimation technique.

Although the reconstruction time is huge, 2D MTERA solved the issue of low resolution in IFFT images and suppressed the ringing artifacts. This is the trade off.

The suppression of the truncation artifacts and the improvements in resolution were observed to be related to the order of model order. Maximum model order calculated were 17, while high model order tends to generate spikes in final image. This spike can be viewed as bands of thick horizontal bars on image.

5.10 SUMMARY

A thorough analysis on MR image data has been presented in this chapter; ranging from the raw data to implementation of proposed modified TERA algorithm. Basically, DATA files are binary data file with headers which estimate noise and followed by the valuable raw data. The raw data is stored in IEEE single precision complex format as a continuous bytes starting after the header section. Each data points are differentiated by their offsets which can be computed based on IEEE single precision complex format (4 bytes for REAL and 4 bytes for IMAGINARY) in each row sequence. To read the binary files, a converter program is needed. An algorithm for a simple raw data file and a complete raw data file has been presented as well with lengthy explanation.

Implementation and results of 2D IFFT and 2D ARMA using modified TERA has been presented as well. Results were explored in three different aspects, that is from intensity graphs, final image and performance metrics in image statistics such as SNR, mean and standard deviation.

CHAPTER SIX

CONCLUSION

6.1 INTRODUCTION

In this thesis, a modified TERA or MTERA algorithm has been proposed to reconstruct MRI Images from raw data. The algorithm of MTERA has been presented in Chapter 4, while implementation and results has been presented in Chapter 5. In this chapter, conclusion of this thesis is presented and finally future work is recommended for this research work.

6.2 CONCLUSION

The MR Image is a map of the spectral information in the data. Normally this spectral information is obtained by applying the FFT algorithm to rows and columns of the matrix raw data, which eventually become the image.

2D IFFT is the current standard reconstruction technique used to reconstruct images acquired through various data acquisition techniques. If 2D IFFT could not be applied directly as in echo planner imaging, then some pre-processing steps are required. For data acquisition technique such as Parallel Imaging or spiral reconstruction technique, the 2D IFFT could not be applied directly. In this case the MR data are interpolated or data are restored from multiple beams before applying Fourier Transform (Bernstein et al, 2004). The intensive use of Fourier transform is due to its fast reconstruction time and its reliability in producing clinically trustable images. An evident of fast reconstruction timing can be viewed at Table 5.13, where each slice was reconstructed in 3 seconds. While practically, in Philips® MRI scanner

such as Achieve 3.0 T or Interra 1.5, by adopting parallel imaging technique, Fourier transform were used to reconstruct about 1200 images with size of 256 X 256 per second.

Despite the success of Fourier Transform, it has some inherit limitation which leads to loss of resolution, Gibbs phenomena viewed as spurious ringing in the image, and limited resolution. This limitation is due to fitting the finite discrete data sampling into an infinite smooth reconstruction equation as in equations 1.4, 3.13 and 3.15. These limitations are presented in detail as problem statement in Chapter 1.2.2, discussed as issues for MR Reconstruction in Chapter 2.5 and again in Chapter 3.2.2

Although the resolution can improved and filters can be applied on IFFT images, it leads to other issues such as suppression of tiny pathological representation in images and there are wide ranges of filter selections applied to various imaging sequence.

To overcome the limitation of Fourier transform, many alternate proposals has been made such as Modified Backprojection Method, Gegenbauer which concentrated on edge detection, Neural Network, Wavelet Method, Parametric modeling such AR and ARMA, etc. Among the alternate solution, one successful method is ARMA method. In solving for ARMA, method, one specific algorithm; Transient Error Reconstruction Approach (TERA) was proven to be a potential replacing algorithm for Direct Fourier technique. Despite the successful studies on TERA, however, this algorithm is not been selected for practical purpose due to its limitation especially lengthy computation time and image dependent due to model orders are not computed dynamically .

Realizing this limitation, a modified TERA (MTERA) approach was proposed in this thesis in Chapter 4.4. MTERA were proposed to compute the model order

dynamically for each series rather than fixing it. Taking advantage of current computing speed, the complex computation of model orders are made easy. Model orders are computes dynamically using TPE. This is discussed in detail in section 4.4.2. Example of computed model order is presented in Figure 4.4.

Based on this model order, AR coefficients for each series is determined using Yule-Walker method which utilized the correlation of input data to determine the AR coefficients. YW method as presented in section 4.4.3 is solved with Levinsion-Durbin Algorithm. This definitely reduces the computation time compared to Barrowdale method used by Smith which has many intrinsic computations. Then the prediction error is computed using equation 4.14 that is the prediction error alone, unlike in original TERA. The proposed MTERA is discussed in detail in section 4.4.

Basically, MTERA is different from TERA algorithm form 3 different perspective:

i. Use of TPE to compute model order dynamically for each row data and column data
ii. Model parameters are calculated using YW method
iii. Final data are estimated from Transient Error Sequence alone

1D parametric modeling using original TERA has been successfully implemented by Smith (Smith et al, 1986) and exhibit the significant improvements compared to Fourier transform. A 2D approach were attempted but not studied in detail. ID TERA application is applied by applying the TERA on truncated axis of MR data, while the non-truncated axis were reconstructed using IFFT. This is to reduce the reconstruction time.

Implementation of 2D MTERA is presented in sections 5.6 and 5.7. Algorithms were presented in detail and implementation results were presented in

section 5.8. Results were presented in 3 perspectives, the intensity graphs, final image and statistical analysis of reconstructed images. The results were discussed in detail in section 5.8.

Table 5.13 displays statistical description of reconstructed image. Out of 6 parameters computed, only 2 could be considered useful, that is the mean signal and reconstruction time. Mean signal shows the intensity of pixels indicating resolution level in the image. Both images show high level of resolution when reconstructed using 2D MTERA.

A huge difference in reconstruction time is shown in Table 5.13. IFFT images are reconstructed in 3.43 seconds and 3.36 seconds for image slices numbered 13 and number 1. While the same image slices were reconstructed in 166.76 seconds and 204.98 seconds respectively. As been explained earlier, the dynamic computation of model orders and AR coefficients contributes this delayed reconstruction time. However, the delayed reconstruction time paid off with high resolution images.

Finally From the intensity graphs, final images and Table 5.13 in chapter 5, it is clearly indicating and concluded that 2D ARMA with MTERA method provide higher resolution images with suppressed truncation artifacts.

6.3 SUMMARY AND RECOMMENDATTION FOR FUTURE WORK

It is clear from previous section, the 2D m-TERA produces high resolution image with suppressed truncated artifacts. The major problem with modeling algorithms is their success in image independent. The rate of independent has been reduced in m-TERA by adopting dynamic model order computation.

Although, it has been shown in this thesis that modeling produces image with higher resolution and suppressed truncated artifacts, this is not very clearly visible in a

phantom images as been used for this thesis. A much fairer justification is by testing on clinical images such as brain sequence which is rich of Gaussian noise. This will reveal more information such as clearly visible truncation artifacts.

The success of m-TERA depends on model order estimation. Model order has been a factor in producing stable images. Low model order tends to produce images which has no difference than IFFT image while higher model order tends to produces spikes in the image. Model order determination is factor contribute to computation time in ARMA method. Such a shorter and exact model order determination would be very beneficial in contributing more to this research. A faster reconstruction time could be achieved by faster model order determination algorithm.

Although Neural Network algorithm failed the clinical testing, but a combination of Neural network and m-TERA is proposed for future work on this title. The NN could be applied to determine exact model order in a short time, and then this model order can be feed into m-TERA for reconstruction.

Therefore, using of NN to determine model orders and feed into m-TERA to reconstruct clinical images is recommended for future work.

BIBLIOGRAPHY

Akaike, H. (1970). *Statistical predictor identification*. Annals of the Institute of Statistical Mathematics 22 (1970), pp. 203–217.

Barrowdale, I., & Erickson, R.E. (March 1980). *Algorithm for least square prediction and maximum entropy spectral analysis – Part 1: theory, geophysics.* Vol. 45(3) pp. 420 – 432 .

Basu, S., & Bresler, Y. (Oct 2000). *O(N2log2N) filtered backprojection reconstruction algorithm for tomography*. IEEE transaction on Image Processing, Volume 9, (10), Pg. 1760 – 1773.

Beatty, P.J., Nishimura, D.G., & Pauly, J.M. (2005). *Rapid gridding reconstruction with a minimal over sampling ratio*, IEEE Transactions on Medical Imaging, Vol. 24 (6)

Bernstein, M.A., King, K.F., & Zhou, X.J. (2004). *Handbook of MRI pulse sequences.,* USA: Elsevier Academic Press.

Blaimer, M., Breuer, F., Mueller, M., Robin, M.H., Mark, A., & Peter, M. J. (2004). *SMASH, SENSE, PILS, GRAPPA how to choose the optimal method*. Top Magnetic Resonance Imaging. Vol. 15 Number 4. Lippincott Williams and Wilkins. pp. 232 – 236.

Blanchet, G., & Charbit, M. (2006). *Digital signal and image processing using MATLAB*® (1st edtn.). United Kingdom: International Scientific and Technical Encyclopedia (ISTE).

Charles, W. T. (1992). *Discrete random signals and statistical signal processing*. (1st edn.). London: Prentice Hall International (UK) Limited.

Clare, S. (1997). *Functional MRI: methods and application.* Unpublished doctoral dissertation, University of Nottingham.

Davila, C.E., & Chiang, H.L. (1995). *An algorithm for pole-zero system model order estimation*. IEEE Transaction on Signal Processing, Vol. 43, No.4.

Ellard, D. (NA). *History of MRI*. Department of Clinical Radiology, University of Manchester. Retrieved September, 4, 2004. http://www.isbe.man.ac.uk/personal/dellard/dje/history_mri/history of mri.htm

EMRF (2003). *A short history of magnetic resonance imaging from a european point of view*. Retrieved September, 4, 2004. http://www.emrf.org/FAQs%20MRI%20History.html

Gottlieb, D., Shu, C.W., Solomonoff, A., & Vandeven, H. (1992). *On the gibbs phenomenon i: recovering exponential accuracy from the fourier partial sum of a non-periodic analytic function*. Journal of Computational Applied Mathematics. Vol 43 , pp. 81–98 .

Haacke, E.M., & Liang, Z.P. (2000). *Challenges of imaging structure and function in MR I*. IEEE Engineering in Medicine and Biology. Vol. 19, (5), Pg. 55 – 62.

Hendricks, R.E. (2000). *Image contrast and noise. Chapter 4 in methods in biomedical magnetic resonance imaging and spectroscopy,* Edited by I.R.Young, Vol. 1, New York: John Wiley Inc

Hornak J.P. (1996). *The basics of MRI*
http://www.cis.rit.edu/htbooks/mri/chap-11/chap-11.htm#11.1

Jackson, J.I, C.H Meyer & D.G. Nishimura (Sept 1991). *Selection of a convolution function for fourier inversion using gridding [computerized tomography application*]. IEEE Transactions on Medical Imaging, Vol 10, Issue 3, pg 473 – 478.

Kumar, A., Welti D., & Ernst, R. (1975). *NMR fourier zeugmatography*. Journal of Magnetic Resonance. Vol 18, pp. 69 – 83.

Liang, G., Wilkes M. (1993). *ARMA model order estimation based on the eigenvalues of the covariance matrix*. IEEE Transaction on Signal Processing. Vol. 41 (10).

Liang, Z .P, & Haacke, E.M. (1999). *Magnetic resonance imaging*. Encyclopedia of Electrical and Electronics Engineering , Edited by J.G. Webster , John Wiley and Sons, Vol.2 , pp. 412 – 426.

Liang, Z.P. & Lauterbur, P.C. (1999.). *Principles of magnetic resonance imaging: a signal processing perspective.* New York: IEEE Press.

Manolakis, G., Ingle, V.K., & Kogon, S.M. (2000), *Statistical and adaptive signal processing – spectral estimation, signal modeling, adaptive filtering and array processing*. Singapore: McGraw Hill International Editions.

McColl, R.W. & Scarlat, M.A.(1999). *Partial AR models with SVD*. Nuclear Science Symposium (IEEE), Vol.3, pg. 1292. Seatle, USA.

Nichols, S.T., Smith, M.R., & Salami, M.J.E. (1985). *Application of ARMA modeling to multi-component signals*. IPAC, United Kingdom.

Noll, D.C., & Sutton, B.P. (2003). *Gridding procedures for non-cartesian k-space trajectories.* Dept of Biomedical Engineering, University of Michigan. ISRSM Seminar MR Physics for Physicists.

Penner, A.R., Smith, M.R., & Nichols, S.T. (1989). *Noise reduction in magnetic resonance images using IDFT and TERA model reconstruction.* IEEE Engineering in Medicine and Biology Society. 11th Annual International Conference. Vol. 2, pp 642 – 643.

Philips® Medical Systems (2002 November, 29). Philips enables open access with new Medical IT family. PR Newswire Europe Ltd. Retrieved August 17,2004. http://www.prnewswire.co.uk/cgi/news/release?id=94849

Philips® Medical Systems (2006). *Online product information*. http://www.achats-publics.fr/Site-IRM/Achieva3,0T/Panorama-3,0T.htm

Pispatsrisawat, T., Gacic, A., Franchetti, F., Puschel, M. & Moura, J.M.F. (2005). *Performance analysis of the filtered backprojection image reconstruction algorithms.* IEEE International Conference on Acoustics, Speech, and Signal Processing. Vol. 5 , pg. 153 – 156.

Press, W.H., Flannery, B.P., Teukolsky, S.A., & Veterling, W.T. (1992). *Numerical recipes in C*. United Kingdom: Cambridge University Press, Cambridge,.

Rodriguez, A.O., (2004). *Principle of magnetic resonance imaging.* Universidad Autonoma Metroplolinata Istapalapa.

Rogers, B.P. (2004). *Examples of MRI artifacts.* University of Wisconsin-Madison Retrieved February, 23, 2005 http://vuiis.vanderbilt.edu/~rogersbp/mrartifacts.html

Salami, M.J. (1986). *Modified cadzow method for ARMA.* Unpublished doctoral dissertation, University of Calgary, Canada.

Schomberg, H., & Timmer, J. (Sept 1995). *The gridding method for image reconstruction by fourier transformation*. IEEE Transaction on Medical Imaging. Vol. 14 ,pp 596-607.

Semmlow, J.L (2004). *Biosignal and biomedical image processing – Matlab based pplications*. USA: Marcel Dekker Inc.

Sijbers, J. (1998). *Signal and noise estimation from magnetic resonance imaging*. Unpublished doctoral dissertation, Universitaire Instelling Antwerpen.

Smith, M.R. (1992). *Constrained ARMA method for magnetic resonance imaging,* IEEE 6th Workshop pp. 481-484, Canada.

Smith, M.R., & Nichols, S.T. (1989). *A Two – Dimensional modeling reconstruction technique for magnetic resonance data.* Journal of Magnetic Resonance, Vol 85, pp 573 – 580, Academic Press.

Smith, M.R., Nichols, S.T., Henkelmen, R. M., & Constabel, R.T. (1991). *A quantitative comparison of the TERA modeling and DFT magnetic resonance image reconstruction techniques.* Magnetic Resonance in Medicine, Vol. 19, pp 1 -19 , Academic Press.

Smith, M.R., Nichols, S.T., Henkelmen, R.M., & Wood, M.L. (1986). *Application of autoregressive modeling in magnetic resonance imaging to remove noise and truncation artifact.* Magnetic Resonance Imaging , Vol. 4 , pp. 257-261.

Smith, M.R., Nichols, S.T., Henkelmen, R.M., & Wood, M.L. (1986). *Application of autoregressive moving average parametric modeling, in magnetic resonance image reconstruction.* IEEE Transactions on Medical Imaging. Vol. MI-5 (3) pp 132 – 139.

Wilkes, D.M., Liang, G., & Cadzow, J.A. (1992). *ARMA model order determination and MDL: A new perspective.* IEEE International Conference on Acoustics, Speech and Signal Processing, ICASSP. San Francisco, CA, USA

Wood, M.L., & Henkelman, R.M. (1985). *Truncation artifacts in magnetic resonance imaging.* Journal of Magnetic Resonance Med. Vol .2.

Yan, H. (2002). *Signal processing for magnetic resonance imaging and spectroscopy* (1st edtn.). USA: Marcel Dekker Inc.

Yang, J., & Smith, M.R. (1996). *Constrained and adaptive ARMA modeling as an alternative to the DFT – with application to MRI.* Chapter in "2D and 3D digital signal processing (Techniques and applications)" . Ed. C. T .Leonades, Control and System Dynamics , Vol 77, pp 225- 299 , Academic Press.

PUBLICATION AND ACHIEVIEMENT

Publication

M.J.Salami, O.Khalifa, K.Ariffin, A.R.Najeeb, "Magnetic Resonance Image Reconstruction using 2D ARMA" IEEE's International Conference on Biotechnology Engineering, ICBE2007, Kuala Lumpur

Award

Gold Medal, Kulliyah of Engineering, IIUM Research and Innovation Exhibition (KERIE 2006) held on 5^{th}- 6^{th} December 2006 at International Islamic University of Malaysia